Synthesis, characterization and optical properties of environmentally benign rare earth based inorganic pigments

Thesis submitted to the
University of Kerala
for the award of the degree of

Doctor of Philosophy
in Chemistry
under the Faculty of Science

By

VISHNU V. S

under the supervision of

Dr. M. L. P. Reddy

NATIONAL INSTITUTE FOR INTERDISCIPLINARY SCIENCE AND TECHNOLOGY
COUNCIL OF SCIENTIFIC AND INDUSTRIAL RESEARCH
THIRUVANANTHAPURAM–695 019, KERALA, INDIA

2011

...Dedicated to my
Parents and Teachers...

DECLARATION

I hereby declare that the Ph.D thesis entitled "**Synthesis, characterization and optical properties of environmentally benign rare earth based inorganic pigments**" is an independent work carried out by me at the Chemical Sciences and Technology Division, National Institute for Interdisciplinary Science and Technology (NIIST), CSIR, Thiruvananthapuram, under the supervision of Dr. M. L. P. Reddy, Scientist–G, and it has not been submitted anywhere else for any other degree, diploma or title.

Vishnu V. S

Thiruvananthapuram
June, 2011

NATIONAL INSTITUTE FOR INTERDISCIPLINARY SCIENCE AND TECHNOLOGY (NIIST)

Council of Scientific & Industrial Research (CSIR)
(Formerly Regional Research Laboratory)
Industrial Estate P.O., Thiruvananthapuram – 695 019
Kerala, INDIA

ISO 9001 REGISTERED
MGMT. SYS. RvA C 024
DNV Certification B.V., The Netherlands

Dr. M. L. P. Reddy
Scientist G
Chemical Sciences and Technology Division

Tel: 91-471-2515 360
Fax: +91-471-2491 712
E-mail: mlpreddy55@gmail.com

CERTIFICATE

This is to certify that the work embodied in the thesis entitled "**Synthesis, characterization and optical properties of environmentally benign rare earth based inorganic pigments**" has been carried out by **Mr. Vishnu V. S** under my supervision and guidance at the Chemical Sciences and Technology Division of National Institute for Interdisciplinary Science and Technology (Formerly Regional Research Laboratory), Council of Scientific and Industrial Research, Thiruvananthapuram and the same has not been submitted elsewhere for any other degree.

Dr. M. L. P. Reddy
(Thesis Supervisor)

Thiruvananthapuram
June, 2011

Acknowledgements

At the onset, I would like to express my heartfelt thanks and deep sense of gratitude to my research supervisor Dr. M. L. P. Reddy, for suggesting the research problem, for his constant encouragement, efficient planning, constructive criticism and valuable guidance during the entire course of my work. I thank you Sir for your help, inspiration and blessings.

I sincerely thank Dr. Suresh Das, Director, NIIST, and former directors Prof. T. K. Chandrasekhar and Dr. B. C. Pai for providing the necessary facilities and infrastructure to carry out this investigation.

I would also take this opportunity to thank Dr. Remya P. N., Dr. Biju S., Ms. Ambili Raj D. B, Ms. Divya V, Ms. Lucky M. V, Ms. Sheethu Jose and Mr. Biju Francis for their timely help and co-operation. I would also extend my thanks to all my labmates for the support bestowed.

I would like to thank

- *Dr. K. J. Sreeram and Mr. Nidhin M (CLRI, Chennai) for their valuable help in coating studies.*
- *Dr. T.P.D. Rajan and Dr. S. Ananthakumar for their help during my research.*
- *Mr. Guruswamy for XRD analysis and Mr. Chandran for SEM analysis.*
- *All former and present colleagues in my division for the help and support.*
- *Library and other supporting staff of NIIST for the help rendered.*
- *All my friends at NIIST for their support.*

I acknowledge the Council of Scientific and Industrial Research, New Delhi for the award of Senior Research Fellowship and Indian Rare Earth Technology Development Council, Mumbai for the fellowship towards a project during the early stages of my research.

I express my earnest thanks to my parents, brothers and my wife who were a constant source of inspiration and support during the entire period of my research.

I would also take this opportunity to thank all my teachers for their blessings.

Above all, I thank Almighty for giving me all these people to help and encourage me, and for the skills and opportunity for the successful completion of this thesis.

Vishnu V. S

Contents

List of Tables

List of Figures

List of Abbreviations

ISO	International Organization for Standardisation
DIN	Deutsches Institute fur Normung (German Standards Organisation)
CIE	Commission Internationale de l'Eclairage
RE	Rare Earth
UV	Ultraviolet
vis	Visible
NIR	Near Infrared
XRD	X–Ray Diffraction
SEM	Scanning Electron Microscope
PTFE	Poly–tetrafluoroethylene
ASTM	American Society for Testing and Materials
TG	Thermogravimety
DTA	Differential Thermal Analysis
C–type	Cubic Type
F–type	Fluorite Type
PMMA	poly(methyl methacrylate)

PREFACE

Inorganic pigments have been utilized by mankind since ancient times, and are still widely used to color materials exposed to elevated temperatures during processing or application. Indeed, in the case of glasses, glazes and ceramics, there is no alternative to inorganic pigments for coloring. However, most inorganic pigments contain heavy metals or transition metals that can adversely effect the environment and human health if critical levels are exceeded. Hence there is a strong incentive to develop new colored inorganic pigments to substitute for industrial pigments that are based on heavy elements hazardous to health and environment. Thus, the main objective of this work is to design and develop novel environmentally benign rare earth based inorganic pigments for various surface coating applications.

The thesis has been divided into five chapters, of which the first chapter highlights the need for the development of new class of rare earth based inorganic pigments. It also incorporates a general introduction to the inorganic pigments about their history, classification and uses, followed by a detailed overview on the recent developments on rare earth based inorganic pigments.

The second chapter describes the results on the synthesis, characterization and optical properties of molybdenum or praseodymium doped yttrium cerate pigments. The pigments having the general formula $Y_2Ce_{2-x}M_xO_{7+\delta}$ (M = Mo or Pr and x ranges from 0 to 0.5) have been synthesized by a traditional solid state process and were characterized using XRD, UV–vis–NIR diffuse reflectance spectroscopy and CIE–1976 $L^*a^*b^*$ color scales. The results demonstrated that the color of the pigment samples change from ivory–white to yellow upon doping of Mo^{6+}. The coloring mechanism of the Mo^{6+} doped pigments can be explained on the basis of O_{2p}–Mo_{4d} charge–transfer transitions. In contrast, the doping of Pr^{4+} for Ce^{4+} gently changes the color of the resultant pigments

from brick–red to dark–brown. The coloring mechanism is based on the introduction of an additional energy level of $4f^1$ electrons of Pr^{4+} between the O^{2-} valence and Ce^{4+} conduction bands. The pigments also possess high near–infrared solar reflectance (>90% for yellow and >70% for the brick–red pigments), thus becoming potential candidates as "cool colorants". The NIR solar reflectance of the developed pigments has also been evaluated after coating it on to a roofing material like asbestos cement sheet **[*Chem. Lett.* *39*,2010, 820–821; *Sol. Energy Mater. Solar Cells*, d.o.i.10.1016/j.solmat.2011.05.042].**

The third chapter reports on the synthesis, characterization and optical properties of a new class of rare earth based pigments as alternatives to toxic inorganic pigments. Investigations reveal that the doping of molybdenum for ceria in $Sm_2Ce_2O_7$ changes the color hue from cream to yellow. The band gap of the resultant pigments decreases from 2.76 to 2.52 eV due to the O_{2p}–Mo_{4d} charge transfer transitions. On the other hand, the doping of praseodymium in ceria matrix changes the color from cream through brick red to dark brown and the band gap shifts from 2.76 to 1.72 eV. The coloring mechanism is based on the introduction of an additional electronic level of energy in the cerianite forbidden band. The influence of various mineralizers on the calcination temperature and optical properties of the pigments have been evaluated. The thermal and chemical stabilities of the pigments have also been examined and the results are depicted in this chapter **[*Dyes Pigm. 85*, 2010,117–123]**.

New rare earth based inorganic pigments having the general formula $Ce_{1-(x+y)}Zr_xTa_yO_{2+\delta}$ (x ranges from 0.15 to 0.2 and y ranges from 0 to 0.05) with a cubic fluorite structure, displaying colors ranging from white to yellow have been synthesized as viable alternatives to lead, cadmium and chromium based yellow toxic inorganic colorants and these results are compiled in Chapter 4. The coloring mechanism is based

on the strong absorptions of the pigments in the visible region under 500 nm, which could originate from the additional energy level between O_{2p} valence band and the Ce_{4f} conduction band by forming a hybrid orbital of Ta_{5d} and O_{2p}. The typical designed pigment sample, $Ce_{0.8}Zr_{0.17}Ta_{0.03}O_2$ was examined for its mass tone/hiding power, tinting strengths and weather resistance by coating on an opacity chart. The results demonstrated that the yellow ceramic pigment obtained in the present study is a potential alternative to the existing classical toxic yellow inorganic pigments for surface coating applications **[*Dyes Pigm. 82*, 2009, 53–57].**

The fifth chapter deals with the development of novel environment friendly yellow inorganic pigments having the general formula $Sm_{6-x}W_{1-y}Zr_xMo_yO_{12+\delta}$ (x ranges from 0 to 0.6 and y ranges from 0 to 1). The pigments were synthesized by simple solid state route and characterized by various spectroscopic techniques. The systematic substitution of Mo^{6+} for W^{6+} in Sm_6WO_{12} gently changes the color from white to yellow. The band gap of the resultant pigments varies from 3.29 to 2.69 eV. The coloring mechanism is based on the O_{2p}–Mo_{4d} charge transfer transitions. Furthermore, the doping of Zr^{4+} for Sm^{3+} in Sm_6MoO_{12} lattice produces intrinsic strain which further intensifies the yellow hue of the resultant compounds with band gap decreasing to 2.58 eV. The designed pigments possess good chromatic properties, especially the hue angle which is found to be similar to those observed for industrial pigments such as $PbCrO_4$, $BiVO_4$, CdS, $NiTiO_3$ and praseodymium yellow and also show thermal and chemical stabilities. The coloring performance of the developed yellow pigments was evaluated by incorporating it into a polymer substrate material **[*J. Am. Ceram. Soc. 94*, 2011, 997–1001].**

The conclusions arrived from this work have been summarized at the end of each chapter. The relevant references cited in this work have been given towards the end of the thesis.

Chapter 1

General Introduction

1.1 Pigments

The word ‘pigment’ is of Latin origin (pigmentum) and originally denoted a color in the sense of a coloring matter, but was later extended to indicate colored decoration. The modern meaning associated with the word pigment originated in the 20th century. According to accepted standards the word pigment refers to a substance consisting of small particles that is practically insoluble in the applied medium and is used on account of its coloring, protective, or magnetic properties. Both pigments and dyes are included in the general term “coloring materials”, which denotes all materials used on account of their coloring properties. The characteristic that distinguishes pigments from soluble organic dyes is their low solubility in solvents and binders (Buxbaum and Pfaff 2002). The pigments can be characterized by their chemical composition, and by their optical or technical properties.

1.2 Inorganic and Organic Pigments – A comparison

In chemical terms, pigments are conveniently classified as either inorganic or organic. In general, inorganic pigments are capable of providing excellent resistance to heat, light, weathering, solvents and chemicals, and in those respects they can offer technical advantage over most organic pigments. In addition, inorganic pigments are generally of significantly lower cost than organics. On the other hand, they commonly lack the intensity and brightness of color of typical organic pigments. Organic pigments are characterised by high color strength and brightness although the fastness properties which they offer are somewhat variable. There is, however, a range of high–performance organic pigments which offer excellent durability while retaining their superior color properties but these tend to be rather more expensive. The ability either to provide opacity or to ensure transparency provides a further contrast between inorganic and

organic pigments. Inorganic pigments are, in general, high refractive index materials which are capable of giving high opacity while organic pigments are of low refractive index and consequently are transparent (Christie 2001). Indeed, in the case of glasses, glazes and ceramics, there is no alternative to inorganic pigments for coloring (Jansen and Letschert 2000).

1.3 History of Inorganic Pigments

Natural inorganic pigments have been known since prehistoric times (Fig. 1.1).

Fig. 1.1. An Egyptian painting (The blue colors are due to Egyptian blue).

60,000 BC Natural ocher ($Fe_2O_3.H_2O$) possessing an yellowish brown color was used in the Ice Age as a coloring material.

3000 BC Vermillion (HgS) was used as a red pigment.

2000 BC Natural ocher was burnt, sometimes in mixtures with manganese ores, to produce red, violet, and black pigments for pottery (Buxbaum and Pfaff 2002; Barnett *et al*. 2006).

1000 BC The ancient Egyptians were probably responsible for the development of the earliest synthetic pigments. The most notable products were Alexandra blue, a ground glass colored with a copper ore, and Egyptian Blue, a mixed silicate of copper and calcium ($CaCuSi_4O_{10}$) which has been identified in

murals dating from around 1000 BC (Barnett *et al*. 2006). Perhaps the oldest synthetic colorant still used extensively today is Prussian Blue, the structure of which has been established as iron(III) hexacyanoferrate(II). The manufacture of this blue inorganic pigment is much less ancient, dating originally from the middle of the 17th century, although this product pre–dates the origin of synthetic organic dyes and pigments by more than a century (Christie 2001). Orpiment (Arsenic sulphide) and Naples yellow (a lead antimonate) were the first clear yellow pigments. Ultramarine (lapis lazuli) and artificial lapis lazuli (Egyptian blue and cobalt aluminum spinel) were the first blue pigments (Fig. 1.2). Terra verte, malachite, and a synthetically prepared copper hydroxychloride were the first green pigments. Calcite, some phases of calcium sulfate, and kaolinite were some of the white pigments used historically. A synthetic lapis lazuli (a silicate of copper and calcium) is still known as Egyptian blue. Antimony sulfide and galena (lead sulfide) were commonly used as black pigments, cinnabar as a red pigment, and ground cobalt glass and cobalt aluminum oxide as blue pigments.

AD 1700's The industrial production of pigments started in the 18th and 19th centuries and a good number of pigments were developed in quick succession.

1704	Iron Blue or Prussian Blue [iron(III) hexacyanoferrate(II)]
1758	Naples Yellow ($Pb_3(SbO_4)_2$
1777	Cobalt Blue ($CoAl_2O_4$)
1778	Chrome Yellow ($PbCrO_4$), Scheele's Green ($CuHAsO_3$)
1780	Cobalt Green ($CoO{\cdot}ZnO$)
1819	Cadmium Yellow (CdS)

1859 Guignet's Green (Hydrated Cr_2O_3)

1860 Cerulean Blue ($CoO \cdot SnO_2$)

1874 Lithopone (70% $BaSO_4$ + 30% ZnS) etc. are a few to mention (Buxbaum and Pfaff 2002; Barnett *et al*. 2006, Bittler and Ostertag, 1980).

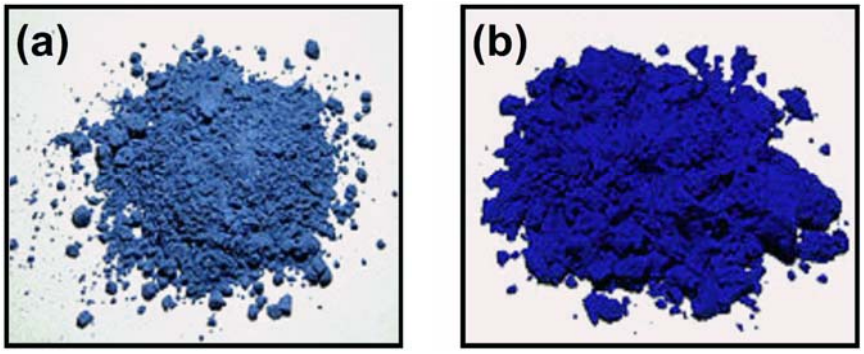

Fig. 1.2. Photograph of ultramarine blue (a) natural (b) synthetic.

Pigments became a matter of scientific investigation in the 20th century. In the past few decades, the synthetic colored pigments cadmium red, manganese blue, molybdenum red, and mixed oxides with bismuth came into the market. Numerous pigment compositions based on bismuth vanadate have been developed. Titanium dioxide with anatase or rutile structures occupied the place of white pigments (Buxbaum and Pfaff 2002; Smith 2002). However, a good number of the pigments known today encompass toxic metals that are hazardous to the health and environment.

Notwithstanding that most inorganic pigments have been known for a very long time, new developments appear on the catwalk of colors in the 21st century. The so–called "high performance pigments" show a lot of modern developments (Smith 2002). Driven by environmental laws, much research in this century is being focused on the development of environmentally benign inorganic pigments to substitute for the classical pigments based on toxic elements (Jansen and Letschert 2000; Garcia *et al*. 2001; Martos

*et al.*2007; [a]Martos *et al.*, 2008; [a]Sreeram *et al*. 2008; Smith *et al*. 2009; Martos *et al*. 2009; Sulcova *et al*. 2010; George *et al*. 2011, Fernandez–Gonzalez *et al*. 2011).

1.4 Classification of Inorganic Pigments

Inorganic pigments can be classified from various points of view. Based on coloristic and chemical considerations, as recommended by ISO and DIN, inorganic pigments can be classified as given in Table 1.1 (Buxbaum and Pfaff 2002).

Table 1.1. Classification of inorganic pigments

Term	Definition
White pigments	the optical effect is caused by nonselective light scattering (examples: titanium dioxide and zinc sulfide pigments)
Colored pigments	the optical effect is caused by selective light absorption and also to a large extent by selective light scattering (examples: iron oxide red and yellow, cadmium pigments, ultramarine pigments, chrome yellow, cobalt blue)
Black pigments	the optical effect is caused by nonselective light absorption (examples: carbon black, iron oxide black)
Effect pigments	the optical effect is caused by regular reflection or interference
Pearl luster pigments	regular reflection takes place on highly refractive parallel pigment platelets (examples: titanium dioxide on mica)
Metal effect pigments	regular reflection takes place on mainly flat and parallel metallic pigment particles (examples: aluminum flakes)
Interference pigments	the optical effect of colored luster pigments is caused mainly due to interference (examples: iron oxide on mica)
Luminescent pigments	the optical effect is caused by the capacity to absorb radiation and to emit it as light of a longer wavelength
Fluorescent pigments	the light of longer wavelength is emitted after excitation without a delay (examples: silver–doped zinc sulfide)
Phosphorescent pigments	the light of longer wavelength is emitted within several hours after excitation (examples: copper–doped zinc sulfide)

1.5 Applications of Inorganic Pigments

The most important areas of use of pigments are paints, varnishes, plastics, artists' colors, printing inks for paper and textiles, leather decoration, building materials (cement renderings, concrete bricks and tiles, mostly based on iron oxide and chromium oxide pigments), imitation leather, floor coverings, rubber, paper, cosmetics, ceramic glazes, and enamels. The paint industry uses high–quality pigments almost exclusively (Buxbaum and Pfaff 2002, Jansen and Letschert, 2000). Pigments are fine particle size materials that confer on a paint its color and opacity. Pigments are used in paint formulation to carry out one or more of the following tasks (Ali *et al*. 2005).

1. Provide color
2. Hide substrate and obliterate previous colors
3. Improve the strength of the paint film
4. Improve the adhesion of the paint film
5. Reduce gloss
6. Reduce cost

When choosing a pigment for a particular application, several points normally have to be considered.

1. Coloring properties (color, tinting strength, hiding power)
2. General chemical and physical properties (chemical composition, moisture and salt content, content of water–soluble and acid–soluble matter, particle size, density, and hardness)
3. Stability properties (resistance toward light, weather, heat, and chemicals, anticorrosive properties, retention of gloss)
4. Behavior in binders (interaction with the binder properties, dispersibility, special properties in certain binders, compatibility, and solidifying effect)

1.6 Colorimetry

The term *color* is used with different meanings in different technologies. The perception of color is a psychophysical phenomenon, and the measurement of color must be defined in such a way that the results correlate accurately with what the visual sensation of color is to a normal human observer. *Colorimetry* is the science and technology used to quantify and describe physically the human color perception. The basis for colorimetry was established by CIE [Commission Internationale de l'Eclairage; International Commission on Illumination] (Ohno, 2000).

Color is defined by the presence of an object, an illuminant and an observer. Standard colorimetric observers and standard light sources (illuminants) are needed in color definition. CIE has defined and standardized the CIE colorimetric system which is based on standard color matching functions and tristimulus values.

1.6.1 Standard Illuminants

Illuminants indicate the predominant light source in which an object is viewed. The colors we see will vary considerably according to the particular illuminant in which we see them. Certain colors show perceptible changes in appearances as they are viewed under different illuminants. Table 1.2 gives a list of standard illuminants.

Table 1.2. CIE illuminants

Illuminant	Characteristics
A	CIE standard illuminant for incandescent illumination, yellow–orange in color, with a correlated color temperature of 2856 K
B	Represent direct sunlight with a correlated color temperature of approximately 4900 K
C	CIE standard illuminant for tungsten illumination that simulates average daylight, bluish in color, with a correlated color temperature of 6774 K
D	CIE standard illuminants for daylight, based on actual spectral measurements of daylight. D_{65} with a correlated color temperature of 6504 K is most commonly used. Others include D_{50}, D_{55}, and D_{75}
F	CIE standard illuminant for fluorescent illumination. F_2 represents a cool white fluorescent lamp (4200 K), F_7 represents a broad–band daylight fluorescent lamp (6500 K).

The D_{65} illuminant represents a standard daylight typical of average daylight and hence is recommended by CIE. The spectral power distribution of the standard D_{65} illuminant is shown in Fig. 1.3.

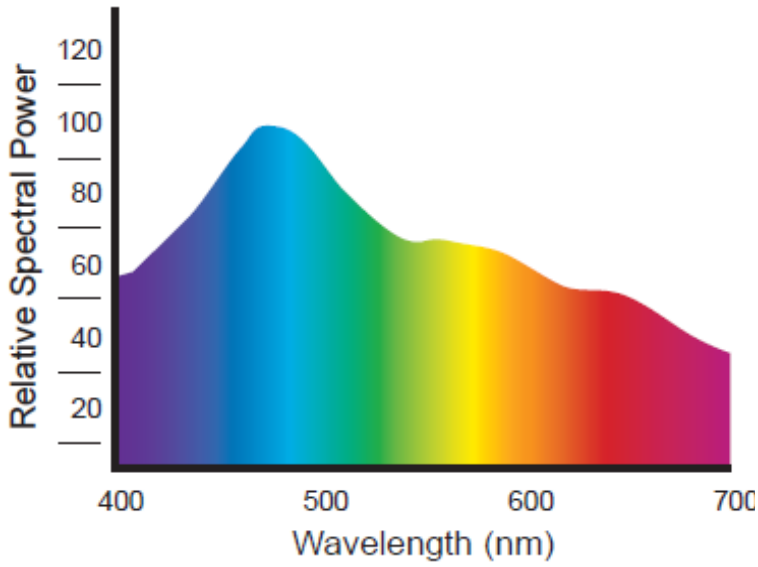

Fig. 1.3. Spectral power distribution of the standard D_{65} illuminant.

1.6.2 Standard Observers

A standard observer is a hypothetical observer having the tristimulus color–mixture data recommended in 1931 by the CIE for a 2° viewing angle. A supplementary observer for a larger angle of 10° was adopted in 1964. A 10° standard observer is to be used when the field of view is larger than 4°. A 2° visual field represents a diameter of about 17 mm at a viewing distance of 0.5 m. A 10° visual field represents a diameter of about 90 mm at a viewing distance of 0.5 m (CIE 1986, CIE 2004). The color matching function for the 2° and 10° standard observer is shown in Fig. 1.4.

1.6.3 Trichromatic principle and the CIE system

It is a well known fact that any color stimulus can be prepared from the spectral colors by mixing. Thus, it has a spectral distribution, which in the case of nonluminous, perceived colors is called the spectral reflectance $\rho(\lambda)$ (Buxbaum and Pfaff 2002; Volz 2002). After defining three reference stimuli, the trichromatic principle allows a three–dimensional

color space to be built up in which the color coordinates (tristimulus values) can be interpreted as components of a vector. For pure white light, the CIE tristimulus values are calculated as

$$X = \int_{400}^{700} \bar{x}(\lambda)\rho(\lambda)d(\lambda)$$

$$Y = \int_{400}^{700} \bar{y}(\lambda)\rho(\lambda)d(\lambda)$$

$$Z = \int_{400}^{700} \bar{z}(\lambda)\rho(\lambda)d(\lambda)$$

If light other than pure white light is used for illumination, $\rho(\lambda)$ must be replaced with the product of $\rho(\lambda).S(\lambda)$. The three CIE tristimulus values will then depend on the spectral reflectance $\rho(\lambda)$ and the spectrum of the illuminant $S(\lambda)$ as follows:

$$X = \int_{400}^{700} \bar{x}(\lambda)\rho(\lambda)S(\lambda)d(\lambda)$$

$$Y = \int_{400}^{700} \bar{y}(\lambda)\rho(\lambda)S(\lambda)d(\lambda)$$

$$Z = \int_{400}^{700} \bar{z}(\lambda)\rho(\lambda)S(\lambda)d(\lambda)$$

where $\bar{x}, \bar{y}$ and $\bar{z}$ are the CIE tristimulus values of the spectral colors and are called the CIE spectral tristimulus values (color matching function). The CIE chromaticity coordinates (x, y, and z) are given by

$$x = \frac{X}{X + Y + Z}$$

$$y = \frac{Y}{X + Y + Z}$$

$$z = 1 - x - y$$

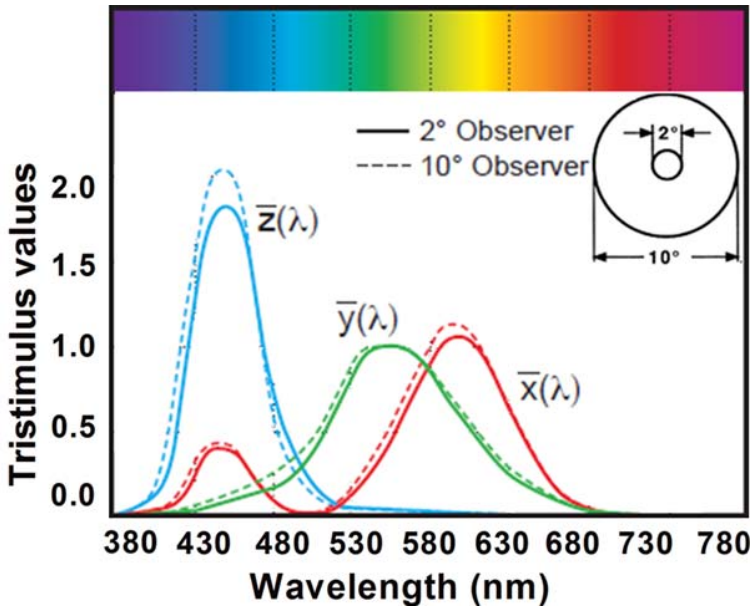

Fig. 1.4. The color matching function for the 2° and 10° standard observer.

These are treated as coordinates in the color plane and define the CIE chromaticity diagram (Fig.1.5). The chromaticity coordinates *x* and *y* are used to specify the saturation and hue of any color. A third color variable is specified in addition to *x* and *y*, namely the CIE tristimulus value *Y*, which is a measure of lightness.

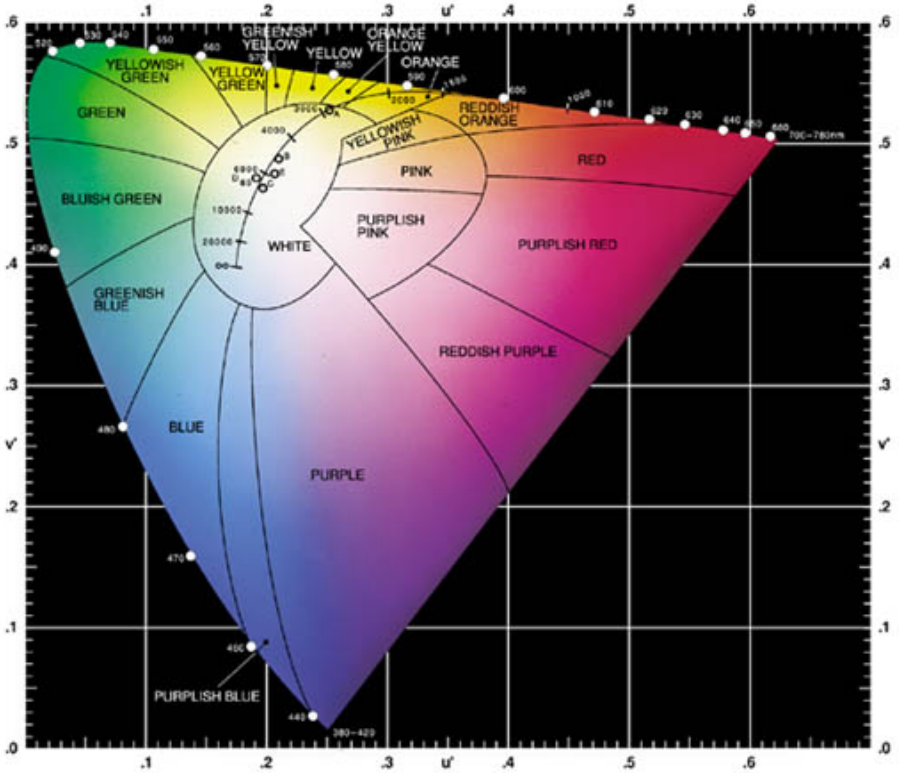

Fig. 1.5. CIE 1976 chromaticity diagram.

This system allows exact measurement of color with worldwide agreement. However, for the testing of pigments, this is not sufficient because small color differences usually have to be determined and evaluated. To determine color difference objectively, one needs to start with a concept that plays an idealized role in the physiology of colors, the concept of "absolute color space", which can be thought of as a three–dimensional arrangement of color stimuli such that the distance between two color stimuli in an arbitrary spatial direction corresponds to the perceived difference. A color space with these properties cannot, however be derived on a purely theoretical basis; its structure must be determined experimentally through color matching tests on samples having small color differences. Such a type of color space can be based on the color qualities lightness, hue, and saturation. Several such systems exist. The most widespread color system is probably the Munsell system. Brightness, hue and saturation are termed value, hue and chroma respectively in the Munsell system.

For the quantitative determination of color differences, the transformation relationships between the CIE system (which has to be used for color measurement) and the physiologically equidistant color system must be established. Color differences can then be calculated in the latter system. A large number of color difference systems have been developed, mainly as needed for industrial color testing. The Adams–Nickerson (AN) system, well known for many decades and derived from the Munsell system, was recommended for pigment testing by DIN and later worldwide by the CIE. CIE $L^*a^*b^*$ color space is perceptually uniform. The three coordinates are denoted by L^* is the vertical lightness axis [black (0) to white (100)], a^* is the green (–ve) to red (+ve), and b^* is the blue (–ve) to yellow (+ve) axis (Fig. 1.6). The color locus in the color plane (a^*, b^* plane) can also be described as polar coordinates as C^* (chroma) and $h°$(hue angle), where

$$C^* = \sqrt{(a^*)^2 + (b^*)^2}$$

$$h^\circ = \tan^{-1}\left(\frac{b^*}{a^*}\right)$$

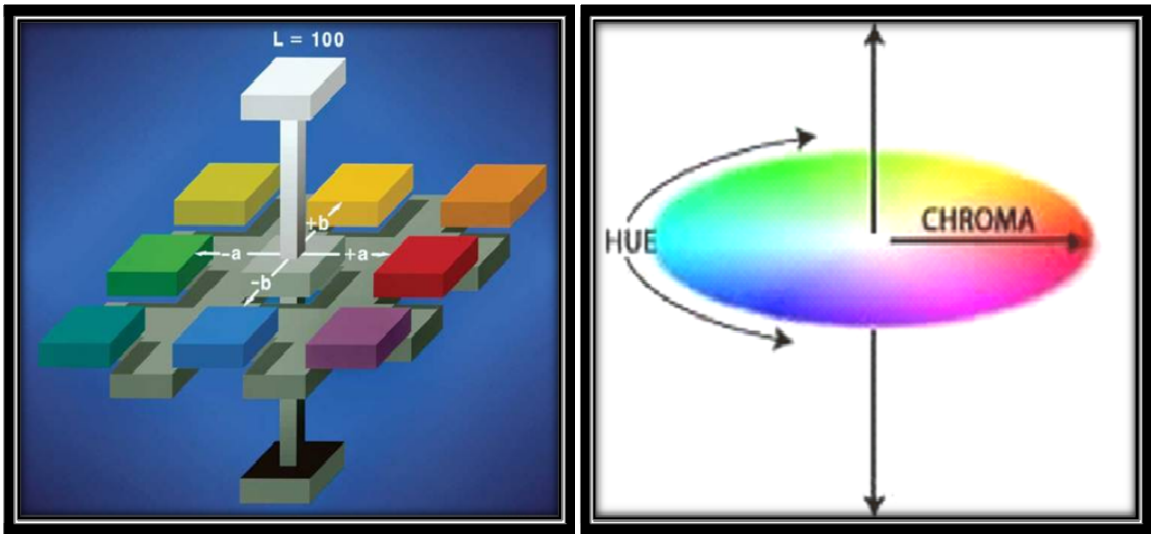

Fig. 1.6. CIE 1976 color scale.

To calculate the CIELAB coordinates, *X*, *Y*,and *Z* are first converted into the functions *X**, *Y**, and *Z** by using a relationship that approximately takes account of the physiologically equidistant lightness steps.

$$X^* = \sqrt[3]{\frac{X}{X_n}}; \qquad Y^* = \sqrt[3]{\frac{Y}{Y_n}}; \qquad Z^* = \sqrt[3]{\frac{Z}{Z_n}}$$

Where X_n, Y_n *and* Z_n are the CIE tristimulus values of the illuminant, especially a standard illuminant.

For radicands ≤0.008856, these equations become

$$X^* = 7.787\frac{X}{X_n} + 0.138$$

$$Y^* = 7.787\frac{Y}{Y_n} + 0.138$$

$$Z^* = 7.787\frac{Z}{Z_n} + 0.138$$

The $L^*a^*$and b^* can then be calculated as

$$L^* = 116Y^* - 16$$

$$b^* = 200\ (Y^* - Z^*)$$

$$a^* = 500\ (X^* - Y^*)$$

The components of the color difference are obtained as differences between the test sample (T) and the reference pigment (R).

$$\Delta E^*_{ab} = \sqrt{(\Delta L^*)^2 + (\Delta a^*)^2 + (\Delta b^*)^2}$$

where $\Delta L^* = L^*_T - L^*_R$

$\Delta a^* = a^*_T - a^*_R$

$\Delta b^* = b^*_T - b^*_R$

A significant advantage of the CIE system is that the color difference can be broken down into components in another way: into brightness, chroma and hue, corresponding to the arrangement in the color space.

Lightness difference, $\Delta L^* = L^*_T - L^*_R$

Chroma difference, $\Delta C^*_{ab} = C^*_{ab(T)} - C^*_{ab(R)} = \left(\sqrt{(a^*_T)^2 + (b^*_T)^2} - \sqrt{(a^*_R)^2 + (b^*_R)^2}\right)$

Hue difference, $\Delta H^*_{ab} = \sqrt{\left(\Delta E^*_{ab}\right)^2 - \left(\Delta L^*\right)^2 - (\Delta C^*_{ab})^2}$

Modern testing of coloring materials is able to establish an almost perfect connection between the color stimulus (and hence the optical properties of pigments) and the fundamental physical quantities. Fig. 1.7 represents a schematic diagram connecting the color properties and the theoretical fundamentals (Volz 2002).

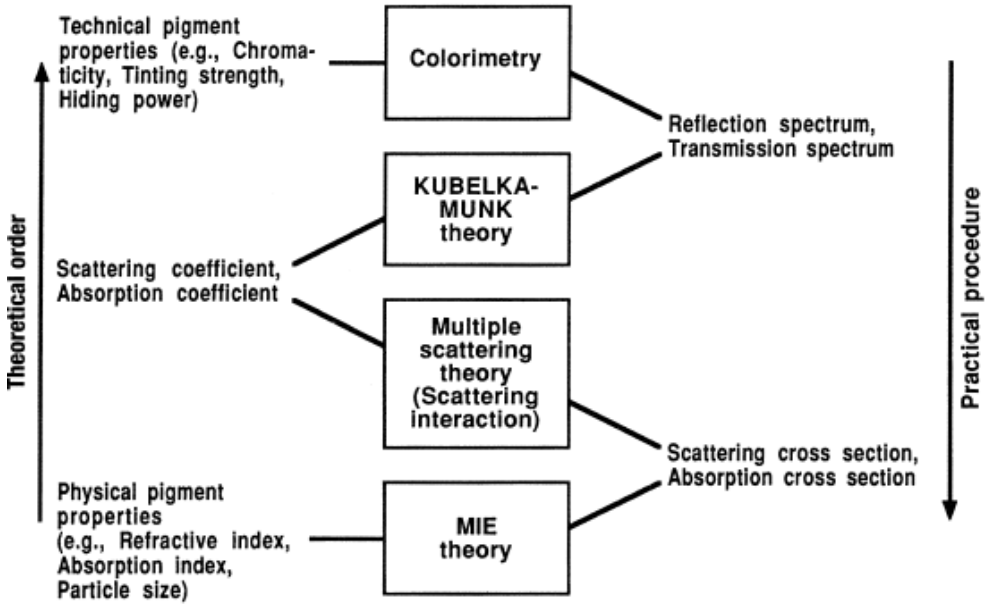

Fig. 1.7. Schematic diagram showing the relation between color properties and theoretical fundamentals

Colorimetry relates the perceived color quality to the color stimulus and this in turn, to the reflection spectrum $\rho(\lambda)$.

Kubleka–Munk theory relates $\rho(\lambda)$ to the scattering coefficient, absorption coefficient, and coating thickness. The theory is based on the fact that the optical properties of a film which absorbs and scatters light may be described by two constants: the absorption coefficient *K* and the scattering coefficient *S*. In a simplification, the flux of the diffuse incident light is represented by a single beam L+, and the flux of the light scattered in the opposite direction by a beam L−. Each beam is attenuated by absorption and scattering losses, but is reinforced by the scattering losses of the respectively opposite beam. The absorption and scattering losses are determined quantitatively by the two coefficients *K* and *S*. A simple system of two linked differential equations can be written. These can be integrated for the valid boundary conditions at the incident light side, and at the opposite

side. Solutions for the transmittance τ and the reflectance ρ are obtained from these integrals as a function of the absorption coefficient *K*, the scattering coefficient *S*, the film thickness *h*, and in special cases of the reflectance ρ_0 of a given substrate.

The most important and widely used quantity derived from the Kubelka–Munk theory is the reflectance of an opaque (infinitely thick) film that is described by a very simple eqn:

$$\frac{K}{S} = \frac{(1-\rho_\infty)^2}{2\rho_\infty}$$

From this expression (Kubelka–Munk function) it follows that, within the range of validity of the theory, ρ_∞ depends only on the ratio of the absorption coefficient to the scattering coefficient, and not on their individual values. The equation has been most useful where reflectance measurements are used to obtain information about absorption and scattering (e.g., in textile dyeing, thin layer chromatography and IR spectroscopy).

This theory is especially useful for computer color matching of pigmented systems: absorption and scattering coefficients are combined additively using the specific coefficients of the components multiplied by their concentrations (Buxbaum and Pfaff 2002).

Multiple scattering theory relates scattering coefficient to the scattering cross section of the individual particle and the pigment concentration (The absorption coefficient is directly proportional to the absorption cross section and pigment concentration).

Mie theory, finally relates scattering coefficient and absorption coefficient to the particle size, the wavelength, the refractive index and the absorption index; the last two optical properties being constants of the material.

1.7 Rare earth based inorganic pigments: State of the art

1.7.1 Rare earth based blue inorganic pigments

Currently employed blue inorganic pigments in the pigment industry are cobalt blue ($CoAl_2O_4$), cerulean blue ($CoO{\cdot}SnO_2$), ultramarine ($Na_7Al_6Si_6O_{24}S_3$), prussian blue ($Fe_4[Fe(CN)_6]_3$), and azurite $[Cu_3(CO_3)_2(OH)_2]$ (Fig. 1.8). However, all the above pigments suffer from environmental and/or durability issues. Cobalt is considered to be highly toxic. Ultramarine and azurite are not stable with respect to heat and acidic conditions. Prussian blue liberates HCN under mild acidic conditions. In addition, the manufacture of ultramarine involves a large amount of sulphur dioxide emission. Hence, the identification of intense blue inorganic pigments that are environmentally benign, earth–abundant, and durable is important but remains a challenge today (Smith *et al.* 2009).

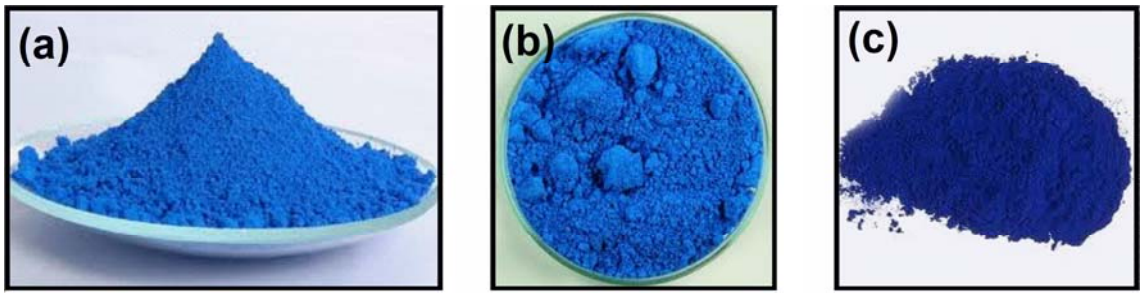

Fig. 1.8. Toxic blue pigments (a) Cobalt blue, (b) Cerulean blue and (c) Prussian blue.

An intense bright–blue colored pigment was reported based on the formula $YIn_{0.9}Mn_{0.1}O_3$ (Smith *et al.* 2009). The blue color was obtained when Mn^{3+} is introduced into the trigonal bipyramidal sites of $YInO_3$ by partial replacement of Mn^{3+} (Fig. 1.9). The intense blue color appears at lowest concentration of Mn^{3+} doping in $YInO_3$. With increasing Mn^{3+} composition, the color darkens until $YMnO_3$, which is found to be black. The blue color was also obtained when Mn^{3+} was introduced into trigonal bipyramidal sites in other layered oxides ($ScAlMgO_4$, $ScGaMgO_4$, $LuGaMgO_4$, $ScGaZnO_4$, and

$InGaMgO_4$). It was concluded that the blue color is a consequence of both the crystal field splitting associated with the trigonal bipyramidal coordination and the short apical Mn–O bonds.

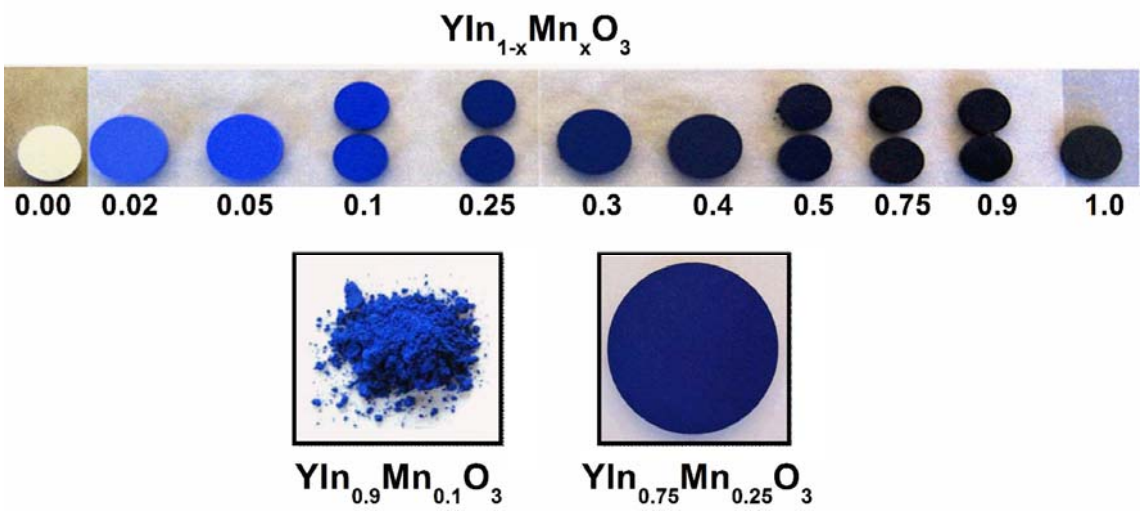

Fig. 1.9. Representative photographs of $YIn_{1-x}Mn_xO_3$ blue pigments.

The use of rare–earth cuprates $R_2Cu_2O_5$ (R = rare earth) type compounds for high temperature (above 1000 °C) ceramic pigment application has been disclosed (Kar *et al*. 2008). A bluish–green color was obtained for $R_2Cu_2O_5$ (R = Dy, Yb, Ho, Er and Y) powders with a variation in their intensity when calcined between 950 and 1050 °C with a 2 h soaking time. The generation of color in $R_2Cu_2O_5$ is considered to be due to the crystal field splitting of the d–orbitals of Cu^{2+} followed by d–d electronic transitions.

1.7.2 Rare earth based green inorganic pigments

The most popular green pigments (Fig. 1.10) in the ceramic industry are chrome green (Cr_2O_3), cobalt green ($CoO{\cdot}ZnO$) and cobalt titanate green (Co_2TiO_4). However, these pigments encompass toxic elements and hence there is a need for environment friendly counterparts. In this perspective, new inorganic pigments that are based on non–toxic rare earth elements have been developed by many researchers.

Fig. 1.10. Toxic green pigments (a) Chrome green, (b) Cobalt green and (c) Cobalt titanate.

Green ceramic pigments based on $YCrO_3$ perovskite structure, doped with Ca, Al and Ti were developed through a ceramic route (Ardit *et al.* 2009). It has been reported that the doping of Al, Ti and Ca affected the phase composition and induced a series of structural rearrangements in perovskite and their optical properties. Furthermore, the authors observed that the oxidation of Cr^{3+} to Cr^{4+} had a deleterious effect on its green color, tuning it to a grey–brown color.

An yellow–green pigment that consists of non–toxic elements was developed by doping calcium ions into the cerium orthophosphate lattice (Imanaka *et al.* 2003; [b]Masui *et al.* 2004). Doping of divalent alkaline earth ions into the $CePO_4$ lattice induce a change in the 4f–5d transition energy and also supported partial oxidation of the Ce^{3+} ion. By combination of the principal 4f–5d transition of Ce^{3+} and the additional O_{2p}–Ce_{4f} transition of Ce^{4+}, the color of the cerium phosphate changes from white to yellow–green. Nanocrystalline rod shaped calcium doped cerium phosphate yellow–green pigment particles having an average length of ~ 100 nm have been realized through an aqueous sol–gel process (Sumaletha *et al*. 2009).

A series of Ca–doped $PrPO_4$ compounds with the general formula, $Pr_{1-x}Ca_xPO_4$ (x = 0–0.4) has been synthesized by solution route (Sivakumar and Varadraju 2005). The compounds exhibit yellowish–green color and the coloring mechanism is attributed to the electronic transitions between $4f^2 \rightarrow 4f^15d^1$ states of Pr^{3+}.

A new class of inorganic pigments based on praseodymium molybdate having the general formula $Pr_{2-x}Ca_xMo_2O_{9-\delta}$ (where x ranges from 0 to 1.0), displaying colors ranging from green to greenish–yellow (Fig. 1.11) were synthesized by traditional solid state route, and reported as alternatives to lead, cadmium and chromium based colorants. The coloring mechanism is based on the strong absorptions of pigments in the blue and red regions due to electronic transitions between $4f^2 \rightarrow 4f^15d^1$ of Pr^{3+} (George *et al*. 2005; [a]George *et al*. 2008).

Fig. 1.11. Photograph of the $Pr_{2-x}Ca_xMo_2O_{9-\delta}$ (x = 0, 0.1–1.0) pigments.

Thermally and chemically stable, and non–toxic inorganic colorants, characteristically green and well suited for coloration of wide variety of materials and substrates, for example, plastics, ceramics, etc. comprising at least one mixed oxide of the formula: Y_2BaCuO_5, Sm_2BaCuO_5 and Yb_2BaCuO_5 were described in the U. S. Patent (Chopin and Macaudiere 2001).

The structural characterization and optical properties of calcium doped Nd_2S_3 have been investigated and found that the doping of CaS into the α–Nd_2S_3 matrix induces a change in color from dark–red to green (Urones–Garrote *et al*. 2006).

1.7.3 Rare earth based yellow inorganic pigments

Yellow pigments form an important class among inorganic pigments. Some of the renowned inorganic pigments that are in commercial use are cadmium yellow,

praseodymium–zircon yellow, lead chromate, lead antimonite, nickel rutile yellow, chrome rutile yellow, naples yellow, vanadium–zirconia yellow and tin–vanadium yellow (Fig. 1.12). Among these the utility of lead, cadmium and chromium based pigments are restricted due to their toxicity ([b]Badenes *et al.* 2002) while that of iron oxide yellow gets constrained due to its poor thermal stability as they decompose above 220 °C (Cornell and Schwertmann 1996). Though praseodymium–zircon yellow and vanadium–zircon yellow are popular in the pigment industry, their efficacy suffers a setback due to their limitations in bulk coloration of porcelain stoneware at high temperature (Sorly *et al.* 2004; Biswas *et al.* 2008) and in weak color strengths caused by the low concentrations of the dopants forming solid solutions with the host oxides (Ishida *et al*. 1993; Seabright and Draker 1961; Ray *et al*. 1961).

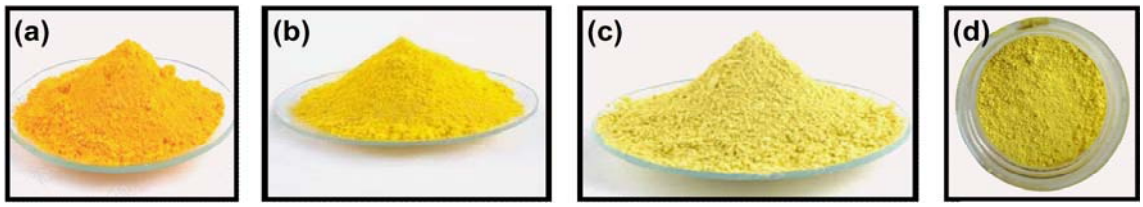

Fig. 1.12. Toxic yellow pigments (a) Cadmium yellow, (b) Chrome yellow, (c) Nickel antimony titanium yellow and (d) Naples yellow.

Pigments based on zircon ($ZrSiO_4$) are widely used in ceramic industries because they can withstand high temperatures and corrosive environments. Their color, obtained by doping the zircon lattice with guest metal species, is yellow, blue or pink when praseodymium, vanadium or iron ions, respectively, are introduced (Nero *et al.* 2004; Llusar *et al*. 2001; Ocana *et al.* 1998). In the case of praseodymium doping, the cations are generally assumed to form a solid solution with the zircon lattice. In general, praseodymium ions are considered to be located at the triangular dodecahedral positions (Ocana *et al.* 1998) of Zr^{4+}, however it is also suggested that Pr^{4+} may substitute for both Zr^{4+} and Si^{4+} of the zircon lattice (Shoyama *et al*.1998). U. S. Patent No. 2,992,123

(Seabright 1961) reported the use of praseodymium doped zirconium silicate crystals as a pigment for use in ceramic glazes for the first time. Ever since, numerous patents, on various aspects of this pigment have been granted (Blonski 1994; Linke *et al.* 1994; Huguenin *et al.* 1996). Since its discovery in the late 1950s, much work has been conducted to get an insight on the processing parameters as well as to improve the optical properties of this pigment (Hill *et al.* 2000; [b]Badenes *et al.* 2002; Nero *et al.* 2004; Kar *et al.* 2004; Kar *et al.* 2005; Kar *et al.* 2007). Studies reveal that, temperature, particle size, reactivity of the zirconia, and mineralizer content are important variables that decide the color of the pigment. Various formulations in the literature indicate that, to obtain an intense yellow color, the praseodymium oxide content should be in the range of 3–8 wt%. Lesser contents are too weak to produce a homogeneous, bright color. In high percentages, praseodymium oxide imparts a greenish–yellow color, because the coloring component is not fully incorporated into the zircon lattice. (Linke *et al*.1994; Hill *et al.* 2000). When praseodymium oxide is incorporated into the zircon host lattice, Pr^{3+} replaces the Zr^{4+} and owing to the interaction of the surrounding f electrons with the host lattice, the f orbitals split into two groups, of which one has a higher energy and the other has a lower energy. Since the transition of energy from the higher energy level to a lower energy falls in the yellow region of the visible spectrum, a yellow color is observed. Addition of CeO_2 shifts the color towards the orange region of the spectrum because of the change in the splitting of the energy levels owing to the change in the interaction of the f electrons with the surrounding electrons of the host lattice, thereby inducing the color change (Kar *et al.* 2007). It is also been reported elsewhere that the incorporation of terbium oxide into the zircon host lattice in the presence of different types of mineralizes creates various shades of yellow which are different from the praseodymium–zircon yellow (Kar *et al.* 2004).

The Ce–S–Si system has been explored in search of new, yellow non–toxic pigments. As yellow pigments to substitute for CdS, $PbCrO_4$ and $PbMoO_4$, sulfides of Ce^{3+} ions are also appropriate if their Ce^{3+} $4f^1 \rightarrow 5d^0$ transition starts at ~ 2.5 eV (Gauthier *et al.* 2003). This might be achieved by increasing the net positive charge on the Ce atoms, i.e., by increasing the ionicity of the Ce–S bonds. According to the inductive effect, one can increase the ionicity of a Ce–S bond by forming a Ce–S–M bond linkage with a third element M that makes a strong covalent bond with S. An increase in the net positive charge on a cation lowers the energies of its orbitals. In a Ce–S–M compound, one might expect that this energy–lowering effect is larger for the 4f than for the 5d orbitals of Ce, thereby increasing the Ce $4f^1 \rightarrow 5d^0$ gap, because the Ce 4f orbitals are much more localized on the Ce atom than are the Ce 5d orbitals. Thus cerium thiosilicates (Ce_2SiS_5, $Ce_6Si_4S_{17}$ and $Ce_4Si_3S_{12}$) and cerium thiophosphates ($CePS_4$) were synthesized as novel yellow pigments. Among these, $Ce_4Si_3S_{12}$ and $Ce_6Si_4S_{17}$ (Fig. 1.13) possess chromatic properties similar to those found for industrially used pigments and are chemically and thermally stable.

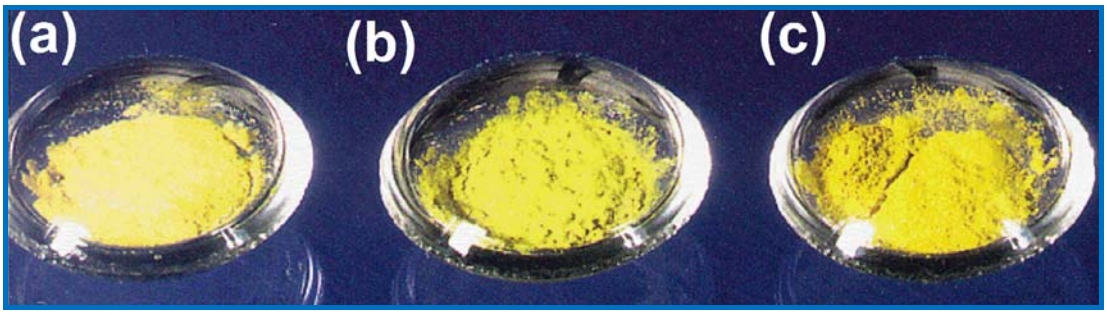

Fig. 1.13. Photographs of (a) $CePS_4$ (b) $Ce_4Si_3S_{12}$ and (c) $Ce_6Si_4S_{17}$.

U. S. Patent. No. 6,419,735 (Busnot and Macaudiere 2002) discloses a process for the preparation of samarium sesquisulfide pigment. The process consist of reacting samarium, trivalent rare earth metal, and alkali metal or alkaline earth metal compounds with a gaseous mixture of hydrogen sulfide and carbon disulfide. The designed pigments

exhibit a strong yellow color and are projected as suitable candidates for the coloring of polymer substrates.

New oxynitride compositions with a defect fluorite–type structure have been synthesized by a thermal ammonolysis of rare earth tungstates in search of non–toxic yellow pigments (Diot *et al*. 2001). Starting from the tungstates $Re_{14}W_4O_{33}$ and Re_6WO_{12} (where Re = Rare earth ions) a progressive substitution of nitrogen for oxygen within the anionic network is shown to be possible with the formation of two oxynitride solid solution domains ranging from $A_4X_{7.33}\square_{0.67}$ and $A_4X_{6.85}\square_{1.15}$, respectively, to $A_4X_6\square_2$ in both cases ($\square$ indicates an anion vacancy). The color of the nitrided powders changes continuously from white to yellow with the nitrogen enrichment as a function of the nitridation temperature and time. The coloring mechanism is explained by a decrease in the energy band gap, as nitrogen gives with cationic elements more covalent bonds than oxygen. This progressive N^{3-}/O^{2-} anionic substitution gives access to a new class of pigments with, in addition, the possibility to tune the absorption edge position to a precise value.

Earlier investigations reveal that the classical toxic inorganic pigments can be replaced by solid solutions of perovskites $CaTaO_2N$ and $LaTaON_2$, which gives colors ranging from yellow to deep red (Jansen and Letschert 1997; Jansen and Letschert 2000). Although these pigments are non–toxic and show excellent color hue, it is necessary to heat the starting materials in a flow of toxic and inflammable ammonia gas for a long time (20–60 h) to synthesize them.

Recently, a series of inorganic pigments based on Si^{4+} doped Y_6MoO_{12} has been reported as yellow pigments (George *et al*. 2011). Replacing Si^{4+} for Y^{3+} in Y_6MoO_{12} changed the color from light–yellow to dark–yellow and the band gap decreased from 2.60 to 2.45 eV due to O_{2p}–Mo_{4d} charge–transfer transitions (Fig. 1.14). The introduction

of Si^{4+} into the Y_6MoO_{12} lattice results in the formation of an additional phase of α–$Y_2Si_2O_7$ which tends to increase the apparent concentration of Mo^{6+} ions in the lattice. These results in a red shift of the charge–transfer band and intensify the yellow hue of Y_6MoO_{12} pigments.

Fig. 1.14. Photographs of $Y_{6-x}Si_xMoO_{12+\delta}$(*x* ranges from 0 to 1) pigments.

Yellow pigments based on the composition $Y_{2-x}Ca_xTi_{2-x}V_xO_7$ with *x* varying between 0.02 and 0.3 were prepared by solid state route and studied the effect of annealing temperature, vanadium concentration and post mechanical grinding on the phase purity and color (Pailhe *et al*. 2009). These compounds exhibit colors varying from pale–yellow (E_g = 2.7 eV) to deep–orange (E_g = 2.2 eV) depending on the vanadium concentration and the synthesis temperature. The coloring mechanism is based on the O^{2-} – V^{5+} charge–transfer transitions.

Rare earth based yellow pigments based on cerium molybdenum oxides has been reported (Sreeram *et al*. 2007) as non–toxic pigments. The coloring properties of the pigment compositions prepared by varying the Ce:Mo ratio in the presence and absence of phosphates was also evaluated in this investigation. The reflectance spectrum of the cerium double molybdates revealed strong absorptions in both visible and ultraviolet regions, which could originate from the O_{2p}–Ce_{4f} and the O_{2p}–Mo_{3d} double charge transitions and as a result the pigments show yellow color. The color of these pigments, especially the chroma was found to be dependent on the presence/absence of phosphate, with phosphate ion increasing the chroma.

$Ce_{1-x}Zr_xBi_yO_{2-y/2}$ solid solutions were synthesized as new inorganic yellow pigments and their color properties have been investigated as possible ecological materials (Masui *et al.* 2006; Furukawa *et al.* 2008). The most effective yellow hue was obtained at x = 0.37 and y = 0.20.The doping of Bi^{3+} ions into the CeO_2 lattice results in enhancement of visible light absorptions due to the transition from a new valence band, made up of a hybrid orbital of Bi_{6p} and O_{2p}, to the Ce_{4f} conduction band. The importance of the presence of Bi^{3+} in the CeO_2–ZrO_2 lattice has been elucidated by comparing the color of $Ce_{0.43}Zr_{0.37}Bi_{0.20}O_{1.9}$ with that of $Ce_{0.43}Zr_{0.37}La_{0.20}O_{1.9}$. However, in comparison with an ideal yellow color, the synthesized pigment was slightly reddish (Fig. 1.15).

Fig. 1.15. Photographs of (a) $Ce_{0.43}Zr_{0.37}La_{0.20}O_{1.9}$, (b) $Ce_{0.43}Zr_{0.37}Bi_{0.20}O_{1.9}$ and (c) praseodymium yellow.

The synthesis of a rare earth containing pyrochlore system $Ce_2Ti_2O_7$ as an ecological colored material by sol–gel synthesis has been reported ([b]Martos *et al.* 2008). The coloration of titanates was ascribed to charge–transfer transitions in which an electron is transferred from the metal ion to the empty 3*d* orbitals of the Ti^{4+} ion. In contrast, the presence of Ce^{4+} ions can generate charge–transfer bands that are also related to the color mechanism, which, in this case, a yellow coloration. Calcination in air or with the use of soft reducing agents leads to CeO_2–TiO_2 compositions (including solid solutions) with yellow to–green colorations. In contrast, with the use of an aggressive reducing agent

such as H_2, the pyrochlore structure is obtained, and the color changes to brownish shades.

The preparation and characterization of SiO_2–CeO_2 mixed oxides as environmentally benign yellow pigments was reported ([a]Masui *et al*. 2004). Accompanying with the change of the band gap energies, all the mixed oxide samples have brilliant colors varying from white to bright yellow, which depends on the Si/Ce ratio. Later the effect of Bi^{3+} doping on this system was studied (Imanaka *et al*. 2008) by synthesizing pigments with the general formula $Ce_{1-x-y}Si_xBi_yO_{2-y/2}$. The coloring of these materials is due to synergetic modification of the band structure of CeO_2 by the hybrid orbital formed from the Bi_{6s} and O_{2p} orbitals, as well as the formation of intermediate energy levels due to Si^{4+} doping. However the bismuth doped compounds possess a reddish hue (Fig. 1.16).

Fig. 1.16. Photograph of $Ce_{0.36}Si_{0.31}Bi_{0.33}O_{1.835}$.

Compositions based on amorphous cerium tungstate, $Ce_{1-x}M_xW_2O_8$ (M=Zr or Ti, $0 \leq x \leq 0.6$), were synthesized and their color properties were characterized from the viewpoint of possible ecological inorganic pigments (Masui *et al.* 2005; Furukawa *et al*. 2006). The pigments absorb the visible and the ultraviolet light under 500 nm efficiently, exhibiting a brilliant yellow color. The coloring mechanism is based on O_{2p}–Ce_{4f} and O_{2p}–W_{5d} double charge–transfer transitions. The optical absorption edge of these pigments depends on the Zr or Ti content, and the effective yellow hue was observed at $x = 0.2$ for both pigments (Fig. 1.17).

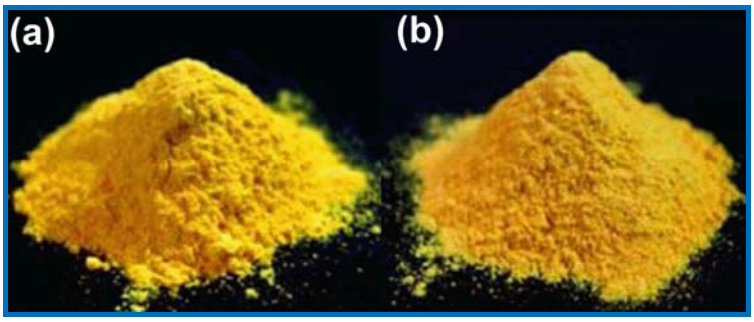

Fig. 1.17. Photographs of (a) $Ce_{0.8}Zr_{0.2}W_2O_8$ and (a) $Ce_{0.8}Ti_{0.2}W_2O_8$.

1.7.4 Rare earth based red inorganic pigments

The development of red ceramic pigments with high–temperature stability is of great importance to the ceramic industry. Conventionally iron oxide in $ZrSiO_4$, cadmium sulfoselenide and Pb_3O_4 encapsulated in tin oxide matrices are used as red pigments (Fig. 1.18). The utility of these pigments for use in ceramic industry can be improved by encapsulating some of these pigments in a zircon matrix. Fe_2O_3–$ZrSiO_4$ and $Cd(S_xSe_{1-x})$–$ZrSiO_4$ heteromorphic pigments, based on inclusion of hematite or cadmium sulfoselenide, respectively, in to the zircon structure are employed traditionally. Zircon crystals protect the occluded red Fe_2O_3 or $Cd(S_xSe_{1-x})$ chromophore crystals from vitreous phases. However, the resulting color of both pigments does not achieve the desired color intensity and/or pure shades (Llusar *et al*. 2001; Garcia *et al*. 2001). Among these the cadmium and lead based pigments are being expelled from the market due to toxicity issues. Numerous pigments based on non–toxic rare earth compounds are being introduced as feasible alternatives to the existing toxic red pigments.

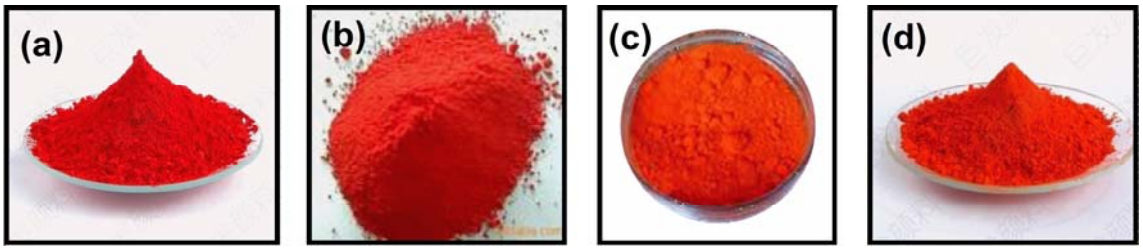

Fig. 1.18. Toxic red and orange pigments (a) Cadmium red, (b) Molybdate red, (c) Vermillion and (d) Cadmium orange.

Pigments based on cerium dioxide represent an important class of inorganic pigments. The synthesis of Pr–doped ceria pigment was first reported in a European patent and published by Olazcuaga *et al*. (Olazcuaga *et al.* 1986; Olazcuaga *et al*. 1987). Thereafter, this system has been studied extensively as ceramic pigments by different authors (Sulcova *et al.* 1998; Bondioli *et al.* 2000; Bondioli *et al.* 2001; Garcia *et al.* 2001; Wang *et al.* 2002; Maso *et al.* 2003; [b]Sulcova and Trojan 2003). These pigments are known to possess high temperature stability and give various pink–orange to red–brown hues, depending on the quantity of praseodymium in the ceria host lattice, synthesis conditions, calcinations temperature (Jayasankar *et al*. 2009). According to Joergensen and Ritterhaus, the red color of praseodymium–doped samples, corresponding to powders with a strong absorption at λ=600 nm, is related to a crystal field effect on the Pr^{4+} cation (Joergensen and Rittershaus 1967). A band structure model proposed by Koelling for CeO_2 and PrO_2 suggests that the electronic spectra arise due to the electron transfer from the ligand orbitals to the localized $4f^1$ level of the Pr^{4+} cation [Koelling *et al.* 1983].

The synthesis of $Ce_{1-x}Pr_xO_2$ solid solutions by three different methods (flux method, coprecipitation, and solid–state reactivity) was investigated to establish optimal preparation conditions to obtain intense red color of the pigment (Bondioli *et al.* 2000). With respect to the other synthesis method investigated, the flux method produces nanosized and well–crystallized $Ce_{1-x}Pr_xO_2$ (x = 0–10 mol %) powders with enhanced chemical and physical properties. The application of microwave technology to coprecipitation synthesis in the $Ce_{0.9}Pr_{0.1}O_2$ system was also investigated (Bondioli *et al.* 2001). The application of microwaves in both drying and calcination processes of co–precipitated powders seems to be an efficient method to improve powder quality, leading to shorter processing schedules and enhanced color development. Later nanocrystalline

Pr–doped ceria powders were prepared by a microwave–assisted hydrothermal route for the first time. The effect of the microwave treatment in relation to the conventional hydrothermal technique was evaluated (Bondioli *et al.* 2005).

The effect of praseodymium doping on the color of ceria was accounted (Sulcova *et al.* 1998). The color of the pigment was found to increase with increase in praseodymium content and the color changed to reddish–brown when 50% praseodymium was used. The effect of various mineralizers on the color hue was also evaluated and found that the color became darker in presence of the mineralizers.

Praseodymium–doped ceria red pigments, $Ce_{1-x}Pr_xO_{2-\delta}$ (x = 0–0.5) have also been prepared by the thermal decomposition of the redox compound $Ce_{1-x}Pr_x(N_2H_3COO)_3.3H_2O$ as well as by the combustion of aqueous solutions containing cerous nitrate, praseodymium nitrate and oxalyl dihydrazide/ammonium acetate. Pigment formation was confirmed by its characteristic red color and reflectance spectrum which shows the reflection edge ~ 690 nm corresponding to charge–transfer from the ligand orbitals to the localized $4f^1$ of Pr^{4+} [Aruna *et al.* 2001].

Low–toxicity red ceramic pigments from lanthanide–cerianite solid solutions have been reported (Garcia *et al*. 2001). The coloring mechanism is based on the introduction of an additional electronic level of energy in cerianite forbidden band, arising from unpaired 4f electrons of lanthanide ions. The red ceramic pigments obtained have been found to be interesting alternatives for the coloration of porcelainised stoneware bodies.

Terbium doped ceria red pigments have also been reported for use in ceramics (Llusar *et al*. 2010; Sulcova *et al.* 2010). These pigments were prepared through both classical and non–conventional routes. The results disclose that nice reddish colors can be obtained at lower temperatures (400–1100 °C) as compared to traditional methods.

Recently, zirconium/tin doped CeO_2–Pr systems displaying colors ranging from brick–red to dark–brown have also been suggested as non–toxic inorganic pigments (Kumari *et al*. 2010). The coloring mechanism is based on the introduction of an additional electronic energy level of unpaired 4f electron of the praseodymium ion into the cerianite band.

Novel inorganic pigments having the general formula $Ce_{0.95-y}Pr_{0.05}M_yO_{2-y/2}$ (where M = La, Nd, Gd and Sm and *y* ranges from 0.05 to 0.85) displaying wide range of colors have been reported ([a]Sulcova and Trojan 2000; [b]Sulcova and Trojan 2000; Sulcova 2002; [a]Sulcova and Trojan 2003). The investigations revealed that the color of the pigment is influenced by both the nature and concentration of the rare earth element used as the dopant.

Reddish–yellow pigments based on $Ce_{10}Pr_xW_yO_z$, (where *x* and *y* varied from 0.075 to 0.6) solid solutions have been reported ([b]Sreeram *et al*. 2008). The use of tungsten gives a red–yellow hue to the pigments with corresponding band–gap energy around 2.2 eV.

Recently, new insights on the structural and optical properties of praseodymium doped cerium–titanium mixed oxide systems as red pigments has been reported (Fernandez–Gonzalez *et al*. 2011). These nanostructured compounds were prepared by solvothermal method and well characterized. The experimental results suggest that, different colored materials ranging from yellow to red can be obtained by varying the firing temperature, quantity of doping praseodymium and pH of the reaction.

A new series of inorganic pigments exhibiting wide range of colors ranging from white to brick–red (Fig. 1.19) have been obtained through traditional solid state route by doping praseodymium into CeO_2 matrix of $TiCeO_4$ (Kumari *et al.* 2008). The color mechanism has been explained on the basis of shift of the charge–transfer band of CeO_2

to higher wavelengths and the band gap of the pigment reduces from 2.96 to 1.84 eV with increasing dopant concentration.

Fig. 1.19. Photographs of $TiCe_{1-x}Pr_xO_{4-\delta}$ pigments.

A new class of inorganic pigments have been reported based on the general formula $Ce_{1-(x+y)}Ti_xPr_yO_2$ (x ranges from 0.05 to 0.195 and y ranges from 0.005 to 0.15). These pigments have been synthesized by solid–state route with a goal of preparing environmentally secure red colorants (George *et al.* 2006). The pigments display colors ranging from brick–red to dark–brown. It is suggested that the coloring mechanism is based on the shift of the charge–transfer band of CeO_2 to higher wavelengths, introducing an additional electronic level by doping praseodymium. $Ce_{1-(x+y)}Ti_xPr_yO_2$ absorbs in the wavelength region below 600 nm producing a red color.

Ceramic pigments with color hues varying from orange to brown based on Fe_2O_3 doped rare earth pigments synthesized by both solid state route and sol–gel methods have been disclosed (Melo *et al*. 2007; Dohnalova *et al.* 2008; Nunes *et al.* 2008). In the case of calcinations route, the color of the pigment changes as the calcination temperature increases from 900 to 1000 °C. On the other hand, in sol–gel route, ceramic pigments free of secondary phases and with different red and brown colors were obtained after heat treatment at 800 °C for 2 h in air atmosphere.

Recently environmentally benign inorganic pigments having colors ranging brick–red to dark–brown (Fig. 1.20) based on Pr^{4+} doped Y_6MoO_{12} has been investigated in our laboratory (George *et al*. 2011). The doping of 2.1 mol % Pr^{4+} for Y^{3+} in the host lattice of Y_6MoO_{12} introduces an additional energy level due to the $4f^1$ electrons between the O^{2-} valence and Mo^{6+} conduction bands resulting in a decrease of band gap from 2.60 to 1.99 eV. Further, the more and more substitution of Pr^{4+} gently red shifts the absorption edge and changes the band gap from 1.99 to 1.90 eV.

Fig. 1.20. Photographs of $Y_{6-x}Pr_xMoO_{12+\delta}$ (x = 0 to 1).

U. S. Patent No. 5,401,309 (Chopin and Dupuis 1995) discloses a process for the synthesis of Ce_2S_3 based pigments having colors varying from brown to red according to the conditions for the preparation thereof, in particular the calcination temperature. These pigments are brown or blood–red depending on whether they have the orthorhombic β–Ce_2S_3 phase or the cubic γ–Ce_2S_3 phase.

A novel erbium titanate pink pigment synthesized by sol–gel methodology has been reported ([a]Martos *et al.* 2008). The success on the development of color is completely related to the sol–gel preparation method, underlying its higher reactivity compared to classical solid–state synthesis. Erbium ions possess a constricted environment and the Er–O bond covalence is higher than in a regular cubic pyrochlore structure. The higher covalent character reduces the interaction between the electrons, since they spread out over wider orbitals, and electron transitions require lower energy, leading to the shift of absorption bands to higher wavelengths. Thus, the change in the Er–O bond covalence

from fluorite to pyrochlore structure would be responsible for the color evolution. The above study also revealed that $Er_2Ti_2O_7$ exhibits a pink color only in its defect fluorite type structure. Further it demonstrated that the intense coloration depends on the presence of fluorite structure, which transforms to pyrochlore at temperature over 700 °C causing loss of intensity. An attempt to improve the color hue of these pink pigments by substituting the Ti^{4+} with larger Zr^{4+} ions in $Er_2Ti_2O_7$ was also conducted (Marthos *et al.* 2009). The study also revealed that the color was dependent on the calcination temperature as well. A loss in coloration was noticed with increase in temperature (Fig. 1.21).

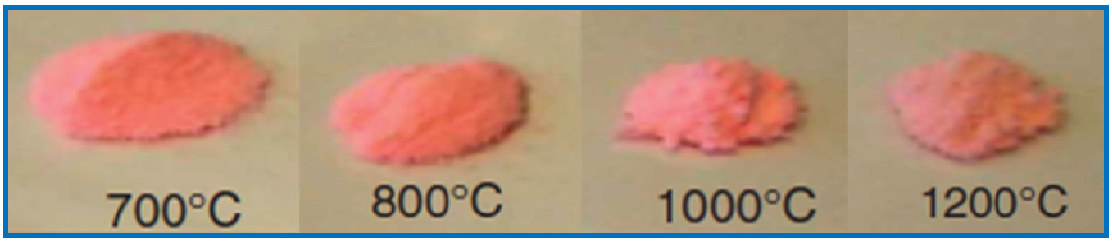

Fig. 1.21. Photograph of the $Er_2Ti_{0.6}Zr_{1.4}O_7$ powders fired at different temperatures.

1.7.5 Rare earth based near–infrared reflective inorganic pigments

Most of the NIR reflective inorganic pigments particularly yellow (eg. cadmium yellow, lead chromate, chrome titanate yellow etc.) contain toxic metals and hence their consumption is being limited. Quite a few infrared reflective inorganic pigments have been reported recently; mostly as patents, which is an indication of their vast potential applications (Swiler *et al.* 2003; Swiler and Axtell 2003).

Novel, yellow, brown and brick–red colored, near–infrared reflective pigments based on yttrium molybdate doped with metal ions such as Si^{4+} or Pr^{4+} have been reported (George *et al.* 2011). The ability of these pigments to confer their NIR reflectance properties to a roofing material like asbestos cement sheet was evaluated. The pigments

exhibited high NIR reflectance (75–85%) when coated on asbestos cement sheet, thus rendering them excellent candidates for use as 'Cool Pigments'.

Cool pigments based on $Ce_{25}Pr_{0.8}FeO_y$ and $Ce_{25}Pr_{0.8}MoO_y$ exhibiting reddish–brown and reddish–orange colors have been investigated ([a]Sreeram *et al*. 2008). The pigments possessed above 65% reflectance in the NIR region and hence can well serve as cool colorants.

1.8 Objectives of the present investigation

Inorganic pigments are currently widely used in numerous industries, especially in those of paints, inks, plastics, rubbers, ceramics, enamels and glasses (Swiler *et al*. 2003). Unfortunately, many of the inorganic pigments which are today actually employed on an industrial scale generally comprise toxic metal ions like cadmium, lead, chromium, antimony and cobalt. The use of these metal ions is becoming increasingly strictly controlled, indeed banned, by legislation in many countries because of their allegedly very high toxicity. This is the case as regards red pigments based on cadmium sulfoselenide encapsulated in zircon matrix and lead oxide in tin oxide matrix and yellow pigments such as lead antimonite, lead chromate and cadmium sulfide. Similarly, green pigments based on chromium oxide. Thus, serious economic and industrial need continues to exist for substitute inorganic pigments devoid of the above disadvantages and drawbacks.

Rare earth elements offer a vast opportunity for development of environmentally secure alternatives for many of the eco–constrained colorants (Garcia *et al.* 2001). The industrial utilization of rare earths is growing very rapidly because of their known low toxicity. The main industrial application in the field of rare earths is the ceramic industry, which consumes up to 31% world production of rare earth compounds. India is rich in rare earth resources and possesses 3% of the total rare earth reserves in the world.

It is clear from the literature review that there exists a large body of literature on rare earth based inorganic pigments displaying various colors. However, their color properties are not satisfactory as compared to the existing industrially used toxic pigments. Further, the synthesis procedure employed for the preparation of many of these pigments involves the use of toxic and inflammable gases. Furthermore, many of the rare earth based pigments exhibit poor thermal and chemical stability, which hinders their use in real

world applications. Thus it has been always a challenging task to develop new class of inorganic pigments that are both non–toxic and environmentally unimpeachable, while preserving or even exceeding the optical, thermal and chemical characteristics of the existing commercial pigments.

Thus, the objectives of the present investigation are as follows:

- To develop non–toxic rare earth based yellow and red inorganic pigments as viable alternatives to the traditional toxic pigment formulations.
- To convert the developed inorganic pigment formulations suitable for various surface coating applications.
- To develop environmentally benign NIR reflective colored inorganic pigments based on rare earths and their application towards building roofing materials as ‘cool pigments’.

Chapter 2

Near–infrared reflecting inorganic pigments based on molybdenum and praseodymium doped yttrium cerate: Synthesis, characterization and optical properties

2.1 Summary

A series of novel environmentally benign near–infrared (NIR) reflecting inorganic pigments based on yttrium cerate doped with metal ions such as Mo^{6+} or Pr^{4+} have been synthesized and characterized using XRD, UV–vis–NIR diffuse reflectance spectroscopy and CIE–1976 *L*a*b** color scales. The substitution of Mo^{6+} for Ce^{4+} in $Y_2Ce_2O_7$ gently changed the band gap of the designed pigments from 3.01 to 2.44 eV due to O_{2p}–Mo_{4d} charge–transfer transitions. This results in a change of the color from ivory–white to yellow. Most importantly, the molybdenum doped pigments exhibit bright yellow hue with high NIR solar reflectance (> 90%) in the range 700–2500 nm. On the other hand, the doping of Pr^{4+} for Ce^{4+} in $Y_2Ce_2O_7$ drastically shifts the absorption edge of the pigments from 410 nm to 725 nm and as a result the band gap of the compounds changes from 3.01 to 1.70 eV. As a consequence, the praseodymium doped pigments exhibit colors ranging from brick–red to dark–brown. These colorants also show significant NIR solar reflectance (> 50%). The ability of the developed pigments to transfer their NIR reflectance properties to a roofing material like asbestos cement sheet was evaluated.

Vishnu, V. S. and Reddy, M. L. P. *Chem. Lett. 39*, **2010**, 820–821;
Sol. Energy Mater. Solar Cells, d.o.i.10.1016/j.solmat.**2011**.05.042

2.2 Introduction

Rising energy cost continues to drive advances in new technologies designed to improve energy efficiency across the globe. One such technology is the use of speciality infrared reflective pigments used to impart color to an object, and to reflect the invisible heat from the object to minimize heat build–up, when exposed to solar radiation. Ultimately the reflection of solar energy lowers the heat build–up resulting in reduction on the load of the cooling system and therefore energy saving. Inorganic class of NIR reflectors are mainly metal oxides and are primarily useful in two major applications: (i) visual camouflage and (ii) reducing heat build–up on the surface of building roofing materials (Jeevanandam *et al.* 2007). Most of the literatures on these pigments exist as patents, which again indicate their wide potential applications (Swiler *et al.* 2003; Sliwinsky *et al.* 2002; Swiler 2002; Modly 1986).

Complex inorganic pigments based on mixed metal oxides (eg:– chromium green, cobalt blue, cadmium stannate, lead chromate, cadmium yellow and chrome titanate yellow) which have been widely used in camouflage absorb visible light but reflect the NIR portion of the incident radiation (Levinson *et al.* 2007; [a]Levinson *et al.* 2005; [b]Levinson *et al.* 2005). However many of these pigments encompass toxic metals and hence their use is restricted. Thus there is a strong incentive to develop new colored NIR reflecting pigments to substitute for industrial pigments that are based on heavy metals hazardous to health and environment. Recently lanthanide based NIR reflective pigments have been proposed as viable alternates to traditional toxic pigments due to their low toxicity (Swiler *et al.* 2003; [a]Sreeram *et al.* 2008; George *et al.* 2011). In this chapter, a series of NIR reflective colored inorganic pigments of the formula $Y_2Ce_{2-x}M_xO_{7+\delta}$ (M = Mo or Pr and *x* ranges from 0 to 0.5) were synthesized, characterized and evaluated their coloring performance by applying on to a roofing material like asbestos cement sheet.

2.3 Experimental Section

2.3.1 Materials and Methodology

Powder samples of the present system, $Y_2Ce_{2-x}M_xO_{7+\delta}$ (M = Mo or Pr and *x* ranges from 0 to 0.5) were synthesized by a solid state reaction, using precursor oxides Y_2O_3 (99.9 %), CeO_2 (99.9 %), $(NH_4)_6Mo_7O_{24}.4H_2O$ (99.9%) and Pr_6O_{11} (99.9%) supplied by M/s. Sigma Aldrich as starting materials. Stoichiometric proportions of the precursors were transferred into an agate mortar and homogenized by wet milling in acetone media. Residual acetone was removed by evaporation and the resultant powders were calcined in platinum crucibles in a Nabertherm high temperature electric furnace at an optimized temperature of 1500 °C for 18 h in air atmosphere, followed by auto–cooling in the furnace. The heating of the furnace was programmed to increase the temperature at 5 °C/min. The pigment compositions thus obtained were ground in an agate mortar in order to refine and homogenize the particle size. The phase purity and chromatic properties were not satisfactory below 1500 °C.

Among the range of pigment compositions prepared, typically $Y_2Ce_{1.5}Mo_{0.5}O_{7+\delta}$ (yellow) and $Y_2Ce_{1.7}Pr_{0.3}O_7$ (reddish–brown), which exhibit better chromatic properties were selected to prepare NIR reflecting coatings on a building roofing material like asbestos cement sheet (made up of small amounts of asbestos fibers locked in cement slurry). The coating was done in a two–step process. In the first step, a small strip of asbestos is pre–coated with TiO_2, an inexpensive white pigment possessing high NIR reflectance. In the second step, the designed typical pigment is applied to the pre–coated substrate material. The pigment samples were ground and sieved under 35 μm mesh size and was ultrasonicated (Vibronics, 250 W, India) for 10 min to ensure the complete dispersion of the pigment particles in an acrylic–acralyn emulsion. The pigment to binder ratio was maintained as 1:1 by weight. The resulted viscous solution was coated on the

asbestos cement sheet surface and was allowed to dry in air. The thickness of the pigment coating on asbestos cement sheet was measured employing LEICA DMRX optical microscope.

2.3.2 Characterization Techniques

The crystalline nature and phase purity of the synthesized samples were characterized by powder X–ray diffraction using the conventional powder techniques in a diffractometer (Philips X'pert Pro) with Ni–filtered Cu K_α (λ = 0.154060 nm) radiation. Data were collected by step scanning over a 2θ range from 10° to 70° with a step size of 0.08° and 5s counting time at each step. The morphology of the synthesized samples was recorded on a scanning electron microscope (SEM) JEOL JSM–5600 model, with an acceleration voltage of 15 kV.

The diffuse reflectance of the powdered pigment samples were measured (380–780 nm) with a UV–vis Spectrometer (Shimadzu UV–2450 with an integrating sphere attachment, ISR–2200) using barium sulfate as a reference. The measurement conditions were as follows: an illuminant D_{65}, 10° complementary observer and measuring geometry d/8°. The band gap values were calculated from the corresponding absorbance spectra by straight forward extrapolation method ([b]George *et al*. 2008) using the formula $E(eV) = 1236/\lambda$ (where λ represents the wavelength in nm).

The color coordinates were determined by coupling an analytical software (UVPC Color Analysis Personal Spectroscopy Software V3, Shimadzu) to the UV–2450 spectrophotometer. The CIE 1976 *L*a*b** colorimetric method was used, as recommended by the Commission Internationale de l'Eclairage (CIE). In this method, *L** is the lightness axis [black (0) to white (100)], *a** is the green (–ve) to red (+ve), and *b** is the blue (–ve) to yellow (+ve) axis (Fig. 1.6). The parameter *C** (chroma) represents saturation of the color and *h*° represents the hue angle. The chroma is defined as

$C^* = \sqrt{(a^*)^2 + (b^*)^2}$. The hue angle, $h°$ is expressed in degrees and ranges from 0° to 360° and is calculated using the formula $h° = \tan^{-1}\left(\frac{b^*}{a^*}\right)$. For each colorimetric parameter of a sample, measurements were made in triplicate and an average value was chosen as the result. Typically, for a given sample, the standard deviation of the measured CIE–*L*a*b** values is less than 0.10, and the relative standard deviation is not higher than 1%, indicating that the measurement error can be ignored.

The near–infrared reflectance of the powdered pigment samples as well as the pigment coated asbestos cement sheet was measured with a UV–vis–NIR spectrophotometer (Shimadzu, UV–3600 with an integrating sphere attachment) using poly–tetrafluoroethylene (PTFE) as a reference. Optical measurements were performed in the 700 to 2500 nm range. The NIR solar reflectance (*R**) in the wavelength range from 700 to 2500 nm was calculated in accordance with the ASTM standard number E891–87 as described elsewhere (Thongkanluang *et al.* 2011; [a]Levinson *et al*. 2010; [b]Levinson *et al*. 2010). Then, the NIR solar reflectance or the fraction of solar radiation incident at wavelengths between 700 and 2500 nm that is reflected by a surface is the irradiance–weighted average of its spectral reflectance, r(λ), can be determined that is,

$$R^* = \frac{\int_{700}^{2500} r(\lambda)\, i(\lambda) d(\lambda)}{\int_{700}^{2500} i(\lambda) d(\lambda)}$$

where r(λ) is the spectral reflectance (Wm^{-2}) obtained from the experiment and i(λ) is the solar spectral irradiance ($Wm^{-2}\ nm^{-1}$) obtained from ASTM standard E891–87.

Thermo gravimetric (TG) and differential thermal analyses (DTA) were performed in a Pyris Diamond TG/DTA Perkin Elmer make. All the experiments were run in a

platinum crucible from 50–1000 °C with a heating rate of 20 °C/min in nitrogen atmosphere.

The particle size distribution of the typical pigment sample was investigated in water medium with calgon as the dispersing agent using the Laser Scattering Particle Size Distribution Analyzer (CILAS 930 Liquid). The samples were ultrasonically homogenized for 180 s during measurement and the signal was evaluated on the basis of Fraunhofer bending.

2.4 Results and Discussion

2.4.1 Powder X–ray diffraction analysis

The optimum calcination temperature of $Y_2Ce_2O_7$ was first established by calcining the precursor oxides at various temperatures ranging from 900 °C to 1500 °C and time ranging from 6–18 h. The corresponding XRD patterns are given in Fig. 2.1. Satisfactory phase purity was attained only after calcination at 1500 °C for 18 h without any impurity peaks of the corresponding precursor oxide systems. On the other hand, the samples calcined at temperatures < 1500 °C exhibits minor peaks corresponding to the precursor oxide (Y_2O_3), which indicates that the solid solution formation is incomplete. The XRD pattern of $Y_2Ce_2O_7$ compound synthesized at the optimized condition (1500 °C/18 h) displays some minor and weak superstructure peaks related to the C–type phase along with the major cubic fluorite (*F*)–type phase (Yamamura *et al*. 2007). However, the peaks corresponding to *C*–type phase are too close to *F*–type phase and hence are difficult to resolve, whereas peaks at higher 2θ value are slightly distorted indicating the possible coexistence of two phases (Mandal *et al*. 2008). The superstructure peaks observed in the XRD pattern may be considered as incomplete due to the weakness of the superlattice lines. Moreover, due to the large coherence length of X–rays it is not often easy to detect weaker super lattice lines amidst a bulk phase using an XRD technique.

The lattice constant of $Y_2Ce_2O_7$ was calculated to be 1.0773 nm, while that of Y_2O_3 having a typical *C*–type structure was 1.0604 nm [JCPDF 41–1105] (Yamamura *et al*. 2007). Despite the ionic radius of Ce^{4+} (0.097 nm) being smaller than Y^{3+} (0.102 nm), the lattice constant of $Y_2Ce_2O_7$ was larger than Y_2O_3 because of the excess oxygen present in the *C*–type structure.

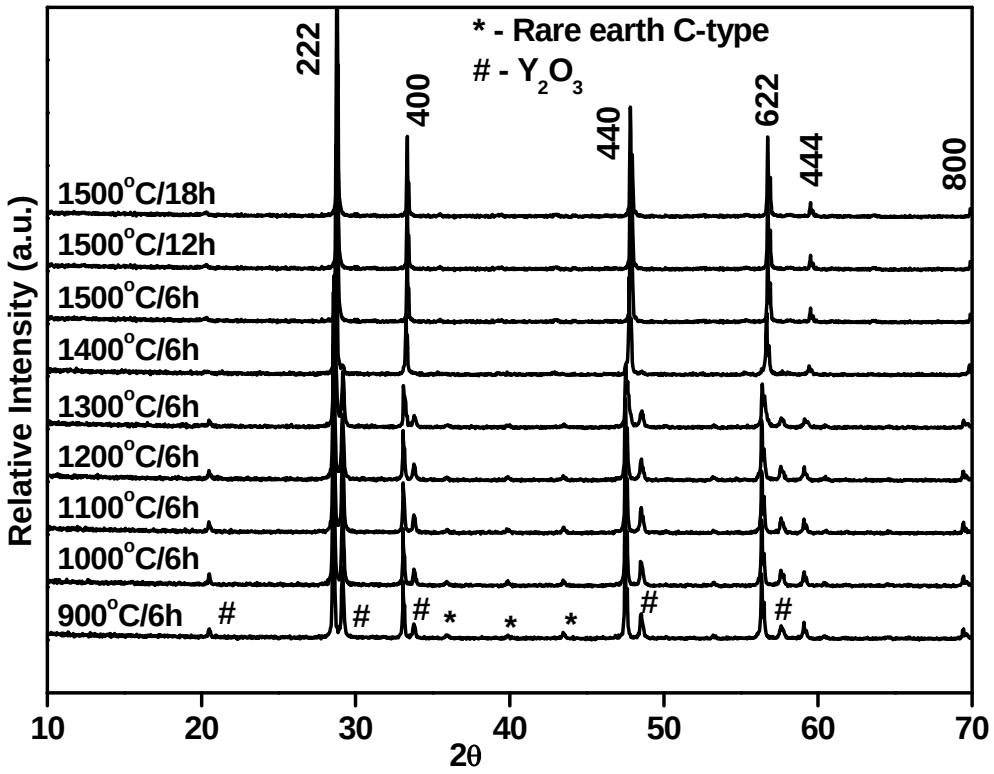

Fig. 2.1. XRD patterns of $Y_2Ce_2O_7$ calcined at different calcination conditions.

The XRD patterns of $Y_2Ce_{2-x}M_xO_{7+\delta}$ (M = Mo and *x* ranges from 0 to 0.5) compounds calcined at an optimized temperature of 1500 °C are summarized in Fig. 2.2. Detailed analysis revealed that all the patterns are systematic in nature and match well with the sole presence of the standard fluorite type cubic phase of $Y_2Ce_2O_7$. From the XRD patterns it could be noted that doping of $Y_2Ce_2O_7$ with 7.5 mol % of Mo^{6+} leads to a marginal shift of diffraction peaks towards lower 2θ angle side. However, the cell parameter value of $Y_2Ce_2O_7$ (1.0773 nm) has not been affected significantly with the doping of small amounts of Mo^{6+}. On the other hand, doping of larger amounts of Mo^{6+}

(>7.5 mol %) results in shift of the XRD patterns to higher angle side. As a consequence, the cell parameter value has been decreased to 1.0747 nm with the substitution of 12.5 mol % of Mo^{6+}. The ionic radius of Mo^{6+} (0.059 nm) is smaller than Ce^{4+} (0.097 nm) and hence a decrease in lattice parameter is expected due to incorporation of Mo^{6+} into the $Y_2Ce_2O_7$ lattice (Shannon 1976).

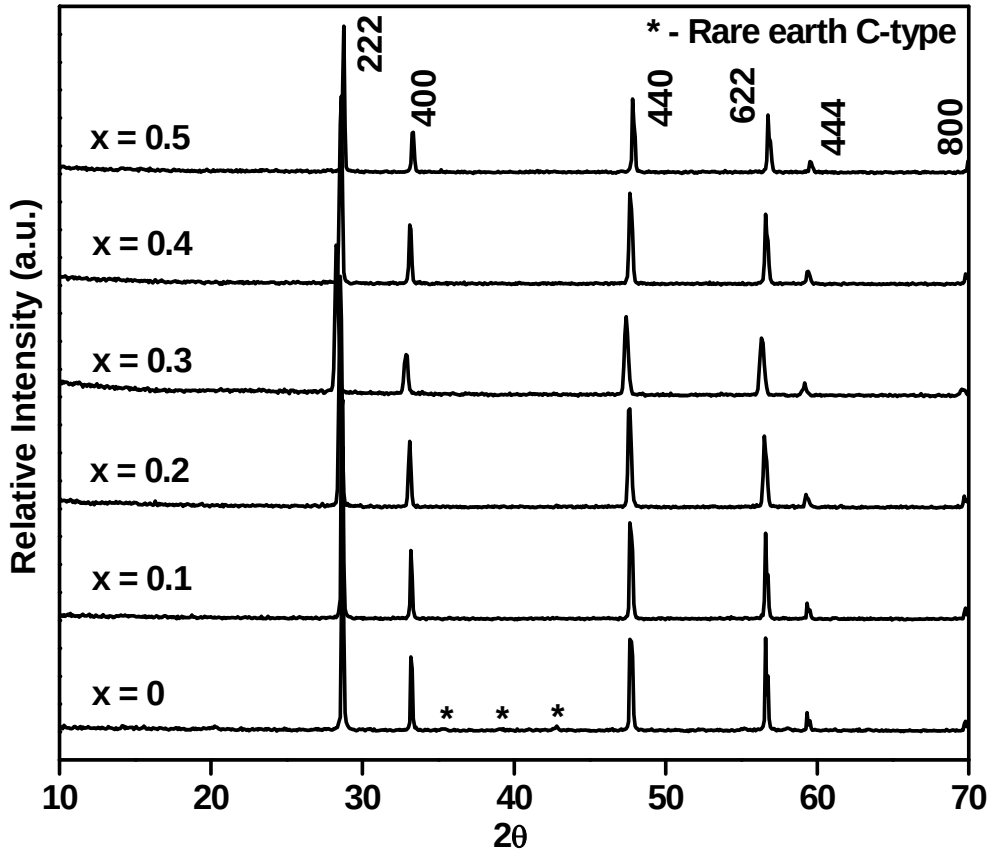

Fig. 2.2. XRD patterns of $Y_2Ce_{2-x}Mo_xO_{7+\delta}$ (x ranges from 0 to 0.5) pigments.

The powder XRD patterns of Pr^{4+} doped $Y_2Ce_2O_7$ compounds show characteristic reflections of cubic fluorite $Y_2Ce_2O_7$ phase (Fig. 2.3). Further, no peaks were observed corresponding to the precursor oxides. This disparate feature compared to pure Y_2O_3 can be explained as due to the formation of solid solutions of these compounds. It is clear from the XRD patterns that no significant shift of diffraction peaks is found with the doping of praseodymium for Ce^{4+} in $Y_2Ce_2O_7$. However the lattice parameter decreases marginally from 1.0773 nm to 1.0765 nm with the introduction of Pr^{4+}, which was not

very significant when compared to the Mo^{6+} doped compounds because the ionic radii of Ce^{4+} and Pr^{4+} in eight fold coordination are very close to each other (0.097 and 0.096 nm) (Shannon 1976).

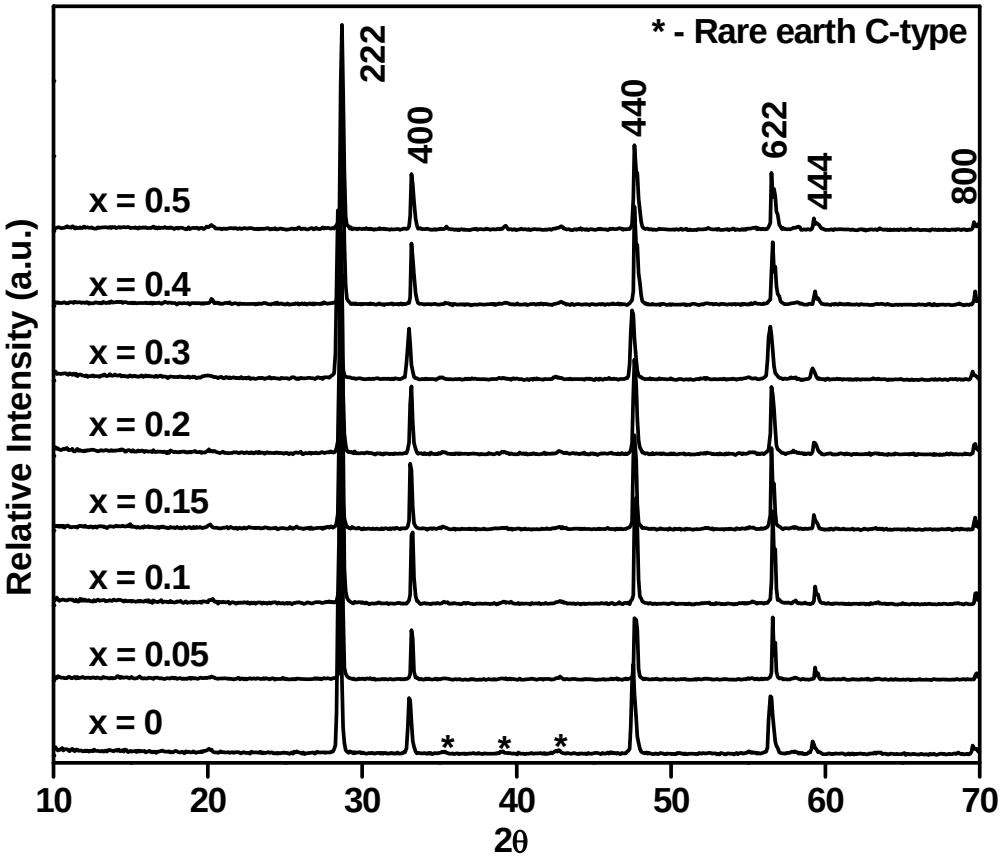

Fig. 2.3. XRD patterns of $Y_2Ce_{2-x}Pr_xO_7$ (x ranges from 0 to 0.5) pigments.

2.4.2 Particle size and morphological analysis

Particle size analysis of the typical yellow pigment, $Y_2Ce_{1.5}Mo_{0.5}O_{7+\delta}$ and reddish–brown pigment, $Y_2Ce_{1.7}Pr_{0.3}O_7$ reveals a mean diameter of 10.62 μm (size of 90% particles < 22.08 μm, 50% particles < 8.66 μm and 10% particles < 2.36 μm) and 12.69 μm (size of 90% particles < 27.43 μm, 50% particles < 9.77 μm and 10% particles < 2.23 μm), respectively. The average particle size of the pigments as observed from the SEM images shown in Fig. 2.4 is approximately 10 μm, which matches well with the results obtained from particle size analysis. The SEM micrographs revealed the presence of

agglomeration in the sample, each agglomerate contained a large number of grains with a grain size <1 μm.

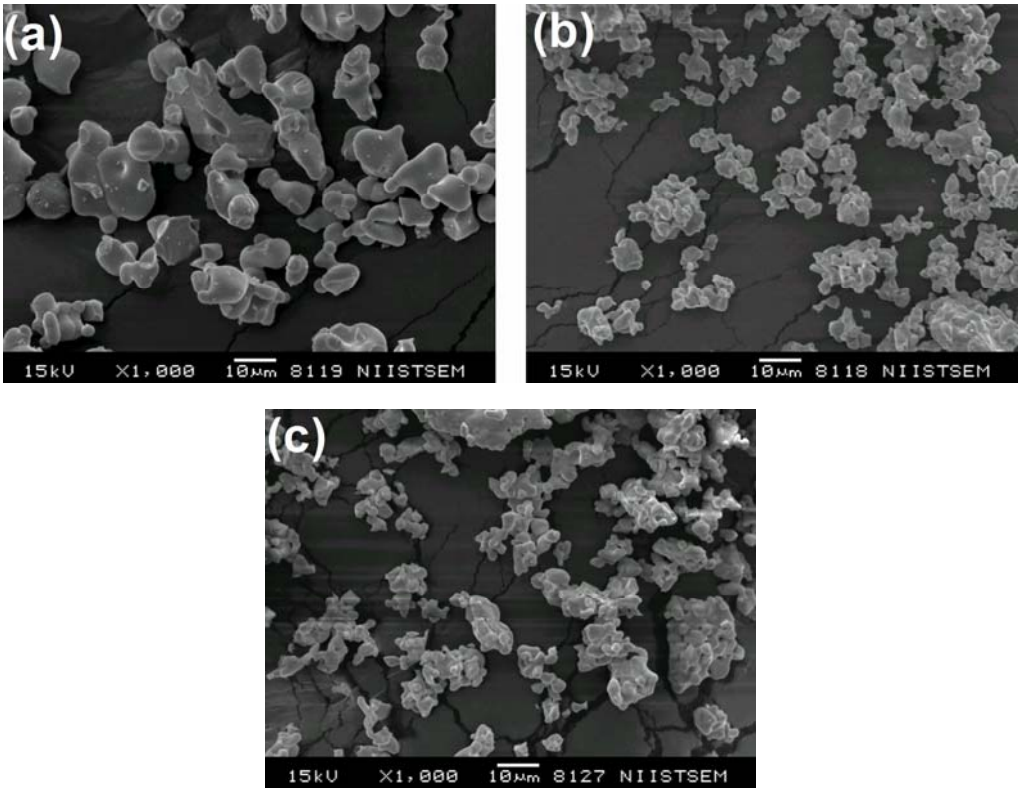

Fig. 2.4. SEM micrographs of (a) $Y_2Ce_2O_7$, (b) $Y_2Ce_{1.5}Mo_{0.5}O_{7+\delta}$ and (c) $Y_2Ce_{1.7}Pr_{0.3}O_7$.

2.4.3 Diffuse reflectance and chromatic properties of molybdenum doped $Y_2Ce_2O_7$

As can be seen from the diffuse reflectance spectrum of $Y_2Ce_2O_7$ compound shown in Fig. 2.5, there exist a strong absorption band at 410 nm. There is no evidence for *f–f* or *f–d* transitions as Y^{3+} and Ce^{4+} displays d^0 and f^0 configurations in their respective stable oxidation states. Hence the UV–vis diffuse reflectance spectrum of $Y_2Ce_2O_7$ is originated mainly from charge transfer transitions between O_{2p} valence and Ce_{4f} conduction bands of Ce^{4+}. The doping of Mo^{6+} for Ce^{4+} in $Y_2Ce_2O_7$ significantly shifts the absorption edge from 410 nm to 506 nm (Fig. 2.5) and as a result the band gap decreases from 3.01 to 2.44 eV. The shift in absorption edge and the consequent change in band gap can be attributed to the O_{2p}–Mo_{4d} charge transfer transitions (Sreeram *et al.* 2007). Thus the color of the pigment samples change from ivory–white to yellow (Fig. 2.6). Fig. 2.7

shows the corresponding absorbance spectra from which the band gap was calculated. The band gap values were obtained by a straight forward extrapolation method and are given in Table 2.1 ([b]George *et al.* 2008).

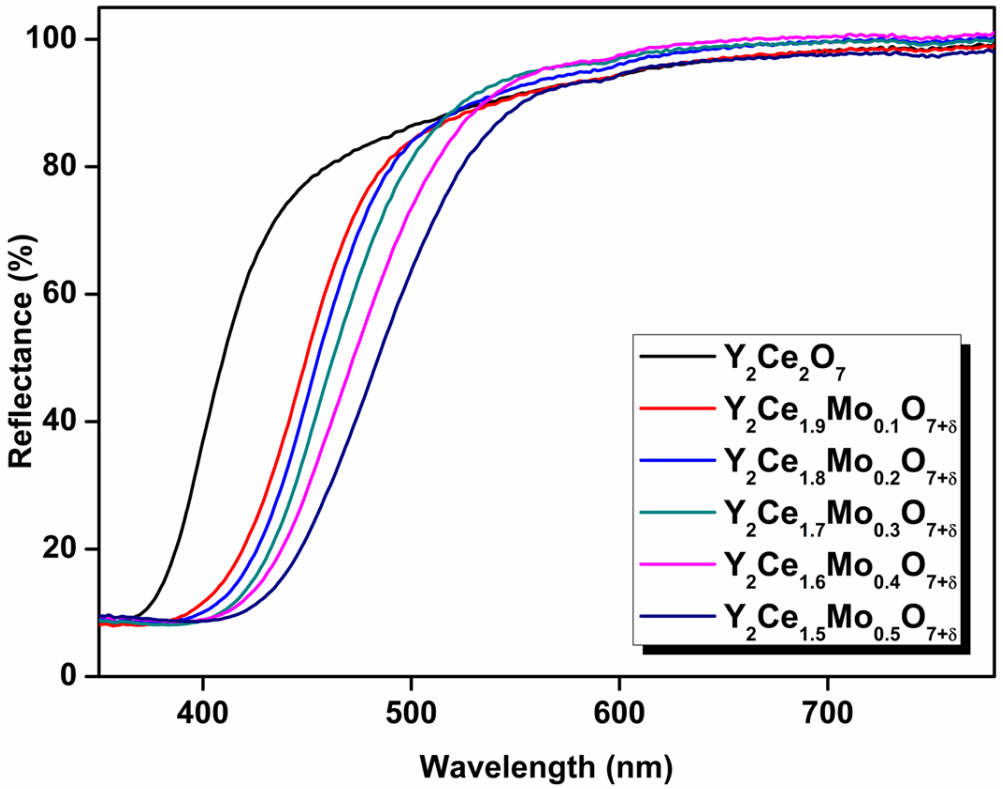

Fig. 2.5. UV–vis diffuse reflectance spectra of $Y_2Ce_{2-x}Mo_xO_{7+\delta}$ (x ranges from 0 to 0.5) powder pigments.

Fig. 2.6. Photographs of $Y_2Ce_{2-x}Mo_xO_{7+\delta}$ (x = 0, 0.1, 0.3, 0.5) and $Y_2Ce_{2-x}Pr_xO_7$ (x = 0, 0.1, 0.3, 0.5) pigments.

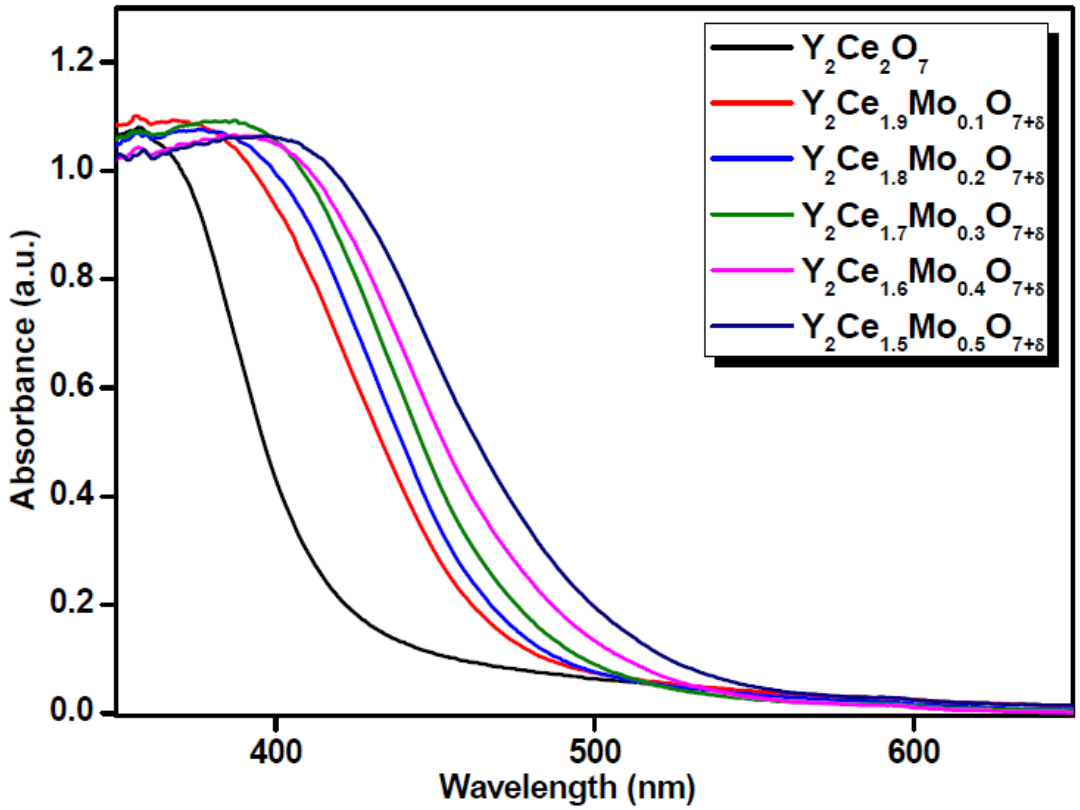

Fig. 2.7. Absorbance spectra of $Y_2Ce_{2-x}Mo_xO_{7+\delta}$ (*x* ranges from 0 to 0.5) powder pigments.

The NIR reflectance spectra of the molybdenum doped $Y_2Ce_2O_7$ powder pigment samples are given in Fig. 2.8. Multiplying the (normalized) spectral irradiance of the sun i(λ) by the spectral reflectivity yields the NIR solar reflection spectrum presented in Fig. 2.9. The parent compound, $Y_2Ce_2O_7$ possesses an NIR solar reflectance (*R**) of 93.5%. The substitution of Mo^{6+} for Ce^{4+} up to 7.5 mol % enhances the NIR solar reflectance to 96%. On the other hand, more and more doping of Mo^{6+} for Ce^{4+} in $Y_2Ce_2O_7$ decreases the NIR reflectance of the pigment samples to 90.2%. However, the high NIR solar reflectance (> 90%) displayed by all the newly designed yellow colored samples makes them as interesting candidates for use as “cool colorants”.

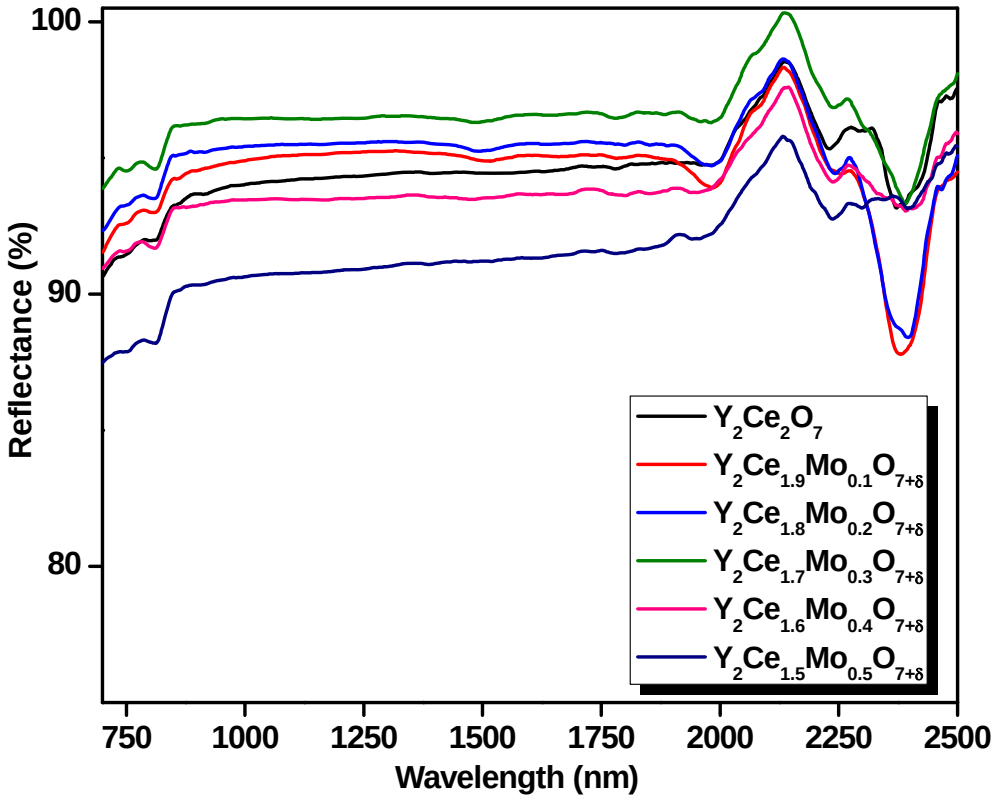

Fig. 2.8. NIR reflectance spectra of $Y_2Ce_{2-x}Mo_xO_{7+\delta}$ (x ranges from 0 to 0.5) powder pigments.

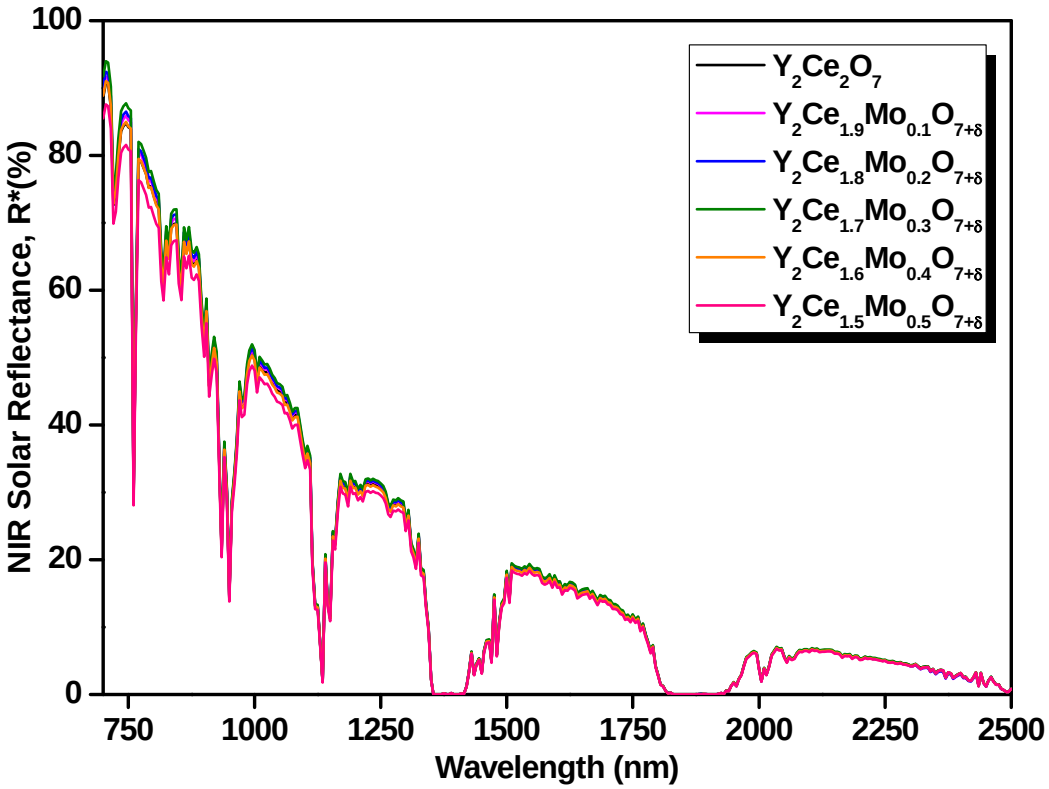

Fig. 2.9. NIR solar reflectance spectra of $Y_2Ce_{2-x}Mo_xO_{7+\delta}$ (x ranges from 0 to 0.5) powder pigments.

The chromatic properties of the synthesized $Y_2Ce_{2-x}Mo_xO_{7+\delta}$ (x ranges from 0 to 0.5) powder pigments can be assessed from their CIE 1976 color coordinate values depicted in Table 2.1. The systematic doping of molybdenum for Ce^{4+} in $Y_2Ce_2O_7$ (from 0 to 12.5 mol %) results in an increase in the b^* value regularly from 11.1 to 62.4, which indicates that the yellowness of the pigment sample enhances. On the other hand, the increase of molybdenum doping upto 7.5 mol % leads to an improvement in green hue of the pigment, which is again evident from the higher values of the color coordinate, $-a^*$ (increases from –0.8 to –9.4). However, more and more doping of molybdenum up to 12.5 mol % decreases the green component of the pigment samples ($-a^*$ value drastically decreases from –9.4 to –4.5). As a consequence to the above, the C^* value which represents the richness of the color hue significantly intensifies by about 6 fold. The observed hue angles of the developed pigments are found to be in the yellow region of the cylindrical color space ($h°$ = 70–105 for yellow) (Sulcova and Trojan 2008). It is interesting to note that the chromatic properties of the typical pigment sample $Y_2Ce_{1.5}Mo_{0.5}O_{7+\delta}$ (L^* = 90.2, a^* = –4.5, b^* = 62.4, C^* = 62.5, $h°$ = 94.1) was found to be significantly higher than the cerium molybdate yellow pigment reported elsewhere, especially the b^* value (L^* = 76.1, a^* = 0.1, b^* = 36.9, C^* = 21.9, $h°$ = 88.2) (Sreeram *et al*. 2007).

Table 2.1. The color coordinates (±0.1) of the $Y_2Ce_{2-x}Mo_xO_{7+\delta}$ (x ranges from 0 to 0.5) powder pigments and band gap values

Pigment composition	Color coordinates					Band gap (*eV*)
	*L**	*a**	*b**	*C**	*h°*	
$Y_2Ce_2O_7$	95.2	–0.8	11.1	11.2	94.0	3.01
$Y_2Ce_{1.90}Mo_{0.10}O_{7+\delta}$	94.6	–7.3	32.0	32.9	102.8	2.66
$Y_2Ce_{1.80}Mo_{0.20}O_{7+\delta}$	95.4	–8.4	38.5	39.4	102.3	2.62
$Y_2Ce_{1.70}Mo_{0.30}O_{7+\delta}$	96.2	–9.4	46.0	46.9	101.5	2.57
$Y_2Ce_{1.60}Mo_{0.40}O_{7+\delta}$	91.9	–7.2	53.6	54.1	97.7	2.49
$Y_2Ce_{1.50}Mo_{0.50}O_{7+\delta}$	90.2	–4.5	62.4	62.6	94.1	2.44

2.4.4 Diffuse reflectance and chromatic properties of praseodymium doped $Y_2Ce_2O_7$

Fig. 2.10 illustrates the diffuse reflectance spectra of the $Y_2Ce_{2-x}Pr_xO_7$ (x ranges from 0 to 0.5) powder pigment samples. The corresponding absorption spectrum is given as Fig. 2.11. As it is evident from the spectra of the pigments, the charge transfer band of $Y_2Ce_2O_7$ at 410 nm is dramatically shifted to longer wavelengths (650 nm) with the substitution of 1.25 mol % of Pr^{4+} chromophore ions. This drastic shift in the absorption edge is due to the introduction of an additional $4f^1$ electronic energy level of Pr^{4+} between the O^{2-} valence and the Ce^{4+} conduction bands. As a consequence, the band gap decreases from 3.01 to 1.90 eV. Therefore the color of the pigment changes from ivory–white to brick–red. Further more and more doping of Pr^{4+} for Ce^{4+} in $Y_2Ce_2O_7$ (from 1.25 to 12.5 mol %) gently shifts the absorption edge from 650 nm to 725 nm and decreases the band gap of the pigment from 1.90 eV to 1.70 eV (Table 2.2). As a result the pigment samples changes their color from brick–red to dark–brown (Fig. 2.6).

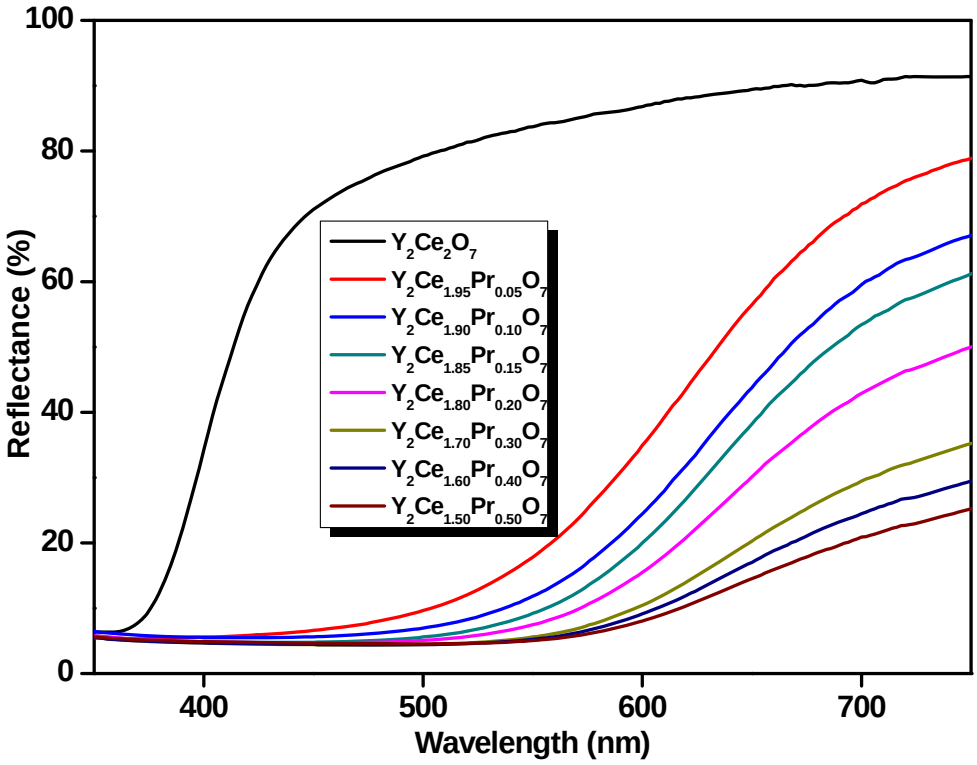

Fig. 2.10. UV–vis diffuse reflectance spectra of $Y_2Ce_{2-x}Pr_xO_7$ (x ranges from 0 to 0.5) powder pigments.

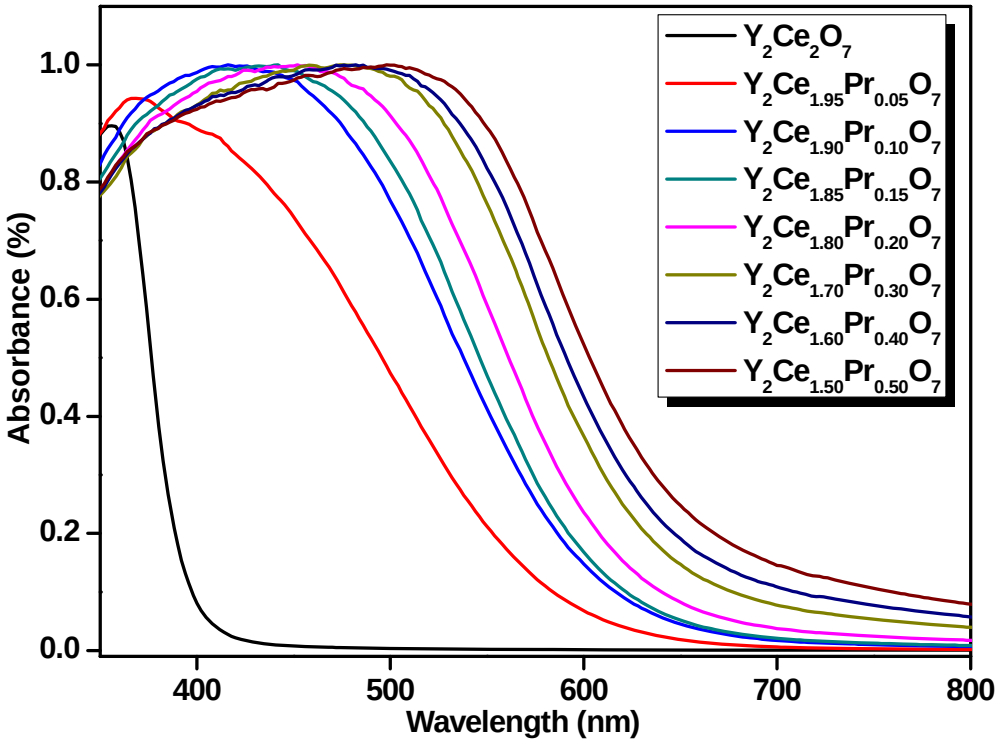

Fig. 2.11. Absorbance spectra of $Y_2Ce_{2-x}Pr_xO_7$ (x ranges from 0 to 0.5) powder pigments.

Figs. 2.12 and 2.13 exemplify the NIR reflectance spectra and the corresponding NIR solar reflectance spectra of $Y_2Ce_{2-x}Pr_xO_7$ (x ranges from 0 to 0.5) powder pigments. The NIR solar reflectance values (R*) decreases from 93.5 to 46 % with a systematic increase of Pr^{4+} concentration from 1.25 mol % to 12.5 mol %. However the high NIR solar reflectance values of some of the brick–red pigments, clearly highlights the potential for the utility of these pigment samples as 'cool pigments'.

The color coordinates of the $Y_2Ce_{2-x}Pr_xO_7$ (x ranges from 0 to 0.5) powder pigment samples are summarized in Table 2.2. Replacing 1.25 mol % of Pr^{4+} for Ce^{4+} in $Y_2Ce_2O_7$ increases the red component (a*) significantly from –0.8 to 26.5 and yellow component (b*) from 11.1 to 37.9. This is also reflected in its chroma value (C*) which gets enhanced from 11.2 to 46.2. A further increase in dopant concentration of the chromophore ion (up to 5 mol %) brings about a slow decrease in the red and yellow hues, the outcome of which is a change in color from brick–red to reddish–brown.

However, when the Pr^{4+} ion concentration is increased to 12.5 mol %, a significant decrease in red and yellow hues as denoted by the chromatic coordinates *a** and *b** were noted. Consequently, the color changes to dark–brown. The hue angle values (*h*°) of the synthesized praseodymium doped $Y_2Ce_2O_7$ pigments lie in the orange–red region of the cylindrical color space (*h*° = 0–35 for red and 35–70 for orange) (Sulcova and Trojan 2008). The color coordinates of the typical pigment $Y_2Ce_{1.7}Pr_{0.3}O_7$ (*L** = 32.6, *a** = 18.1, *b** = 12.0, *C** = 21.8, *h*° = 33.5) sample are found to be higher than that of the red powdered pigment samples of praseodymium doped ceria (*L** = 46.6, *a** = 15.5, *b** = 10.5, *C** = 18.7, *h*° = 34.1) reported elsewhere in the literature (Maso *et al*. 2003).

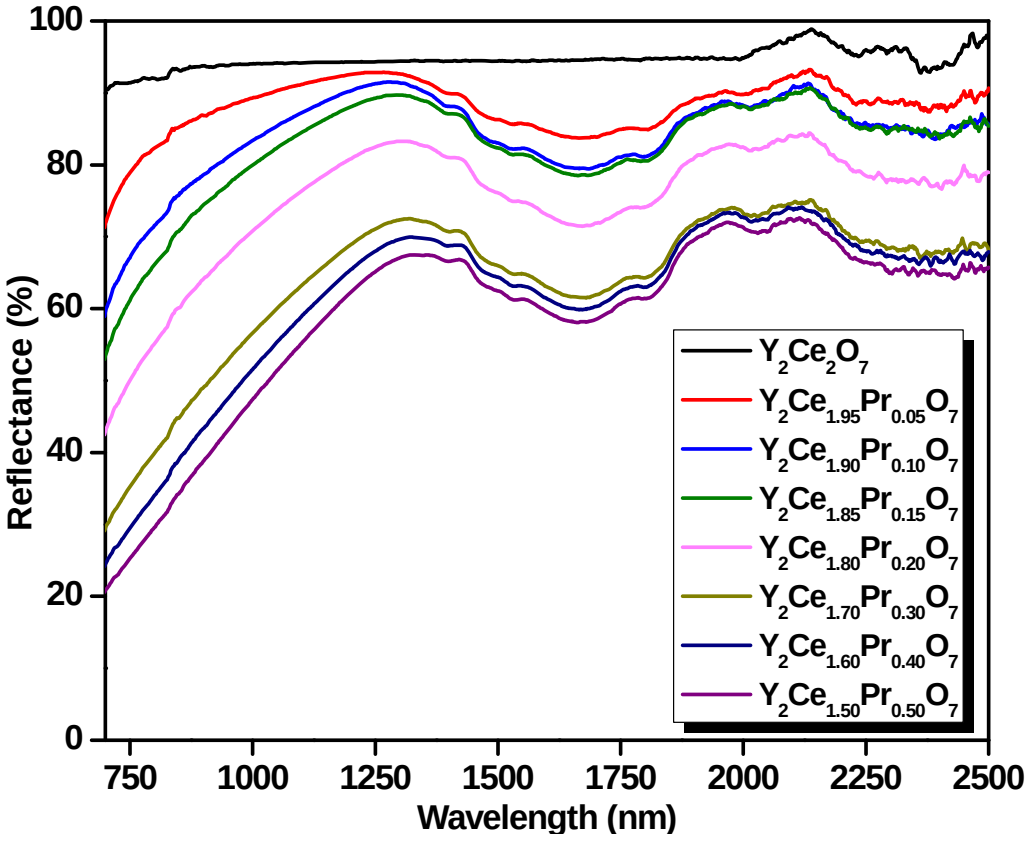

Fig. 2.12. NIR reflectance spectra of $Y_2Ce_{2-x}Pr_xO_7$ (*x* ranges from 0 to 0.5) powder pigments.

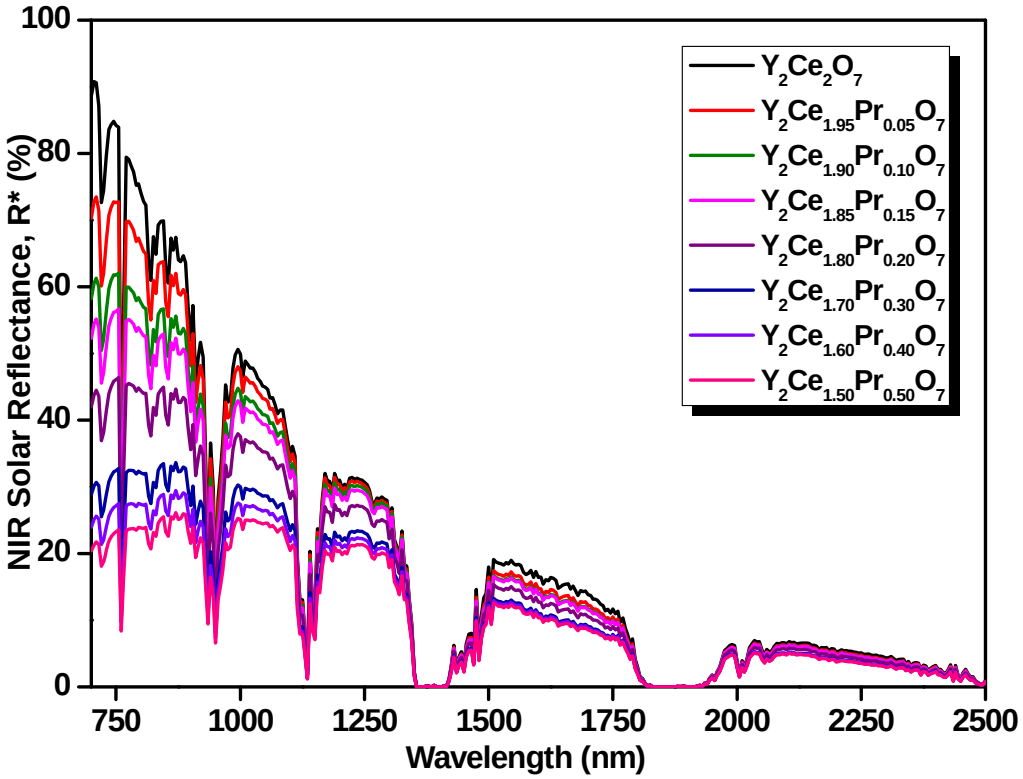

Fig. 2.13. NIR solar reflectance spectra of $Y_2Ce_{2-x}Pr_xO_7$ (*x* ranges from 0 to 0.5) powder pigments.

Table 2.2. The color coordinates (±0.1) of the $Y_2Ce_{2-x}Pr_xO_7$ (*x* ranges from 0 to 0.5) powder pigments and band gap values

Pigment composition	Color coordinates					Band gap (*eV*)
	*L**	*a**	*b**	*C**	*h*°	
$Y_2Ce_2O_7$	95.2	–0.8	11.1	11.2	94.0	3.01
$Y_2Ce_{1.95}Pr_{0.05}O_7$	54.9	26.5	37.9	46.2	55.1	1.90
$Y_2Ce_{1.90}Pr_{0.10}O_7$	44.9	25.1	26.9	36.8	47.0	1.83
$Y_2Ce_{1.85}Pr_{0.15}O_7$	41.5	26.0	25.4	36.3	44.4	1.81
$Y_2Ce_{1.80}Pr_{0.20}O_7$	39.2	22.7	19.1	29.7	40.0	1.77
$Y_2Ce_{1.70}Pr_{0.30}O_7$	32.6	18.1	12.0	21.8	33.5	1.75
$Y_2Ce_{1.60}Pr_{0.40}O_7$	31.6	15.7	9.2	18.2	30.2	1.73
$Y_2Ce_{1.50}Pr_{0.50}O_7$	30.0	13.0	6.5	14.5	26.4	1.70

2.4.5 NIR solar reflectance analysis of the pigment coatings on an asbestos cement sheet surface

Recently, there has been a great demand in building roofing materials with high solar reflectance and high thermal emittance such that the interiors stay cool in the sunlight,

reducing demand for cooling power in conditioned buildings (Thongkanluang *et al.* 2011; Thongkanluang *et al.* 2010; Jeevanandam *et al.* 2007; [a]Levinson *et al.* 2005; [b]Levinson *et al.* 2005). Solar radiation consists of ~ 5% UV radiation, 43% visible radiation and 52% near–infrared radiation (NIR; ~700–2500 nm). The solar energy distribution is shown in Fig. 2.14. Coatings colored with conventional pigments tend to absorb NIR radiation that bears > 50% of the power in sunlight resulting in heat built–up (Levinson *et al.* 2007; Bendiganavale and Malshe 2008). Replacing conventional pigments with 'cool pigments' that absorb less NIR radiation can provide coatings similar in color to that of conventional roofing materials, but with high solar reflectance. The NIR reflectance of such surfaces can be improved further by increasing the number of coating layers, but this increases the cost. The above factors prompted us to evaluate the NIR reflectance of the designed pigments by coating on to a roofing material like asbestos cement sheet adopting a two–step, two–layer process, which is found to be more cost effective.

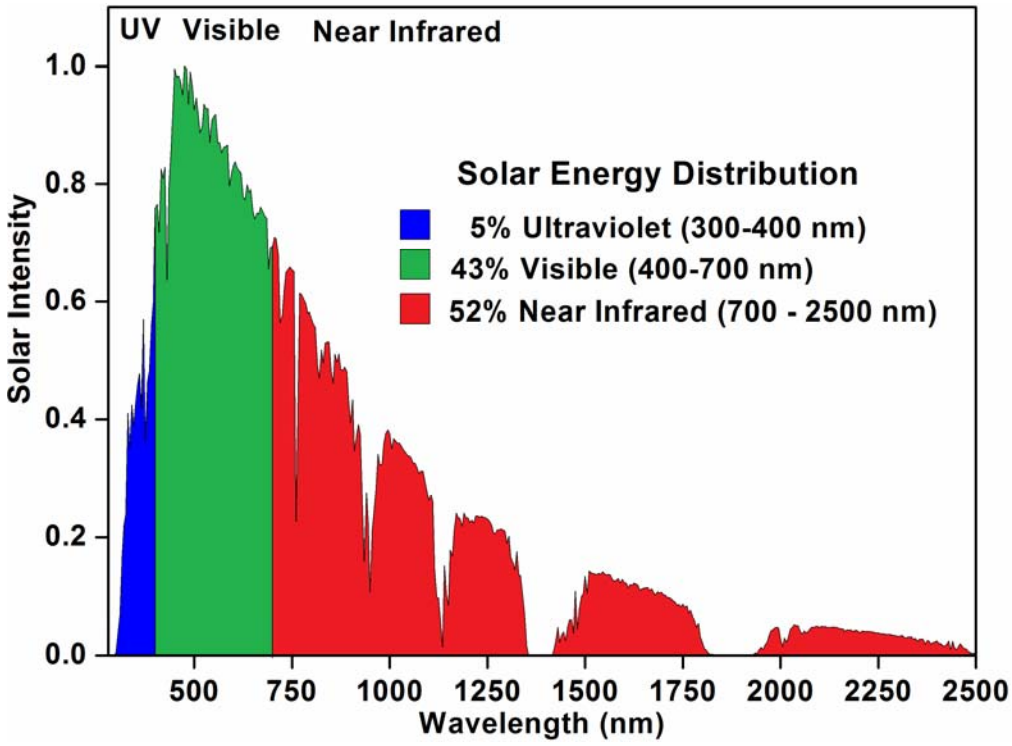

Fig. 2.14. Solar energy distribution.

The pigment having the best chromatic properties was selected to coat on an asbestos cement sheet roofing surface in the current study (Fig.2.15). The NIR reflectance spectrum of the respective pigment samples, $Y_2Ce_{1.5}Mo_{0.5}O_{7+\delta}$ and $Y_2Ce_{1.7}Pr_{0.3}O_7$ coated with varying thickness over a base coat of TiO_2 on a roofing material like asbestos cement sheet are shown in Figs. 2.16 and 2.17, respectively. The corresponding NIR solar reflectance spectra are given in Figs. 2.18 and 2.19 respectively.

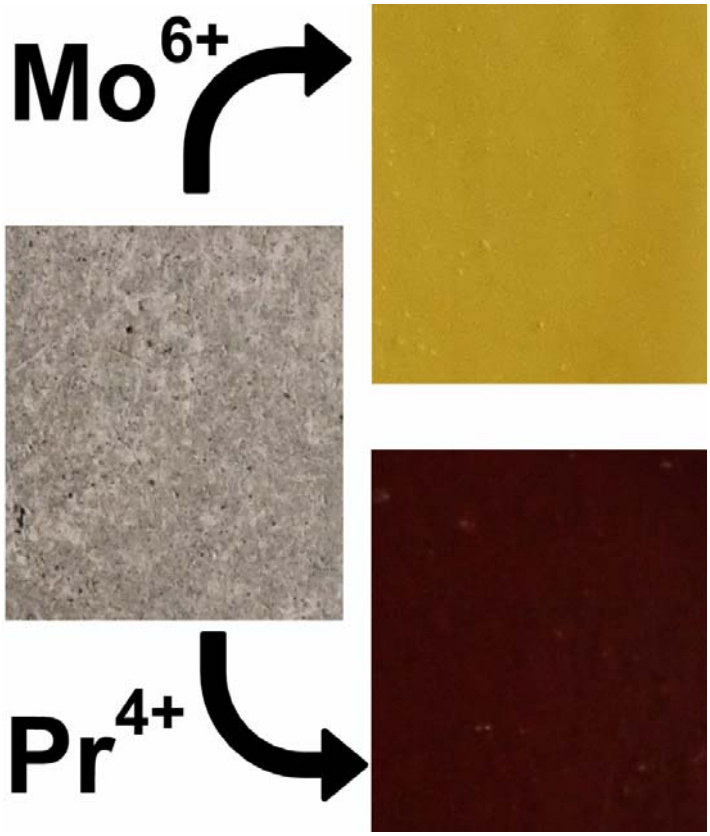

Fig. 2.15. Photographs of $Y_2Ce_{1.5}Mo_{0.5}O_{7+\delta}$ and $Y_2Ce_{1.7}Pr_{0.3}O_7$ pigments coated on an asbestos strip with a TiO_2 base coat.

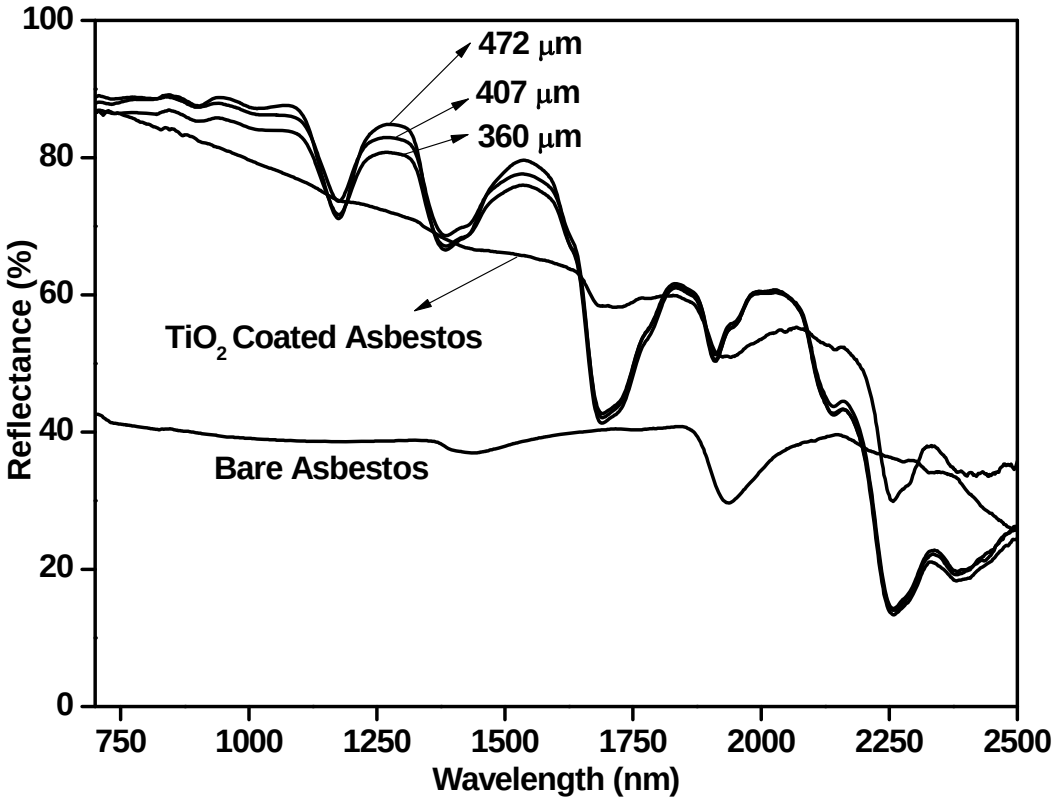

Fig. 2.16. NIR reflectance spectra of $Y_2Ce_{1.5}Mo_{0.5}O_{7+\delta}$ yellow pigment coated at varying thickness over a TiO_2 base coat on an asbestos strip.

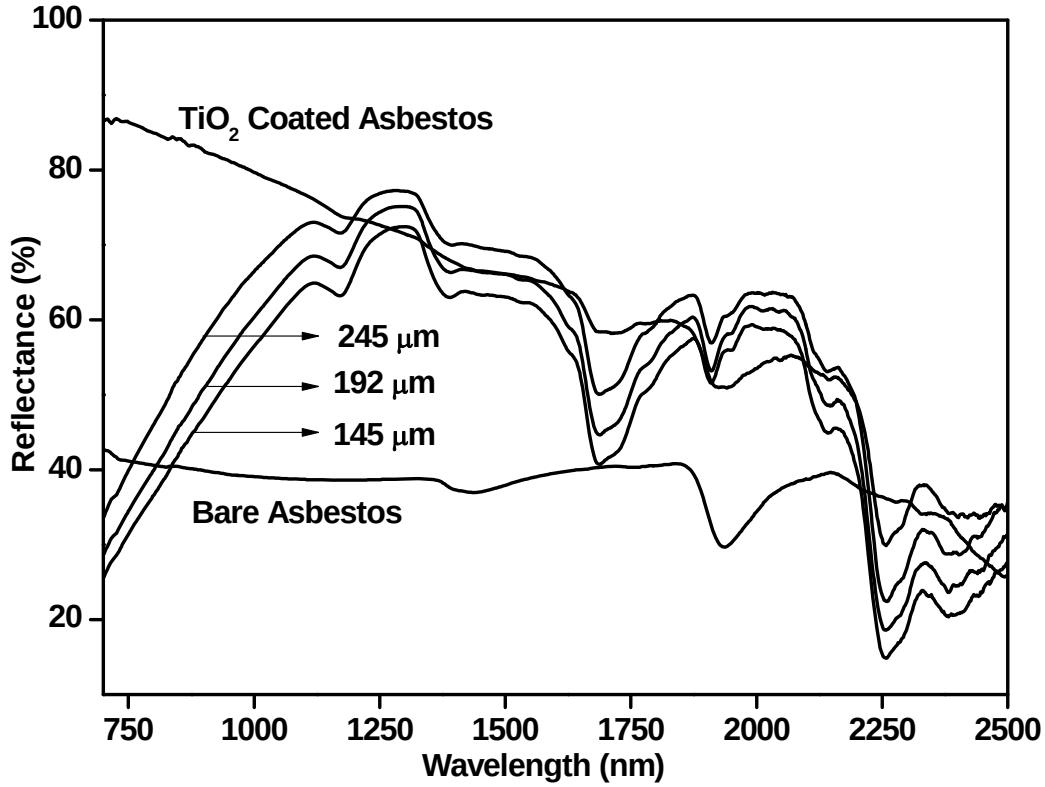

Fig. 2.17. NIR reflectance spectra of $Y_2Ce_{1.7}Pr_{0.3}O_7$ reddish–brown pigment coated at varying thickness over a TiO_2 base coat on an asbestos strip.

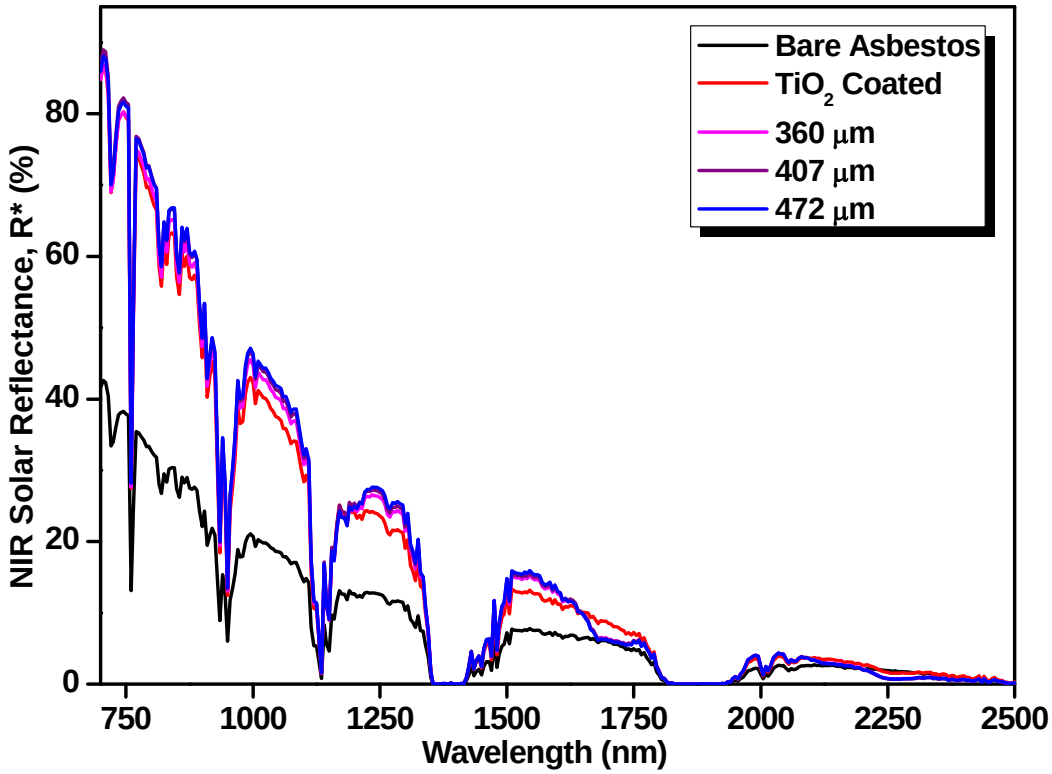

Fig. 2.18. NIR solar reflectance spectra of $Y_2Ce_{1.5}Mo_{0.5}O_{7+\delta}$ yellow pigment coated at varying thickness over a TiO_2 base coat on an asbestos strip.

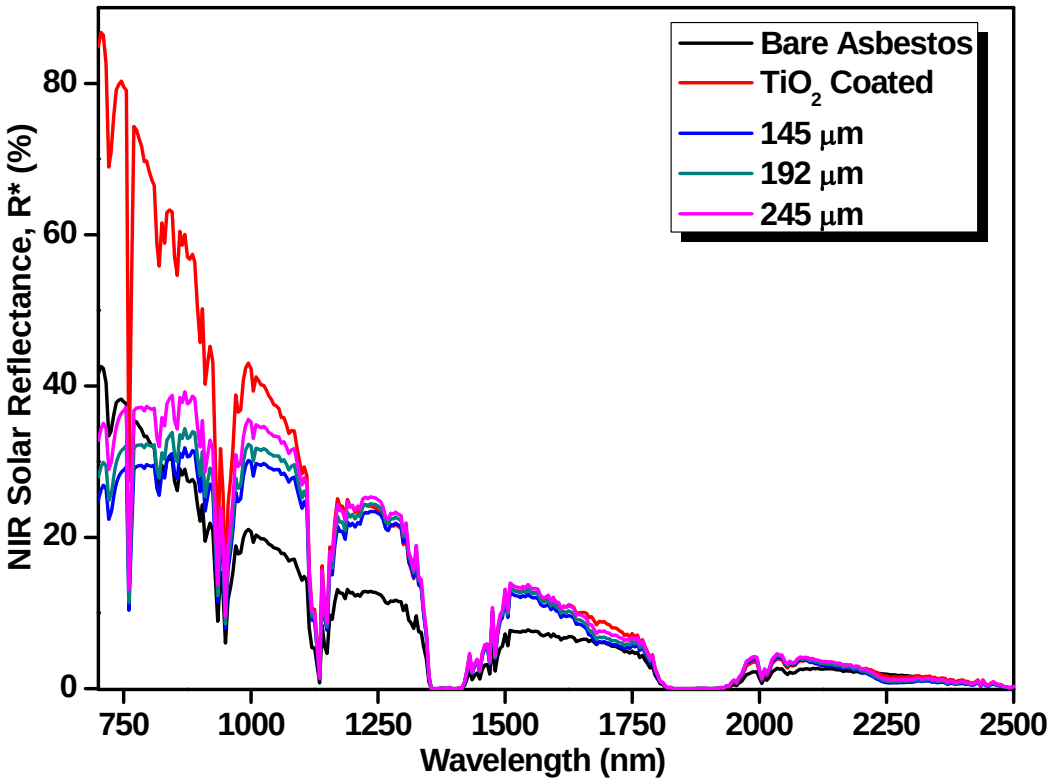

Fig. 2.19. NIR solar reflectance spectra of $Y_2Ce_{1.7}Pr_{0.3}O_7$ reddish–brown pigment coated at varying thickness over a TiO_2 base coat on an asbestos strip.

The results clearly indicate that bare asbestos cement sheet possess a low NIR solar reflectance (*R**) of 39.6%. The TiO_2 coated asbestos cement sheet exhibits an NIR solar reflectance of 76.3%. The application of the pigment on the asbestos cement sheet surface increases its reflectance properties substantially with the increase of coating thickness of the pigment. The yellow pigment over a TiO_2 base coat exhibited an NIR solar reflectance (*R**) of 78.5, 80.3 and 80.5% at 360, 407 and 472 μm thickness, respectively. In the case of reddish–brown pigment, the NIR solar reflectance (*R**) was found to be 49, 52.4 and 57.5% at 145, 192 and 245 μm thickness, respectively. The results of NIR solar reflectance and color coordinates of the yellow and reddish–brown pigment coated asbestos cement sheet specimens are depicted in Table 2.3. It can be seen that the yellowness of the coatings have been improved with increase in coating thickness. This is evident from the hue angle values (*h*°), which decreases from 92.9 to 90.5. The yellow (*b**) component decreased slightly from 64.3 to 62.6 and the green component (–*a**) decreased from –3.3 to –0.5. However the color coordinates did not change significantly with coating thickness for the reddish–brown pigment coated samples.

Table 2.3. NIR solar reflectance and color coordinates of the $Y_2Ce_{1.5}Mo_{0.5}O_{7+\delta}$ and $Y_2Ce_{1.7}Pr_{0.3}O_7$ pigments coated over a TiO_2 base coat on asbestos cement sheet

Parameter	$Y_2Ce_{1.5}Mo_{0.5}O_{7+\delta}$			$Y_2Ce_{1.7}Pr_{0.3}O_7$		
Thickness (μm)	360	407	472	145	192	245
*R** (%)	78.5	80.3	80.5	49.0	52.4	57.5
Color coordinates						
*L**	85.8	84.4	83.3	28.1	27.6	26.9
*a**	–3.3	–0.8	–0.5	17.5	17.1	17.8
*b**	64.3	63.9	62.6	10.4	10.3	10.9
*C**	64.4	63.9	62.6	20.4	19.9	20.9
h°	92.9	90.8	90.5	30.6	31.1	31.4

2.4.6 Thermal and acid/alkali resistance studies of the pigments

Chemical and thermal resistance studies were done using the typical pigments $Y_2Ce_{1.5}Mo_{0.5}O_{7+\delta}$(yellow) and $Y_2Ce_{1.7}Pr_{0.3}O_7$ (reddish–brown). TG–DTA analysis of the pigments was carried out in the temperature range of 50–1000 °C and found that the pigments were thermally stable (Fig 2.20).

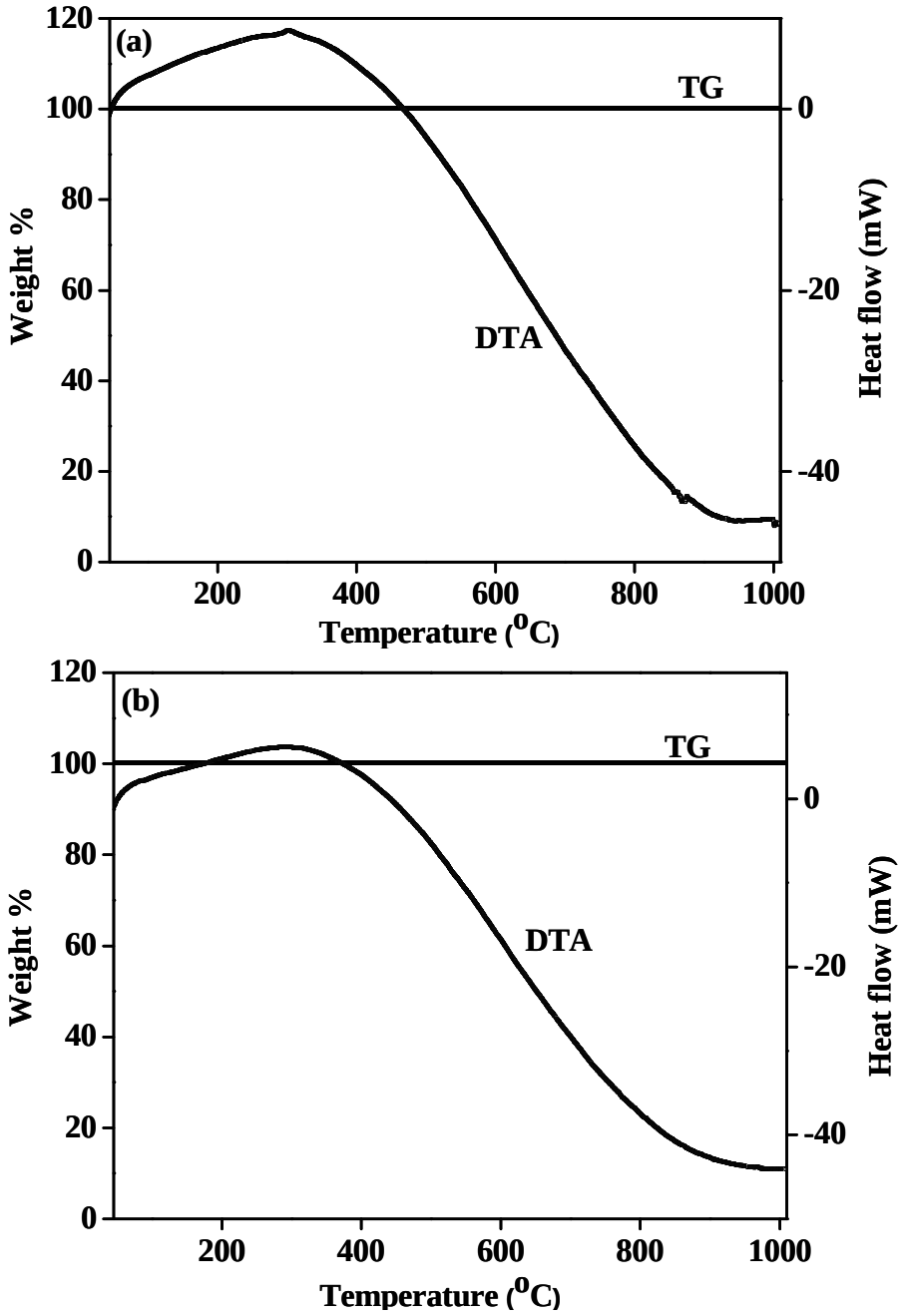

Fig. 2.20. TG/DTA curves of (a) $Y_2Ce_{1.5}Mo_{0.5}O_{7+\delta}$ and (b) $Y_2Ce_{1.7}Pr_{0.3}O_7$ pigment samples.

The acid/alkali resistance of the pigments was carried out in 10% HCl, H_2SO_4, HNO_3 and NaOH. A pre–weighed amount of the pigment was treated with acid/alkali and soaked for half an hour with constant stirring using a magnetic stirrer. The pigment powder was then filtered, washed with water, dried and weighed. Negligible weight loss of pigment was noticed for all the acids and alkali tested. The color coordinates of the resultant tested samples were measured and compared with the untreated samples. The total color difference ΔE^*_{ab} was calculated and is summarized in Table 2.4. The negligible values of ΔE^*_{ab} reveal that the pigments are chemically stable towards the acid/alkali tested. The industrially acceptable limits of ΔE^*_{ab} are as follows: when $\Delta E^*_{ab} \leq$ 1 unit indicate that the color change is almost indistinguishable from the original color, whereas, $\Delta E^*_{ab} \leq 5$ units are considered to be very good.

Table 2.4. The color coordinates (±0.1) of the (a) $Y_2Ce_{1.5}Mo_{0.5}O_{7+\delta}$ and (b) $Y_2Ce_{1.7}Pr_{0.3}O_7$ powder pigments after acid/alkali resistance tests

10 % Acid/Alkali	$Y_2Ce_{1.5}Mo_{0.5}O_{7+\delta}$				$Y_2Ce_{1.7}Pr_{0.3}O_7$			
	L^*	a^*	b^*	[a] ΔE^*_{ab}	L^*	a^*	b^*	ΔE^*_{ab}
HCl	90.7	–4.8	62.8	0.7	38.7	21.9	18.9	1.0
HNO_3	90.3	–4.9	61.4	1.1	38.1	22.4	18.5	1.3
H_2SO_4	90.7	–4.6	62.3	0.5	39.3	22.1	18.9	0.7
NaOH	90.9	–4.8	61.9	0.9	38.8	22.1	18.7	0.8

[a] $\Delta E^*_{ab} = [(\Delta L^*)^2+(\Delta a^*)^2+(\Delta b^*)^2]^{½}$

2.5 Conclusions

- A series of NIR reflective inorganic pigments with the general formula $Y_2Ce_{2-x}M_xO_{7+\delta}$ (M = Mo or Pr and *x* ranges from 0 to 0.5) displaying a wide range of colors from ivory–white to yellow and brick–red to dark–brown have been successfully synthesized by simple calcination route in air atmosphere.
- The X–ray diffraction pattern of $Y_2Ce_2O_7$ can be indexed to a cubic fluorite structure with a lattice constant of 1.0773 nm. The doping of Mo^{6+} or Pr^{4+} for Ce^{4+} in $Y_2Ce_2O_7$ did not alter the cubic phase significantly.
- It is interesting to note that the doping of Mo^{6+} for Ce^{4+} in $Y_2Ce_2O_7$ gently shifted the absorption edge from 410 nm to 506 nm due to O_{2p}–Mo_{4d} charge–transfer transitions. This accounts for the change of color of $Y_2Ce_2O_7$ from ivory–white to yellow.
- The substitution of Pr^{4+} for Ce^{4+} dramatically shifted the charge transfer band of $Y_2Ce_2O_7$ to longer wavelengths (725 nm) and changes the color from ivory–white to dark–brown. The coloring mechanism is due to the introduction of an additional $4f^1$ electronic energy level of Pr^{4+} between the O^{2-} valence and the Ce^{4+} conduction bands.
- Most importantly, the newly designed yellow pigments exhibited high NIR solar reflectance (79–81%) when coated on an asbestos cement sheet, thus rendering them as excellent candidates for use as ‘Cool Pigments’. The currently designed reddish–brown pigment also showed significant NIR solar reflectance (58%).
- The developed pigments do not possess any toxic metal ions, and hence these can be considered as environmentally benign inorganic pigments.

Chapter 3

Effect of molybdenum and praseodymium dopants on the optical properties of $Sm_2Ce_2O_7$: Tuning of band gaps to realize various color hues

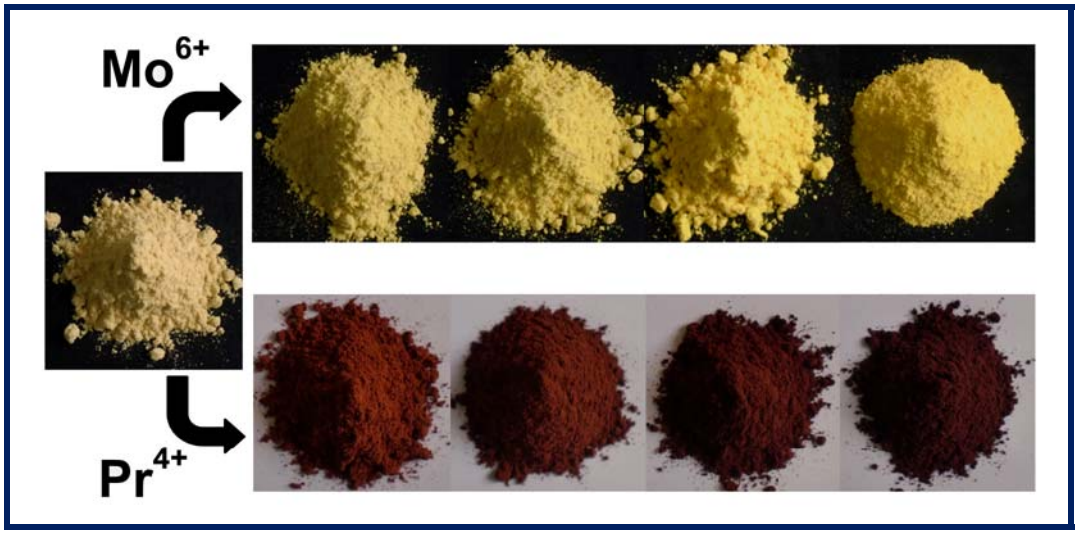

3.1 Summary

This chapter reports on the synthesis, characterization and optical properties of a new class of rare earth based pigments as alternatives to toxic inorganic pigments. Investigations reveal that the doping of molybdenum for ceria in $Sm_2Ce_2O_7$ changes the color hue from cream to yellow. The band gap of the resultant pigments decreases from 2.76 to 2.52 eV due to the O_{2p}–Mo_{4d} charge transfer transitions. On the other hand, the doping of praseodymium in ceria matrix changes the color from cream through brick red to dark brown and the band gap shifts from 2.76 to 1.72 eV. The coloring mechanism is based on the introduction of an additional electronic level of energy in the cerianite forbidden band. The influence of various mineralizers on the calcination temperature and optical properties of the pigments have been evaluated. The thermal and chemical stabilities of the pigments have also been examined.

Vishnu, **V. S.;** George, G and Reddy, M. L. P. *Dyes Pigm. 85,* **2010,** 117–123

3.2 Introduction

Lanthanide ions have attracted considerable attention due to their unique optical properties and specific functions make them useful in a wide range of industrial applications that includes tunable lasers, amplifiers for optical communications, organic light–emitting diodes and inorganic pigments (Taniguchi *et al.* 1995; Bunzli *et al*. 2005; Kido *et al*. 2002; Biju *et al*. 2009; Buxbaum and Pfaff 2005). There is a strong incentive to develop new colored inorganic materials to substitute for industrial pigments that are based on toxic metals hazardous to health and the environment (Jansen and Letschert 2000). Recently, the industrial utilization of lanthanides is growing very rapidly because of their known low toxicity. Hence in the recent past a large number of rare earth based pigments have been proposed as alternatives to traditional toxic inorganic pigments (Dohnalova *et al*. 2009; [a]Martos *et al*. 2008; Sulcova *et al*. 2008). Jansen and Letschert have reported that the colors of the solid solutions $Ca_{1-x}La_xTaO_{2-x}N_{1+x}$ of the perovskite type pigments could be tuned from yellow through orange to deep red by simple composition adjustments. Further, they demonstrated that any color in the range from light yellow to deep red can be tailored by proper adjustment of the O/N ratio in the solid solution. Though these pigments are non–toxic and show excellent color hue, the synthesis procedure of these materials utilizes toxic and inflammable ammonia gas for longer periods. Rare earth sulfides and related compounds have also been proposed as promising candidates for various surface coating applications (Zhukov *et al.* 1997; Perrin and Wimmer 1996; Busnot *et al*. 2002; Gauthier *et al*. 2003). The chromatic properties of cerium sulfides arise from the fact that the optical absorption associated with the $4f \rightarrow 5d$ electronic transition of their Ce^{3+} ions range from ~1.9eV to ~2.1eV (Perrin and Wimmer 1996). In general the synthesis of sulfide based pigments uses toxic hydrogen sulphide gas. Praseodymium yellow ($ZrSiO_4$:Pr) is a well known commercial pigment which has

been widely used in the industry for coloring of ceramics (Hill *et al*. 2000; Blonski 1994).

Among several oxide based rare earth pigments known, CeO_2 and related materials have attracted much attention because of their opacity, low toxicity and high thermal stability (Garcia *et al*. 2001; Imanaka *et al*. 2008; Furukawa *et al*. 2008; [a]Masui *et al*. 2004; Sulcova and Trojan 2004; Kumari *et al*. 2008). However their chromatic properties are not satisfactory as compared to traditional pigments. In general, colors of the inorganic pigment appear brilliant and pure when the corresponding mechanism for a selective absorption of light is related to an electronic interband transition, leading to a steep absorption edge in the visible spectrum. The change in band gap is determined by the extent of overlap of the valence orbitals and by the difference between electronegativities of the ions present in the system (Jansen and Letschert 2000). The present research work has been undertaken to investigate the effect of Mo^{6+} and Pr^{4+} on the color hue of $Sm_2Ce_2O_7$ pigments by tuning the band gaps, which has not been reported in the literature before. The new series of pigments of the formula $Sm_2Ce_{2-x}Mo_xO_{7+\delta}$ (x ranges from 0 to 0.4) and $Sm_2Ce_{2-x}Pr_xO_7$ (x ranges from 0 to 0.2) have been synthesized by solid–state reaction of the respective oxides and characterized by X–ray powder diffraction, UV–vis diffuse reflectance spectroscopy and CIE–$L^*a^*b^*$ 1976 color scales.

Mineralizers have a large effect on the crystal lattice of the synthesized material as well on the color of pigments. The effect of the mineralizer is to form a liquid phase, which loosens the crystal lattice, putting it into an active state. It is known that the reactive power of melt increases sharply when easily polarized components are introduced (Maslennikova *et al*. 2009). The melt thus becomes more mobile and promotes not only earlier completion of the phase–formation process but also the

appearance of new color–carrying phases. These factors have prompted to study the effect of various mineralizers on the calcination temperature and optical properties of the typical pigments $Sm_2Ce_{1.60}Mo_{0.40}O_{7+\delta}$ and $Sm_2Ce_{1.85}Pr_{0.15}O_7$. The thermal and chemical stability of the pigments have also been evaluated.

3.3 Experimental Section

3.3.1 Materials and Methodology

Two series of compounds based on the general formula $Sm_2Ce_{2-x}Mo_xO_{7+\delta}$ (x ranges from 0 to 0.4) and $Sm_2Ce_{2-x}Pr_xO_7$ (x ranges from 0 to 0.2) have been synthesized by solid–state process in air atmosphere. The oxides, Sm_2O_3 (99.9%), CeO_2 (99.9%), Pr_6O_{11} (99.9%) and $(NH_4)_6Mo_7O_{24}.4H_2O$ (99.9%) supplied by M/s. Sigma Aldrich was weighed in stoichiometric proportions and were transferred to an agate mortar. The mixture was then homogenized by wet milling with acetone for 30 min. The resultant powders were then calcined in platinum crucibles in a Nabertherm electric furnace at a temperature of 1500 °C for 18 h, followed by auto–cooling inside the furnace. The heating of the furnace was programmed to increase the temperature at 5 °C/min. The end products were subsequently ground in an agate mortar with the aim of refining and homogenizing the particle size. Typical pigment compositions $Sm_2Ce_{1.60}Mo_{0.40}O_{7+\delta}$ and $Sm_2Ce_{1.85}Pr_{0.15}O_7$ were also prepared in the presence of different mineralizers like NaF, NaCl, CaF_2, H_3BO_3 and Li_2CO_3 with the aim of evaluating their influence on the calcination temperature and optical properties. The mineralizer was used at 1 wt. % level on the total weight of the precursors. The resultant stoichiometric mixtures of samples were calcined at an optimized temperature (1350 °C) and time duration (18 h) in air atmosphere.

3.3.2 Characterization Techniques

The instrumental techniques employed for the characterization of various pigments designed in the present study are the same as that described in the previous chapter 2.

3.4 Results and Discussion

3.4.1 Powder X–ray diffraction analysis

The XRD patterns of the typical pigment sample $Sm_2Ce_2O_7$ calcined at different temperatures ranging from 1000 °C to 1500 °C for 18 h are shown in Fig. 3.1. The samples calcined at temperatures below 1500 °C exhibit poor crystallization, accompanying with peaks corresponding to that of the precursor oxide, Sm_2O_3. (PDF No. 21–1276). On the other hand, the samples calcined at and above 1500 °C can be very well indexed to a cubic fluorite phase accompanied by a weak rare earth cubic–type (C–type) phase. Thus it is clear from the above study that a calcination temperature of 1500 °C and time duration of 18 h is necessary to obtain the desired products.

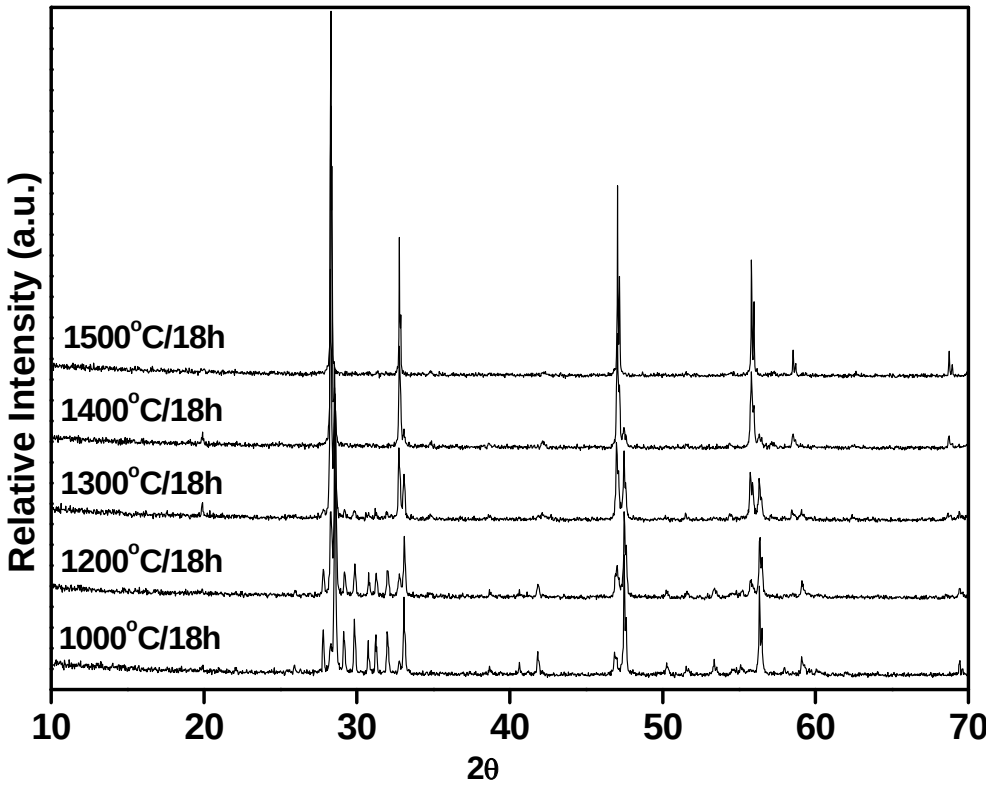

Fig. 3.1. XRD patterns of $Sm_2Ce_2O_7$ calcined at various temperatures for 18 h.

Unlike in the $La_2Ce_2O_7$ system where a complete cubic fluorite type solid solution has been evidenced, as pointed elsewhere (Yamamura *et al*. 2003), the presence of a

major cubic fluorite–type (F–type) phase accompanying by a weak rare earth cubic–type (C–type) superstructure has been observed from the XRD pattern of $Sm_2Ce_2O_7$ depicted in Figs. 3.2 and 3.3. It means that when the ionic radius ratio (Sm^{3+}/Ce^{4+} = 0.109 nm/0.097 nm = 1.12) is smaller than 1.17, the crystal phase can be gently changed from F–type to structure C–type. However, the C–type superstructure noted in the present study may be considered as incomplete due to the weakness of the super lattice lines.

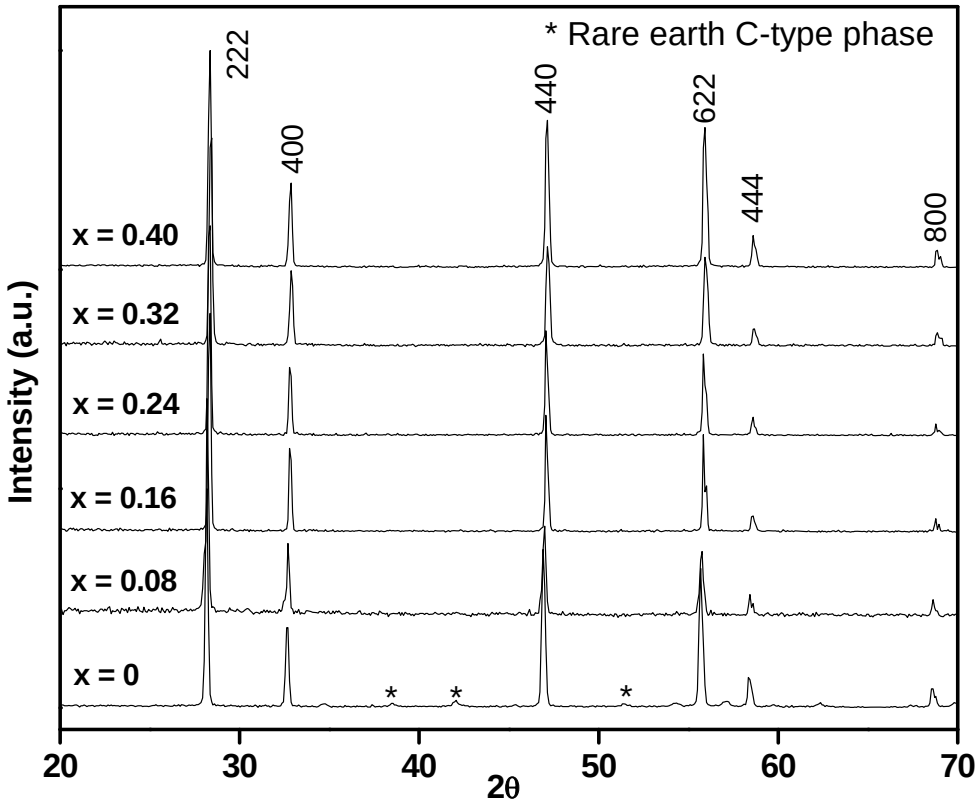

Fig. 3.2. XRD patterns of $Sm_2Ce_{2-x}Mo_xO_{7+\delta}$ (x ranges from 0 to 0.4).

On the other hand, surprisingly the doping of molybdenum or praseodymium for Ce^{4+} in $Sm_2Ce_2O_7$, the superlattice lines of weak C–type superstructure have been completely vanished and shows only cubic F–type phase. Addition of Mo^{6+} (up to 10 mol %) into $Sm_2Ce_2O_7$ produces intrinsic strain which results in a decrease of lattice constant from 1.0970 nm to 1.0890 nm, which further confirms the formation of solid–solution.

This is due to the smaller ionic radii of Mo^{6+} (0.059 nm) compared to Ce^{4+} (0.097 nm). A similar decrease in lattice parameter from 1.0970 nm to 1.0933 nm has been noted with the addition of Pr^{4+} (0.096 nm). However, the decrease in lattice parameter value is not significant as compared to molybdenum doped system. As the ionic radii of Ce^{4+} and Pr^{4+} in eight fold coordination are 0.097 and 0.096 nm, respectively, only minor variations would be expected (Shannon 1976).

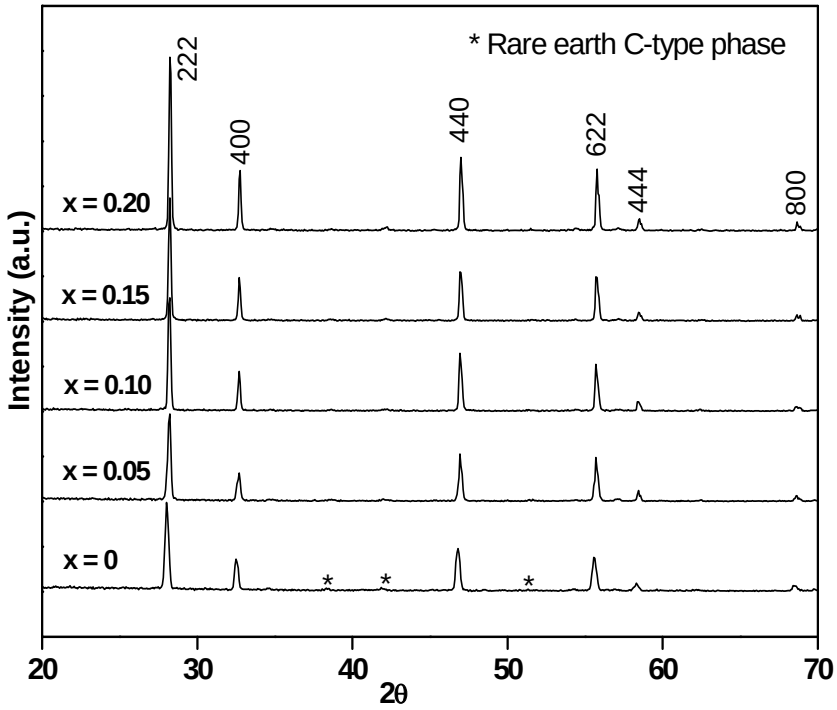

Fig. 3.3. XRD patterns of $Sm_2Ce_{2-x}Pr_xO_7$ (x ranges from 0 to 0.2).

3.4.2 Particle size and morphological analysis

Particle size analysis of the typical pigments $Sm_2Ce_{1.60}Mo_{0.40}O_{7+\delta}$ and $Sm_2Ce_{1.85}Pr_{0.15}O_7$ reveal a mean diameter of 7.96 μm (size of 90% particles < 18.31 μm, 50% particles < 6.03 μm and 10% particles < 1.41 μm) and 8.03 μm (size of 90% particles < 17.73 μm, 50% particles < 5.97 μm and 10% particles < 1.81 μm), respectively. The homogeneous nature of the pigments can be understood from the SEM images (Fig. 3.4), the average

grain size being less than 10 μm, which is again in good agreement with our particle size analysis.

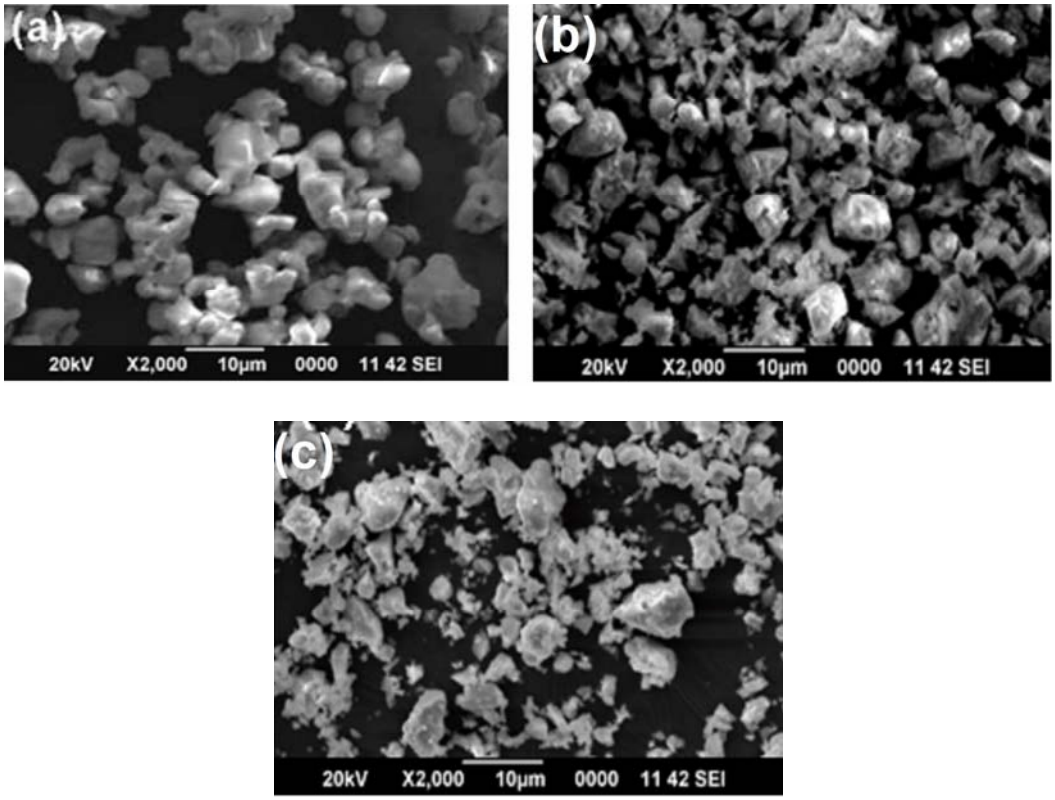

Fig. 3.4. SEM micrographs of (a) $Sm_2Ce_2O_7$ (b) $Sm_2Ce_{1.60}Mo_{0.40}O_{7+\delta}$ and (c) $Sm_2Ce_{1.85}Pr_{0.15}O_7$.

3.4.3 Optical properties of molybdenum doped $Sm_2Ce_2O_7$ pigments

The UV–vis diffuse reflectance and absorption spectra of the pigment samples $Sm_2Ce_{2-x}Mo_xO_{7+\delta}$ (x ranges from 0 to 0.4) are shown in Figs. 3.5 and 3.6, respectively. It can be noted from the reflectance spectrum of molybdenum free $Sm_2Ce_2O_7$ that there is a strong absorption below 450 nm due to the O_{2p}–Ce_{4f} charge transfer transitions of Ce^{4+} (Bunzli *et al*. 2005). In addition, many weak absorption bands in the visible region have also been observed and these can be assigned to f–f electronic transitions of Sm^{3+}. The bands at 402, 465, 478, 490, 530 and 557 nm can be assigned based on the energy levels $^6H_{5/2}$, $^6P_{3/2}$, $^4I_{13/2}$, $^4I_{11/2}$, $^4I_{9/2}$, $^4F_{3/2}$ and $^4G_{5/2}$ of Sm^{3+}, respectively (Carnall *et al*.1968). The

absorptions in the violet blue region along with the O_{2p}–Ce_{4f} charge transfer transition is responsible for the cream hue of $Sm_2Ce_2O_7$.

It is evident from the reflectance spectra of these pigments that the progressive doping of Mo^{6+} for Ce^{4+} in $Sm_2Ce_2O_7$ gently changes the absorption edge from 450 nm to 490 nm, due to the O_{2p}–Mo_{4d} charge transfer transitions (Sreeram *et al*. 2007). Thus, the color of the pigment changes from cream to yellow (Fig. 3.7). The band gap of the colorants as determined from the absorbance spectra is given in Table 3.1 and was obtained by a straight forward extrapolation method ([b]George *et al*. 2008). The band gap of molybdenum free–$Sm_2Ce_2O_7$ sample decreases from 2.76 to 2.52 eV, with the increase of molybdenum concentration.

Table 3.1 summarizes the CIE 1976 color coordinates of the powdered $Sm_2Ce_{2-x}Mo_xO_{7+\delta}$ (x ranges from 0 to 0.4) pigment samples. The progressive doping of Mo^{6+} (from 2 to 10 mol %) for Ce^{4+} in $Sm_2Ce_2O_7$ results in a continuous increase in the yellow component (b^* from 18.8 to 55.0) and chroma (C^* from 18.8 to 55.2) values of the pigments. However, it does not have a significant influence on the hue angle ($h°$). The hue angles ($h°$) of molybdenum doped $Sm_2Ce_2O_7$ pigments were found to be in the yellow region of the cylindrical color space ($h°$ = 70–105 for yellow) (Sulcova and Trojan 2008). On the other hand, the substitution of 2 mol % of Mo^{6+} for Ce^{4+} in $Sm_2Ce_2O_7$ brings about a decrease in a^* (from –0.4 to –5.0). Further incorporation of more and more Mo^{6+} (>2 mol %) has no significant effect on the green component ($–a^*$) of the pigment. The chromatic properties of the typical pigment sample, $Sm_2Ce_{1.60}Mo_{0.40}O_{7+\delta}$ (L^* = 86.3, a^*= –5.0, b^* = 55.0, C^* = 55.2, $h°$ = 90.5) are found to be superior to that of the yellow pigment samples of cerium molybdate reported elsewhere (L^* = 76.1, a^* = 0.1, b^* = 36.9, C^* = 21.9, $h°$ = 88.2) (Sreeram *et al*. 2007).

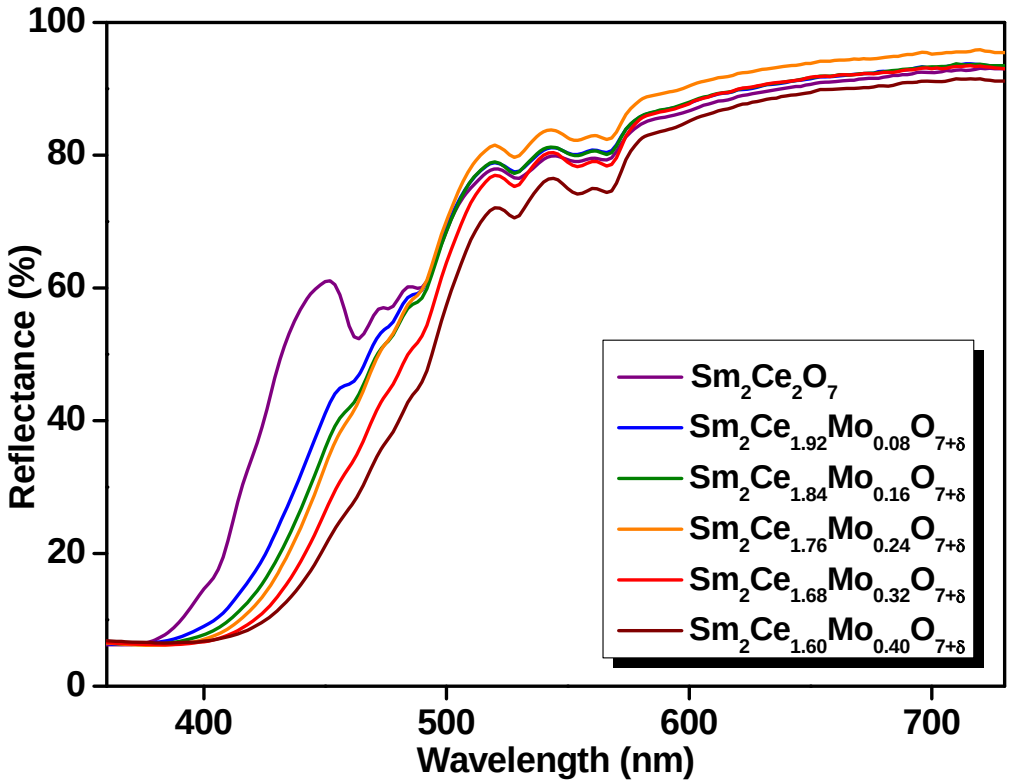

Fig. 3.5. UV–vis diffuse reflectance spectra of $Sm_2Ce_{2-x}Mo_xO_{7+\delta}$ (*x* ranges from 0 to 0.4).

Table 3.1. The color coordinates (±0.1) of the $Sm_2Ce_{2-x}Mo_xO_{7+\delta}$ (*x* ranges from 0 to 0.4) powder pigments and band gap values

Pigment composition	Color coordinates					Band gap
	*L**	*a**	*b**	*C**	*h*°	*(eV)*
$Sm_2Ce_2O_7$	88.9	–0.4	18.8	18.8	90.0	2.76
$Sm_2Ce_{1.92}Mo_{0.08}O_{7+\delta}$	90.5	–5.0	38.3	38.6	91.0	2.64
$Sm_2Ce_{1.84}Mo_{0.16}O_{7+\delta}$	89.1	–5.6	41.9	42.3	91.0	2.60
$Sm_2Ce_{1.76}Mo_{0.24}O_{7+\delta}$	91.2	–6.8	46.0	46.5	91.3	2.57
$Sm_2Ce_{1.68}Mo_{0.32}O_{7+\delta}$	88.5	–6.0	51.9	52.2	90.8	2.54
$Sm_2Ce_{1.60}Mo_{0.40}O_{7+\delta}$	86.3	–5.0	55.0	55.2	90.5	2.52

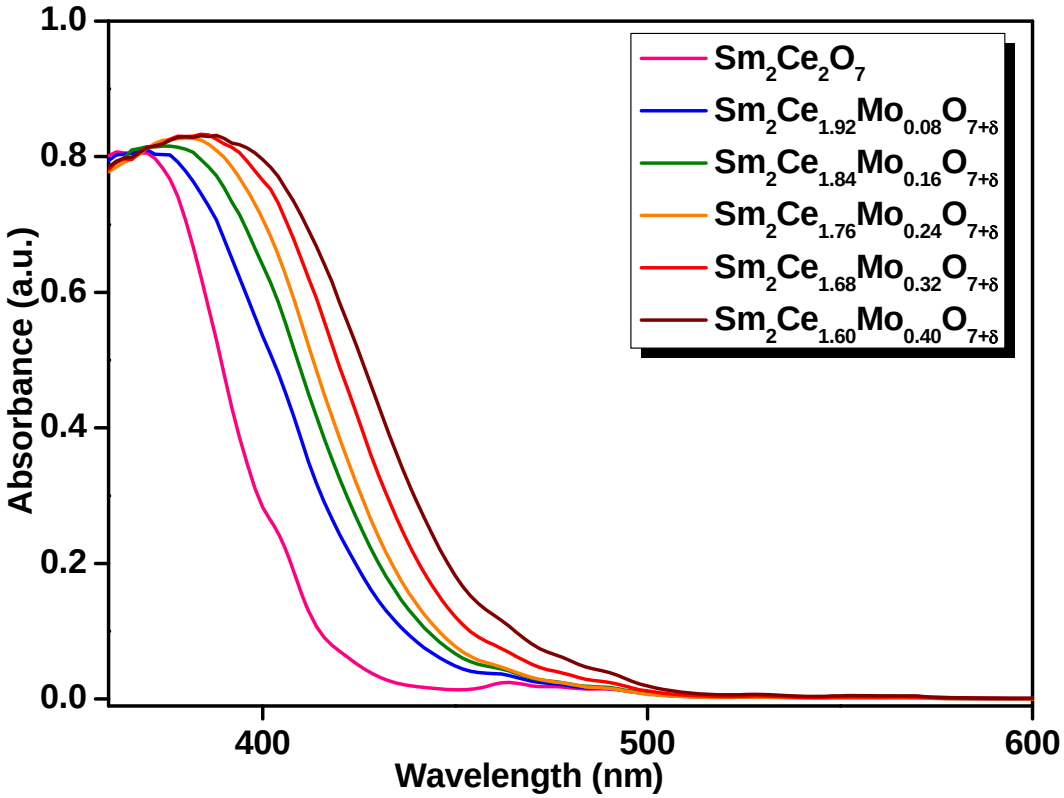

Fig. 3.6. Absorbance spectra of $Sm_2Ce_{2-x}Mo_xO_{7+\delta}$ (x ranges from 0 to 0.4).

Fig. 3.7. Photographs of $Sm_2Ce_{2-x}Mo_xO_{7+\delta}$ and $Sm_2Ce_{2-x}Pr_xO_7$ pigments.

3.4.4 Optical properties of praseodymium doped $Sm_2Ce_2O_7$ pigments

The presence of the tetravalent praseodymium ions in the host lattice of $Sm_2Ce_2O_7$ leads to greater absorptions in the visible region (Fig. 3.8) because the gap between the valence and conduction band narrows. Further it introduces an additional energy level due to the $4f^1$ electrons between the O_{2p} valence and the Ce^{4+} conduction bands. Consequently, the absorption edge is red shifted significantly and the band gap of the pigments decreases from 2.76 to 1.78 eV (Table 3.2) as evident from the absorption spectra depicted in Fig. 3.9. Accordingly the color of the pigments changes from cream to brick–red. On the other hand, with increasing concentration of Pr^{4+} ions, the absorption edge further red shifted and perceptibly thereafter the color changes from brick–red to dark–brown (Fig. 3.7). The band gap of the resultant pigment subsequently decreases to 1.72 eV.

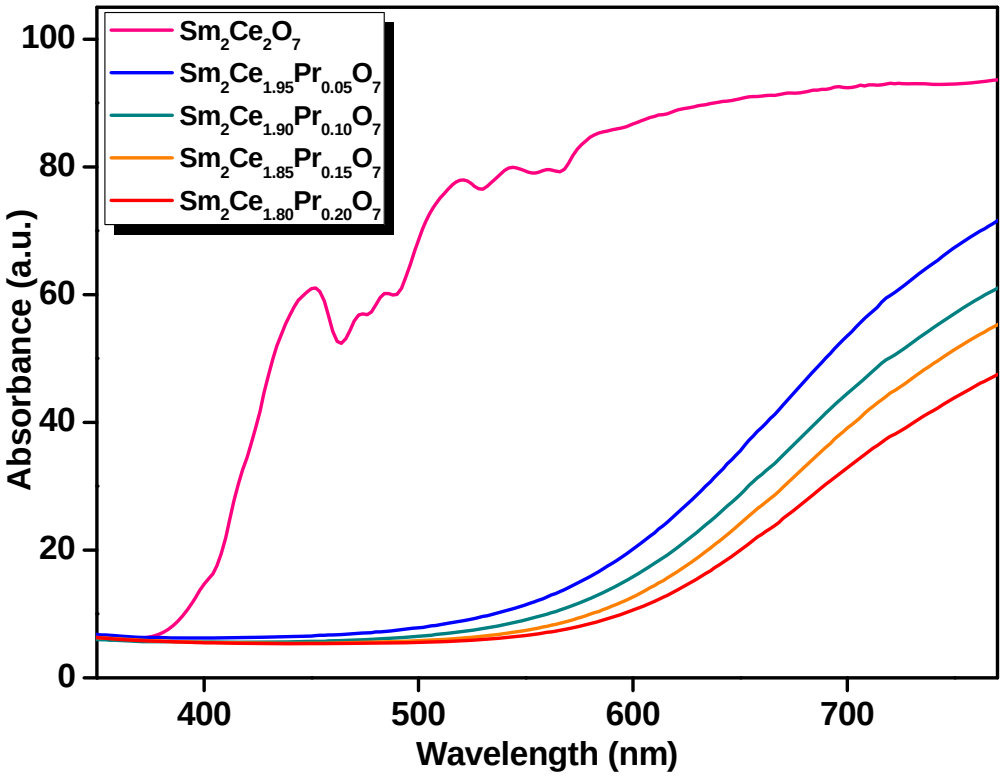

Fig. 3.8. Reflectance spectra of $Sm_2Ce_{2-x}Pr_xO_7$ (x ranges from 0 to 0.2) pigments.

It is clear from Table 3.2 that the substitution of 1.25 mol % of Pr^{4+} for Ce^{4+} in $Sm_2Ce_2O_7$ drastically increases the red component (*a**) from –0.4 to 19.2, while there is no change in the yellow component (*b**) as compared to the praseodymium free sample. In addition to the above, the chroma (*C**) of the pigment has been significantly enhanced from 18.8 to 27.2. On the other hand, the addition of 1.25 mol % of Pr^{4+} has drastically decreased the hue angle (*h*°) from 90.0 to 45.0. This has resulted in a change in the color of the pigment initially from cream to brick–red. Further increase in the dopant concentration of Pr^{4+} from 1.25 to 5 mol % progressively decreases the red component (*a**) from 19.2 to 12.9 and yellow component (*b**) from 19.2 to 6.2, chroma (*C**) from 27.2 to 14.3 and the hue angle from 45.0 to 25.7. These led to the change of the color of the pigment samples to gently change from brick–red to dark–brown. The hue angle values reveal that the Pr^{4+} doped pigments lie in the brick–red to dark–brown region of the cylindrical color space (*h*° = 0–35 for red and 35–70 for orange) (Sulcova and Trojan 2008). The color coordinates of the typical pigment $Sm_2Ce_{1.95}Pr_{0.05}O_7$ (*L** = 46.3, *a** = 19.2, *b** = 19.2, *C** = 27.2, *h*° = 45.0) sample are found to be higher than that of the red powdered pigment samples of praseodymium doped ceria reported elsewhere (*L** = 46.6, *a** = 15.5, *b** = 10.5, *C** = 18.7, *h*° = 34.1) (Kumari *et al*. 2008).

Table 3.2. The color coordinates (±0.1) of the $Sm_2Ce_{2-x}Pr_xO_7$ (*x* ranges from 0 to 0.2) powder pigments and band gap values

Pigment composition	Color coordinates					Band gap
	*L**	*a**	*b**	*C**	*h*º	*(eV)*
$Sm_2Ce_2O_7$	88.9	–0.4	18.8	18.8	90.0	2.76
$Sm_2Ce_{1.95}Pr_{0.05}O_7$	46.3	19.2	19.2	27.2	45.0	1.78
$Sm_2Ce_{1.90}Pr_{0.10}O_7$	39.6	16.6	11.4	20.1	34.4	1.76
$Sm_2Ce_{1.85}Pr_{0.15}O_7$	37.5	14.4	8.4	16.7	30.1	1.74
$Sm_2Ce_{1.80}Pr_{0.20}O_7$	35.7	12.9	6.2	14.3	25.7	1.72

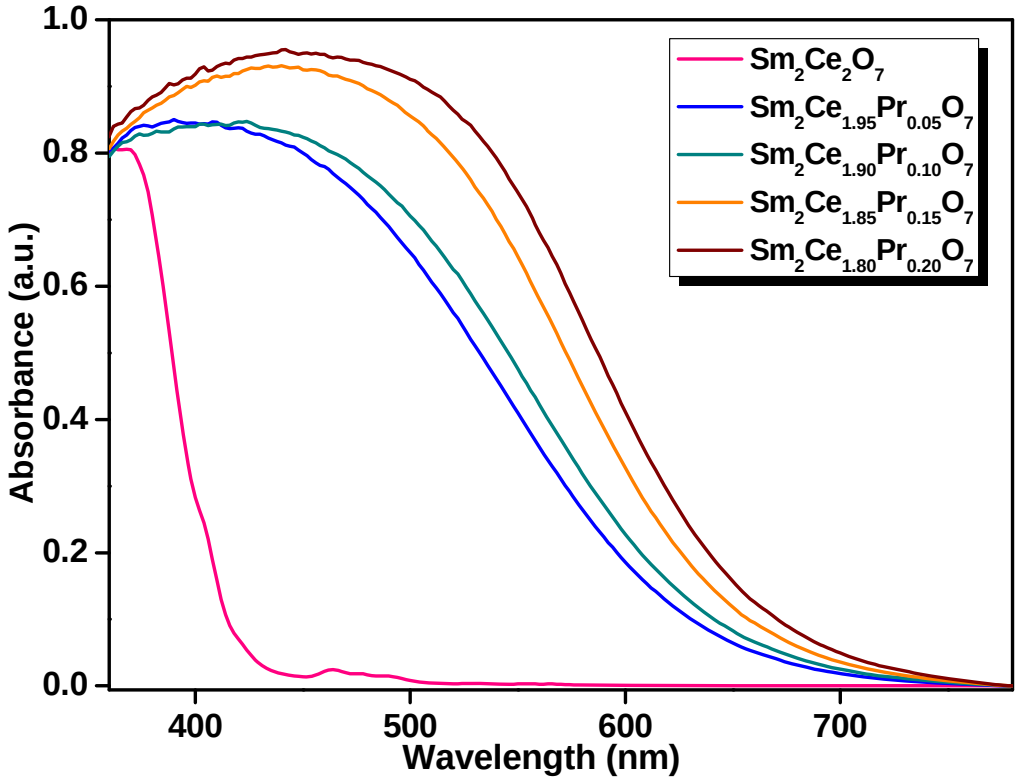

Fig. 3.9. Absorbance spectra of $Sm_2Ce_{2-x}Pr_xO_7$ (x ranges from 0 to 0.2) pigments.

3.4.5 Thermal and chemical stability studies of the pigments

The thermal stability (TG/DTA analysis) of the typical synthesized pigments, namely $Sm_2Ce_{1.60}Mo_{0.40}O_{7+\delta}$ and $Sm_2Ce_{1.85}Pr_{0.15}O_7$ were examined in the temperature range of 30–1000 °C and the results are depicted in Fig. 3.10. The thermogravimetric analysis results clearly indicate that there is negligible weight loss and phase transition of the pigments up to 1000 °C.

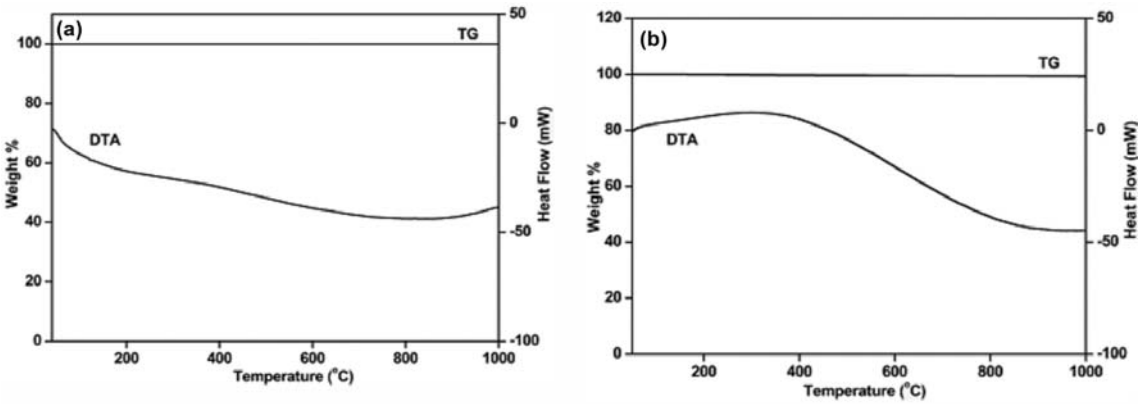

Fig. 3.10. The TG/DTA of (a) $Sm_2Ce_{1.6}Mo_{0.4}O_{7+\delta}$ and (b) $Sm_2Ce_{1.85}Pr_{0.15}O_7$ pigment.

The acid/alkali resistance of the typical pigments $Sm_2Ce_{1.60}Mo_{0.40}O_{7+\delta}$ and $Sm_2Ce_{1.85}Pr_{0.15}O_7$ was investigated using 10% $HCl/H_2SO_4/HNO_3$ and 10% NaOH. A pre–weighed quantity of the pigment was treated with acid/alkali and soaked for half an hour with constant stirring using a magnetic stirrer. The pigment powder was then filtered, washed with water, dried and weighed. Negligible weight loss of pigment was noticed for all the acids and alkali tested. The color coordinates of the typical pigments were measured after acid/alkali treatment and the total color difference, ΔE^*_{ab} of all the pigments are found to be negligible (Table 3.3) except in the case of HNO_3 for $Sm_2Ce_{1.85}Pr_{0.15}O_7$.This indicates that the typical $Sm_2Ce_{1.85}Pr_{0.15}O_7$ pigment exhibits poor resistance towards HNO_3.

Table 3.3. The color coordinates (±0.1) of (a) $Sm_2Ce_{1.60}Mo_{0.40}O_{7+\delta}$ and (b) $Sm_2Ce_{1.85}Pr_{0.15}O_7$ powder pigments after chemical resistance tests

10 % Acid/Alkali	$Sm_2Ce_{1.60}Mo_{0.40}O_{7+\delta}$				$Sm_2Ce_{1.85}Pr_{0.15}O_7$			
	L^*	a^*	b^*	[a] ΔE^*_{ab}	L^*	a^*	b^*	ΔE^*_{ab}
HCl	85.9	–4.8	54.9	0.4	37.0	14.1	8.3	0.6
HNO_3	86.4	–5.0	54.2	0.8	36.0	15.5	8.0	1.9
H_2SO_4	86.1	–4.5	54.1	1.0	38.2	14.8	8.6	0.8
NaOH	86.0	–4.0	54.0	1.4	37.0	14.0	8.0	0.8

[a] $\Delta E^*_{ab} = [(\Delta L^*)^2+(\Delta a^*)^2+(\Delta b^*)^2]^{½}$

3.4.6 Effect of mineralizer on the calcination temperature and optical properties

The influence of mineralizer on the calcination temperature (1250–1350 °C) and optical properties of the typical pigments $Sm_2Ce_{1.60}Mo_{0.40}O_{7+\delta}$, and $Sm_2Ce_{1.85}Pr_{0.15}O_7$ was evaluated. The pigment samples calcined at 1350 °C are found to be crystalline and phase pure. On the other hand, the samples calcined at lower temperatures (1250 °C and 1300 °C) are not phase pure. The XRD patterns of the pigment samples calcined at 1350 °C are shown in Figs. 3.11 and 3.12, and can be very well indexed to the cubic

fluorite structure. The homogeneous and the crystalline nature of the samples can also be seen from the SEM photographs (Fig. 3.13).

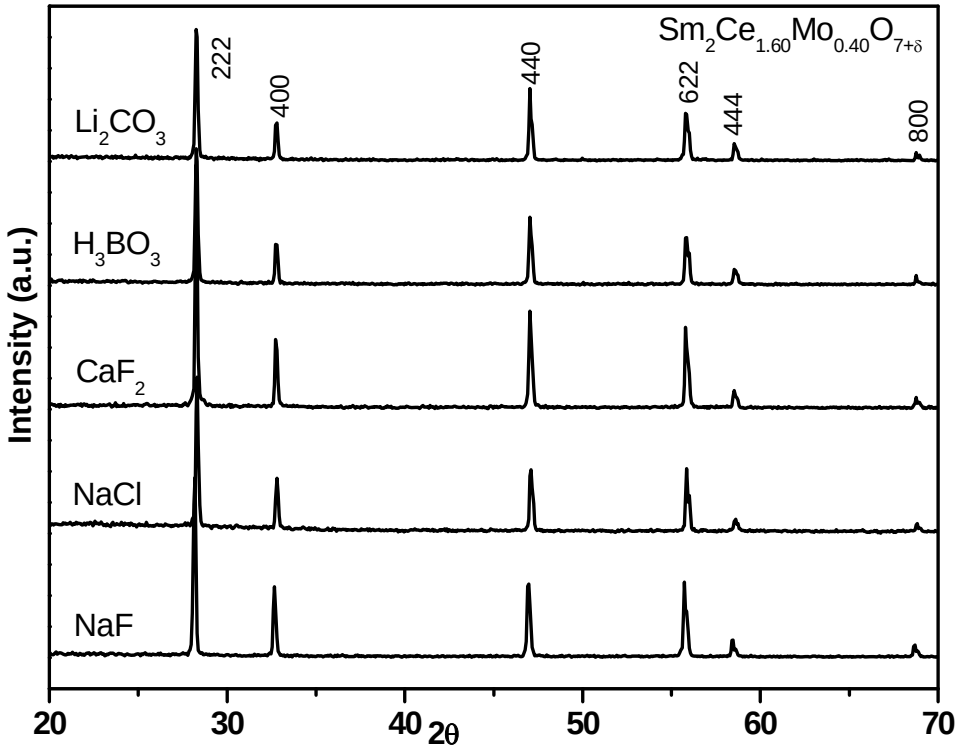

Fig. 3.11. XRD patterns of $Sm_2Ce_{1.60}Mo_{0.40}O_{7+\delta}$ in presence of 1% mineralizer.

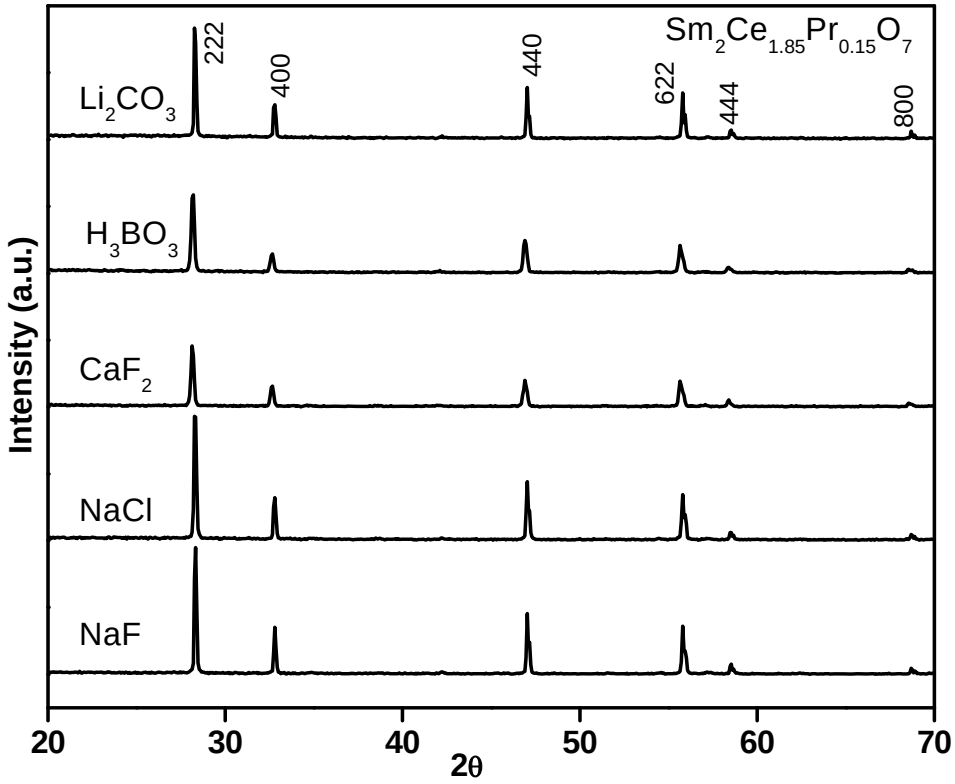

Fig. 3.12. XRD patterns of $Sm_2Ce_{1.85}Pr_{0.15}O_7$ in presence of 1% mineralizer.

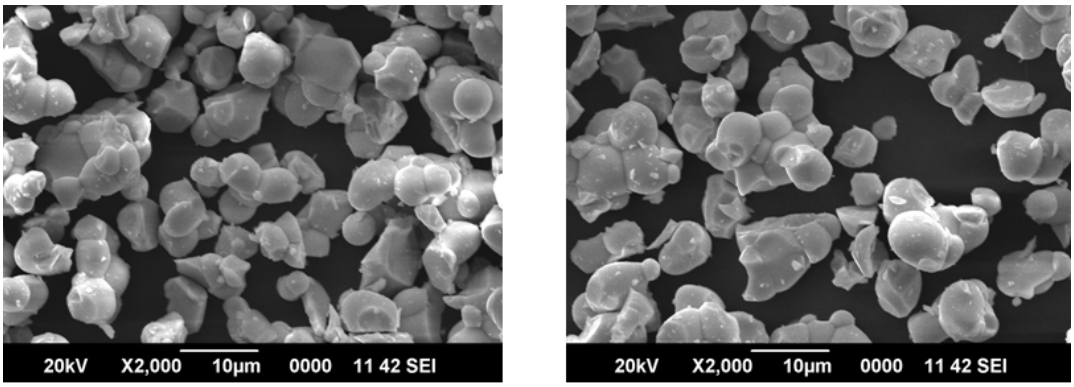

Fig. 3.13. SEM micrographs of $Sm_2Ce_{1.60}Mo_{0.40}O_{7+\delta}$ and $Sm_2Ce_{1.85}Pr_{0.15}O_7$ in presence of NaF mineralizer.

The diffuse reflectance spectra of $Sm_2Ce_{1.60}Mo_{0.40}O_{7+\delta}$, in the presence of various mineralizers are depicted in Fig. 3.14. The corresponding CIE 1976 color coordinates of the powder samples are given in Table 3.4. In the presence of Li_2CO_3, the promotion of fluorite phase at relatively lower temperature was accompanied by slight enhancement of the yellow component (b^*), chroma (C^*) and hue angle ($h°$) of the pigment sample as compared to the mineralizer free sample. However, the green component ($-a^*$) of the pigment sample has not been affected. It is clear from the reflectance spectrum that the absorption edge has been slightly red shifted and consequently the band gap has decreased from 2.52 eV to 2.48 eV as compared to the mineralizer free sample. On the other hand, in the presence of halides of alkali and alkaline earth metals, the a^* (green component), b^* (yellow component) and C^* (chroma) values of the pigment have been decreased with reference to the mineralizer free sample. In addition to the above, the hue angle of the pigment has been increased. The a^* value changes from –5.0 to –2.5, while the yellow component and chroma have not been significantly affected in the presence of H_3BO_3 as a mineralizer.

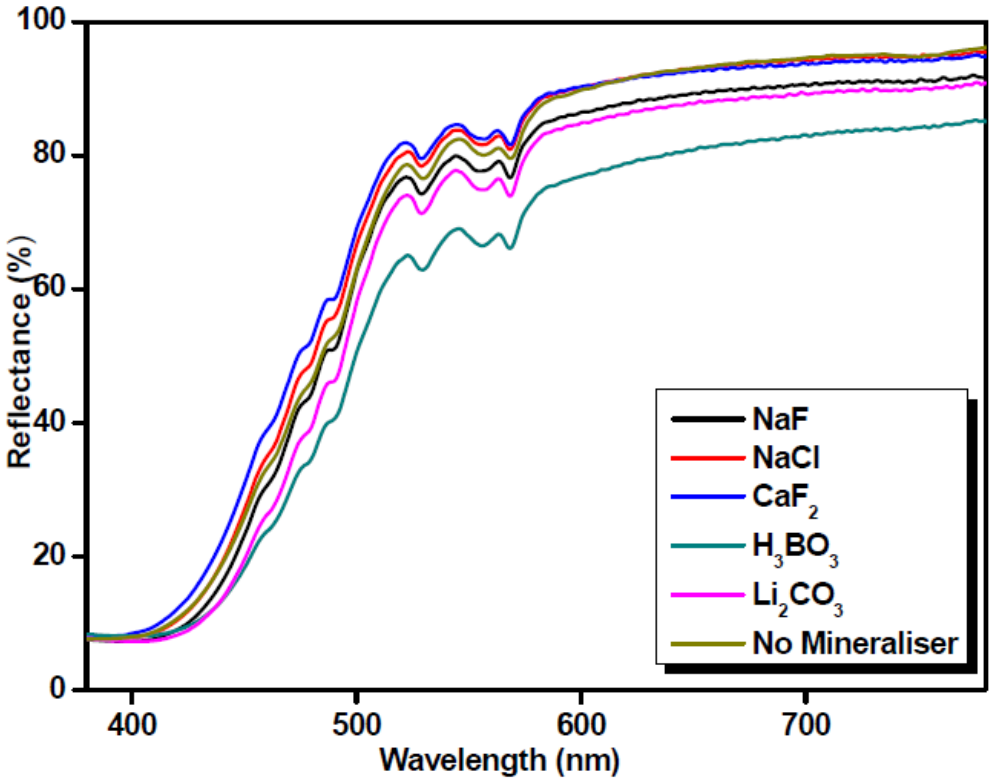

Fig. 3.14. Reflectance spectra of $Sm_2Ce_{1.60}Mo_{0.40}O_{7+\delta}$ in presence of 1% mineralizer.

Table 3.4. Effect of mineralizer on the color coordinates (±0.1) of $Sm_2Ce_{1.60}Mo_{0.40}O_{7+\delta}$

Mineralizer	Color coordinates					Band gap *(eV)*
	*L**	*a**	*b**	*C**	*h*°	
None	86.3	–5.0	55.0	55.2	90.5	2.52
NaF	91.2	–6.0	53.5	53.8	96.4	2.53
NaCl	92.1	–6.1	50.9	51.3	96.9	2.52
CaF_2	92.6	–6.5	47.4	47.8	97.8	2.56
H_3BO_3	85.7	–2.5	54.4	54.5	92.7	2.48
Li_2CO_3	89.9	–5.1	56.8	57.0	95.1	2.48

The optical absorption edge of $Sm_2Ce_{1.85}Pr_{0.15}O_7$ pigment is blue shifted (Fig. 3.15) in presence of NaF, NaCl, CaF_2 and Li_2CO_3 as mineralizer and consequently the band gap also increases marginally as compared to the mineralizer free sample. It can be seen from the color coordinate data of the pigments in presence of the above mineralizers as presented in Table 3.5 that the red component (*a**), yellow component (*b**), chroma (*C**)

and hue angle ($h°$) have been significantly increased when compared to the mineralizer free sample. In the presence of H_3BO_3, the a^*, b^* and C^* values have not been changed significantly. Thus it can be concluded that the presence of mineralizers has a profound influence in bringing down the calcination temperature of pigments (from 1500 °C to 1350 °C). A proper selection of mineralizers can therefore make possible the synthesis of inorganic pigments at comparatively lower temperatures without compromising on their chromatic properties.

Table 3.5. Effect of mineralizer on the color coordinates (±0.1) of $Sm_2Ce_{1.85}Pr_{0.15}O_7$

Mineralizer	Color coordinates					Band gap *(eV)*
	*L**	*a**	*b**	*C**	h°	
None	37.5	14.4	8.4	16.7	30.1	1.74
NaF	40.5	20.8	17.3	27.1	39.7	1.78
NaCl	41.3	20.8	17.4	27.1	39.9	1.79
CaF_2	37.5	16.8	10.0	19.5	30.9	1.75
H_3BO_3	36.6	14.0	9.0	16.7	32.6	1.76
Li_2CO_3	38.2	18.3	11.7	21.7	32.7	1.76

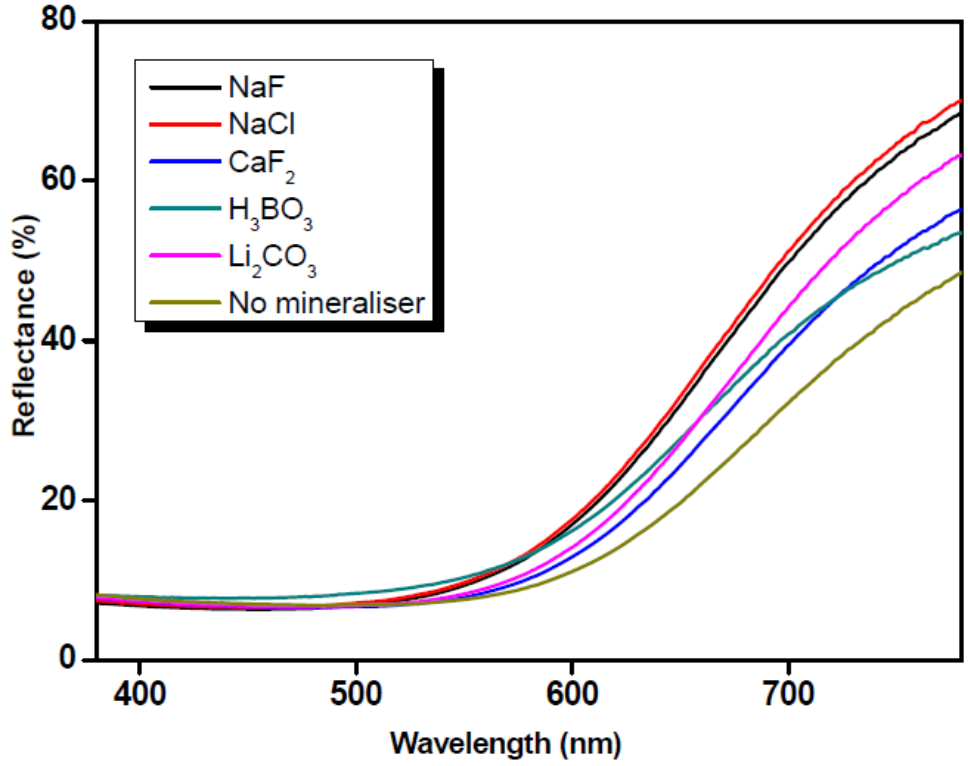

Fig. 3.15. Reflectance spectra of $Sm_2Ce_{1.85}Pr_{0.15}O_7$ pigments in presence of 1% mineralizer.

3.5 Conclusions

- Two new series of non–toxic inorganic pigments having the general formula $Sm_2Ce_{2-x}Mo_xO_{7+\delta}$ (x ranges from 0 to 0.4) and $Sm_2Ce_{2-x}Pr_xO_7$ (x ranges from 0 to 0.2) displaying wide range of colors from cream to yellow and brick–red to dark–brown, respectively, have been developed by traditional solid state route and well characterized.
- By incorporation of chromophore metal ion, Pr^{4+} for Ce^{4+}, in the host compound $Sm_2Ce_2O_7$, the absorption edge (450 nm) has been greatly shifted to the higher wavelengths (695 nm). Further, the position of the absorption edge critically depends on the concentration of Pr^{4+}. The coloring mechanism of Pr^{4+} doped $Sm_2Ce_2O_7$ pigments is based on the introduction of an additional electronic level of energy in cerianite forbidden band, arising from unpaired $4f^1$ electrons of praseodymium ions.
- The absorption edge has been gently changed from 450 nm to 490 nm in the presence of Mo^{6+}, due to O_{2p}–Mo_{4d} charge–transfer transitions.
- The present investigations establish that various color hues can be achieved by the incorporation of suitable chromophore metal ions in $Sm_2Ce_2O_7$ host lattice by tuning of the band gaps.
- The results also highlights that the calcination temperatures can be lowered by employing an appropriate mineralizer along with the precursor oxides.
- The currently developed inorganic pigments possess good thermal and chemical stability.

Chapter 4

Synthesis and characterization of non-toxic tantalum-doped ceria-zirconia mixed oxide yellow pigments: Surface coating studies

4.1 Summary

New inorganic pigments having the general formula $Ce_{1-(x+y)}Zr_xTa_yO_{2+\delta}$ (x ranges from 0.15 to 0.2 and y ranges from 0 to 0.05) displaying colors ranging from white to yellow have been synthesized by a traditional solid–state route, as viable alternatives to lead, cadmium and chromium based yellow toxic inorganic colorants. The products were characterized by X–ray powder diffraction, UV–vis diffuse reflectance spectroscopy and CIE–$L^*a^*b^*$ 1976 color scales. The coloring mechanism is based on the strong absorptions of the pigments in the visible region under 500 nm, which could originate from the additional energy level between O_{2p} valence band and the Ce_{4f} conduction band by forming a hybrid orbital of Ta_{5d} and O_{2p}. The designed yellow pigments consist of non–toxic elements and further found to be thermally and chemically stable. The utility of the designed pigment for surface coating applications is also evaluated.

Vishnu, **V. S.;** George, G.; Divya, V and Reddy, M. L. P. *Dyes Pigm. 82*, **2009**, 53–57.

4.2 Introduction

Thanks to their higher thermal and chemical stability compared to organic pigments, inorganic pigments are widely used in various applications such as paints, inks, ceramics, enamels and glasses (Pailhe *et al*. 2009; Buxbaum and Pfaff 2002). Although $PbCrO_4$, $PbMoO_4$, $Pb_2Sb_2O_7$ and CdS have been widely employed as conventional yellow inorganic pigments, the use of these pigments has been restricted because they contain toxic elements ([a]Badenes *et al*. 2002). Driven by national laws and regulations in the ecological and toxicological area, "sustainable development" and substitution pressures have resulted in the replacement of formerly well known and highly recommended inorganic pigments, by more "environmentally friendly" or less toxic substances. Rare earth–based yellow inorganic pigments cater an important class of environmentally benign inorganic pigments ([a]George *et al*. 2008; Rao and Reddy 2007; Gauthier *et al*. 2003; Jansen and Letschert 2000). Among these, pigments with a ceria host lattice has received due consideration. CeO_2 is a fluorite–structured oxide that can form extensive solid solutions with a variety of alien cations while retaining the fluorite crystal structure. The coloring mechanism is based on the charge–transfer band from O_{2p} to Ce_{4f} in the semi–conducting CeO_2. The band gap between the anionic O_{2p} valence band and the cationic Ce_{4f} conduction band can be modified by the formation of solid solutions, which introduces an additional electronic level between the valence and conduction bands. As a result a shift of the charge–transfer band is observed. Crystalline cerium molybdenum oxides have been reported as novel yellow pigments as alternatives to lead, cadmium and chromium based toxic pigments (Sreeram *et al*. 2007). The reflectance spectrum of the cerium double molybdates indicates strong absorption in both visible and ultraviolet regions, which could originate from the O_{2p}–Ce_{4f} and the O_{2p}–Mo_{3d} double charge transitions and as a result the pigments show yellow color. Earlier investigations reveal

that the classical toxic inorganic pigments can be replaced by solid solutions of perovskites $CaTaO_2N$ and $LaTaON_2$, which gives colors ranging from yellow to deep red (Jansen and Letschert 2000). However the synthesis procedure employed for the above pigments utilizes toxic gases for long periods. Therefore, research needs to be performed in developing novel yellow inorganic pigments with various advantages over traditional toxic pigment formulations.

Thus, the present chapter is focused on the development of a novel class of yellow pigments based on tantalum–doped $Ce_{0.8}Zr_{0.2}O_2$ systems as alternatives to the existing toxic inorganic pigments. The new pigments of the general formula $Ce_{1-(x+y)}Zr_xTa_yO_{2+\delta}$ (x ranges from 0.15 to 0.2 and y ranges from 0.00 to 0.05) have been synthesized by a traditional solid–state reactions of the respective oxides and characterized for their structure and optical properties. The typical designed pigment has also been evaluated for its surface coating applications.

4.3 Experimental Section

4.3.1 Materials and Methodology

Several compositions based on $Ce_{1-(x+y)}Zr_xTa_yO_{2+\delta}$ (x ranges from 0.15 to 0.2 and y ranges from 0.00 to 0.05) stoichiometry were prepared by the ceramic method. The precursors employed for the traditional ceramic pigment synthesis route are the corresponding oxides: CeO_2 (99.9%), ZrO_2 (99.9%) and Ta_2O_5 (99.9%) supplied by M/s. Sigma Aldrich. In this method, the reactants were mixed and homogenized by wet milling with acetone in an agate mortar for 30 min. The mixture was then calcined in platinum crucibles in an electric furnace at a temperature of 1300 °C for 6 h. The heating of the furnace was programmed to increase the temperature at 5 °C/min. In order to ensure the completion of the reaction, the calcinations process was repeated thrice for the

same sample. To refine and homogenize the particle size after calcinations, the resulting products were ground in an agate mortar.

4.3.2 Development of paint formulation

The typical pigment sample, $Ce_{0.8}Zr_{0.17}Ta_{0.03}O_{2+\delta}$ was ground, sieved to obtain the particles in the range of 25–45 μm and analyzed for its mass tone/hiding power and tinting strength. For this, a standard commercial paint composition consisting of a long oil alkyd as a binder, oleic acid as a plasticizer and aluminium stearate as a rheological agent was used. A paint formulation, consisting of 20 g (~ 27 wt.%) pigment, 50 g (~ 68 wt.%) resin, 3 g (~ 4 wt.%) plasticizer and 0.5 g (~ 0.7 wt.%) rheological agent, were mixed along with mineral turpentine in a ball mill for 60 min (Aby *et al.* 2007; [c]Sreeram *et al.* 2008). For tinting strength measurements, the pigment was replaced by a mixture of 15 g (~ 20 wt.%) TiO_2 and 5 g (~ 7 wt.%) pigment. The paint formulation thus developed was used for coating.

4.3.3 Characterization Techniques

The instrumental techniques employed for the characterization of various pigments designed in the present study are the same as that described in the previous chapter 2.

4.4 Results and Discussion

4.4.1 Powder X–ray diffraction analysis

Fig. 4.1 shows the powder X–ray diffraction patterns of the $Ce_{1-(x+y)}Zr_xTa_yO_{2+\delta}$ (x ranges from 0.15 to 0.2 and y ranges from 0.00 to 0.05) pigment samples. The XRD pattern of $Ce_{0.8}Zr_{0.2}O_2$ can be very well indexed to the cubic fluorite structure of CeO_2 with a lattice constant of 0.5363 nm. Addition of Zr^{4+} into CeO_2 produces intrinsic strain which results in a decrease of lattice parameter of CeO_2 from 0.5411 nm (JCPDF 34–394) to 0.5363 nm (Furukawa *et al*. 2008). This is due to the smaller ionic radii of Zr^{4+} (0.084 nm)

compared to Ce^{4+} (0.097 nm) (Shannon 1976). The decrease in lattice parameter further confirms the solid solution formation. The progressive substitution of Ta^{5+} for Zr^{4+} in $Ce_{0.8}Zr_{0.2}O_2$ solid solution, did not change the cell parameter values significantly since the ionic radii of Ta^{5+} (0.074 nm) is moderately smaller than Zr^{4+}. With the increase of tantalum doping in $Ce_{1-(x+y)}Zr_xTa_yO_{2+\delta}$ (x ranges from 0.17 to 0.15 and y ranges from 0.03 to 0.05) beyond 3%, a minor phase of $CeTaO_4$ has also been noticed from the XRD patterns along with the major cubic fluorite phase of $Ce_{0.8}Zr_{0.2}O_2$. The formation of the $CeTaO_4$ can be explained due to the low solubility of tantalum in ceria matrix at higher concentrations of tantalum (Clemente *et al*. 2005). Further, the minor peak observed in the XRD patterns of all the compositions at a 2θ of ~30 is due to the tetragonal phase of $Ce_{0.16}Zr_{0.84}O_2$ (JCPDF 38–1437) (Reddy *et al*. 2003). The presence of excess oxygen in the present system can be accommodated as structural oxygen and not as interstitial sites (van Roosmalen and Cordfunke 1991). The overstoichiometry due to oxygen is, therefore, compensated by cation vacancies. The defect equilibrium in ceria doped with Ta_2O_5, in terms of Kroger–Vink notation (Kroger *et al.* 1956) can be represented as

$$TaO_{2.5} = Ta_{Ce}^{\bullet} + e' + 2O_0^x + \frac{1}{4}O_{2(g)}$$

4.4.2 Particle size and morphological analysis

Fig. 4.2 refers to the SEM micrographs of typical pigment samples, $Ce_{0.8}Zr_{0.2}O_2$ and $Ce_{0.8}Zr_{0.18}Ta_{0.02}O_{2+\delta}$. The homogeneous nature of the pigments can be understood from the SEM images. From the SEM photograph, it is clear that there is an even grain distribution; the average grain size is less than 5 μm.

Color depends on several material properties of a pigment, among which particle size of the pigment is of prime importance. Decrease in particle size of the pigment increases the surface area which further contributes to high surface coverage, higher

number of reflectance points and hence more scattering. The particle size distribution of the typical pigment, $Ce_{0.8}Zr_{0.18}Ta_{0.02}O_{2+\delta}$ was investigated in water with calgon as the dispersing agent. The results reveal a distribution with 90% of the particles with size smaller than 7.54 μm, 50% smaller than 2.59 μm and 10% smaller than 0.36 μm. The mean particle diameter of the pigment sample was found to be 5.65 μm.

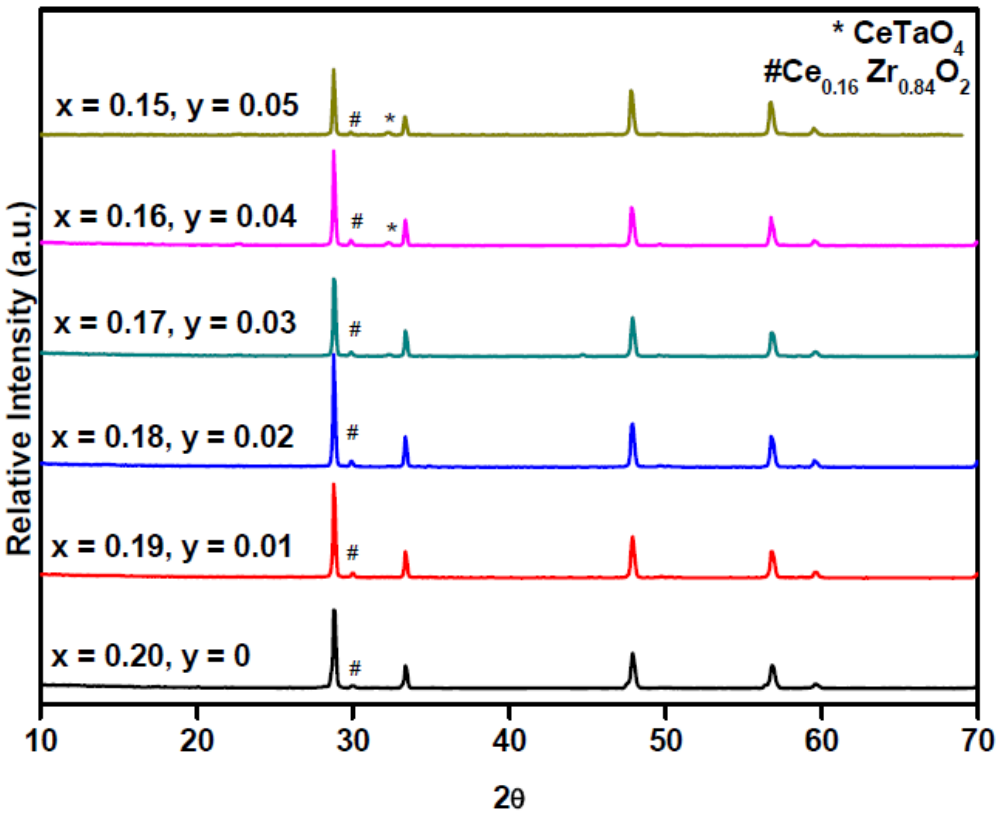

Fig. 4.1. X–ray diffraction patterns of $Ce_{1-(x+y)}Zr_xTa_yO_{2+\delta}$ (x ranges from 0.15 to 0.2 and y ranges from 0.00 to 0.05) pigments.

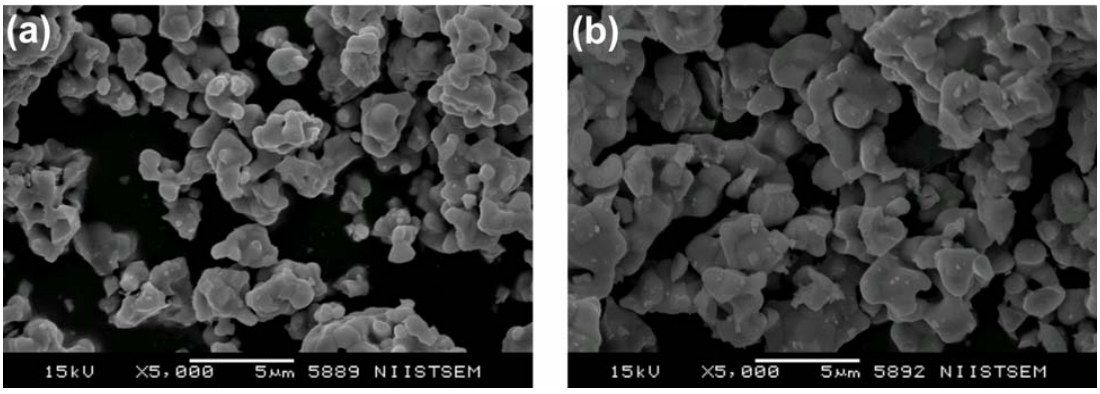

Fig. 4.2. SEM micrographs of (a) $Ce_{0.8}Zr_{0.2}O_2$ and (b) $Ce_{0.8}Zr_{0.18}Ta_{0.02}O_{2+\delta}$.

4.4.3 Optical properties of tantalum doped $Ce_{0.8}Zr_{0.2}O_2$ pigments

The effect of tantalum doping on the optical properties of $Ce_{0.8}Zr_{0.2}O_2$ was analyzed from the diffuse reflectance spectra of the pigment samples (Fig. 4.3). The corresponding absorption spectrum is given as Fig. 4.4. The optical absorption edge critically depends on the concentration of tantalum present in the pigment samples and all these samples absorb blue light efficiently, which is originated from the O_{2p}–Ce_{4f} charge transitions. As a result, the color of the pigment samples becomes yellow because blue is a complimentary color to yellow (Fig. 4.5). Furthermore, the doping of Ta^{5+} into the CeO_2–ZrO_2 lattice will result in an additional energy level between O_{2p} valence band and the Ce_{4f} conduction band by forming a hybrid orbital of Ta_{5d} and O_{2p} (Arranz *et al*. 2002).

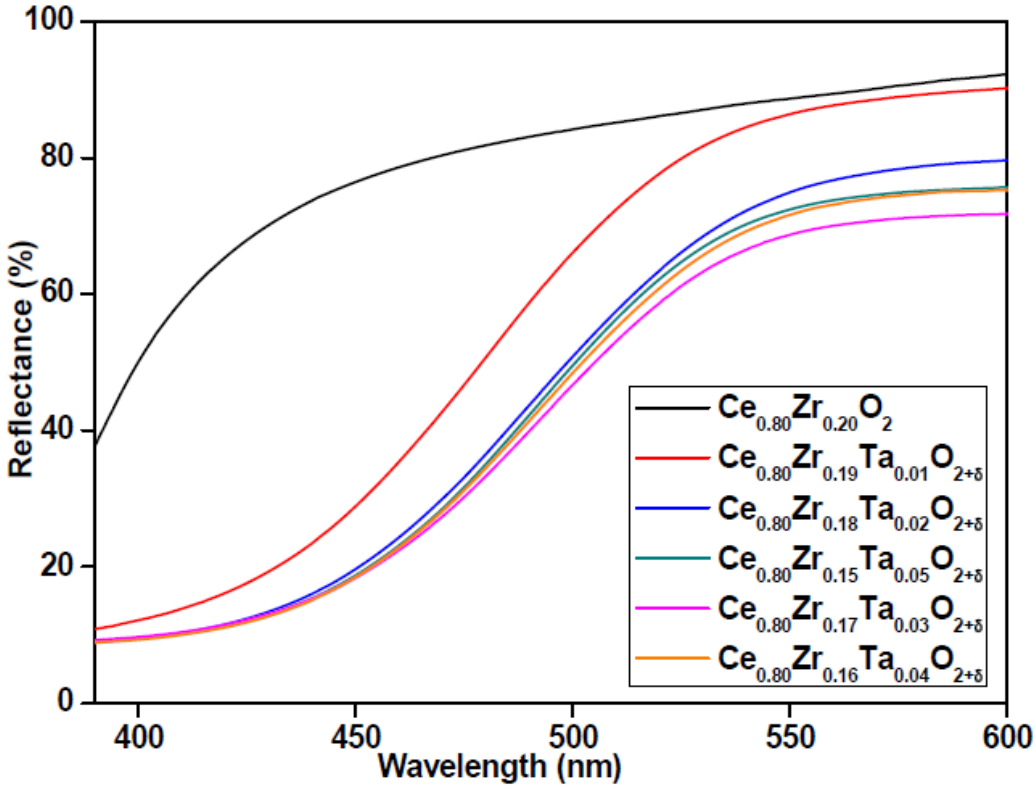

Fig. 4.3. Reflectance spectra of $Ce_{1-(x+y)}Zr_xTa_yO_{2+\delta}$ powder pigments.

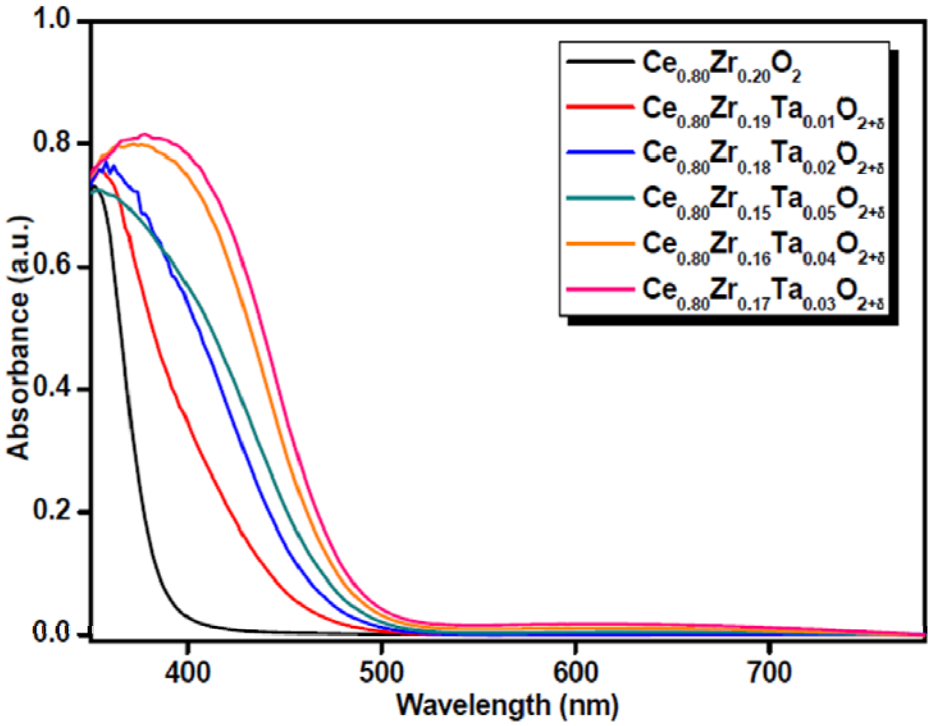

Fig. 4.4. Absorption spectra of $Ce_{1-(x+y)}Zr_xTa_yO_{2+\delta}$ powder pigments.

The band gap of the colorants as determined from the absorbance spectra is given in Table 4.1 and was obtained simply by a straightforward extrapolation method ([b]George *et al*. 2008). It can be clearly seen that the band gap of the $Ce_{0.8}Zr_{0.2}O_2$ (3.0 eV) decreases to 2.34 eV with the progressive doping of Ta^{5+} for Zr^{4+} in $Ce_{1-(x+y)}Zr_xTa_yO_{2+\delta}$ (x ranges from 0.17 to 0.20 and y ranges from 0 to 0.03) samples. Thus the color of the pigment samples gently changes from white to yellow. On the other hand, the band gap of the colorants moderately increases above 3% doping of tantalum due to the formation of minor phase of $CeTaO_4$.

Fig. 4.5. Photographs of $Ce_{0.8}Zr_{0.2}O_2$ and $Ce_{0.8}Zr_{0.17}Ta_{0.03}O_{2+\delta}$ pigments.

The CIE 1976 color coordinates of the powdered pigments are summarized in Table 4.1. The increase of b^* value with the increase of dopant concentration from $y = 0$ to 0.03 in $Ce_{0.8}Zr_{0.2}O_2$, indicates that the color of the pigment gently changes to yellow. It can be seen that there is no appreciable change in a^* which is responsible for the green tinge of the pigment sample after the progressive doping of tantalum into $Ce_{0.8}Zr_{0.2}O_2$. At higher tantalum concentrations, the chroma of the pigment decreases slightly may be due to the formation of minor phase of $CeTaO_4$ (Clemente *et al*. 2005). The color coordinates of the typical pigment, $Ce_{0.8}Zr_{0.17}Ta_{0.03}O_{2+\delta}$ (L^* = 86.7, a^* = –9.2, b^* = 54.7, C^* = 55.5, $h°$ = 80.5), especially the chroma was found to be much higher than that of the commercially available pigment (L^* = 90.0, a^* = –3.5, b^* = 43.3, C^* =43.5, $h°$ = 85.4) Zircon Yellow (Zircon 1561: $(Zr,Pr)SiO_4$ of M/s Kawamura Chemicals, Japan). However, the chroma of the present pigment samples is found to be inferior to that of commercial cadmium yellow (L^* = 75.7, a^* = –7.9, b^* = 99.1, C^* = 99.4, $h°$ = 85.4) (Jansen and Letschert 2000). The hue angles ($h°$) of the present pigments were found to be in the yellow region of the cylindrical color space.

Table 4.1. The color coordinates (±0.1) of the $Ce_{1-(x+y)}Zr_xTa_yO_{2+\delta}$ (x ranges from 0.15 to 0.2 and y ranges from 0.00 to 0.05) pigments and band gap values

Pigment composition	Color coordinates					Band gap
	*L**	*a**	*b**	*C**	*h*º	*(eV)*
$Ce_{0.8}Zr_{0.2}O_2$	97.9	–2.2	12.1	12.3	79.5	3.00
$Ce_{0.8}Zr_{0.19}Ta_{0.01}O_{2+\delta}$	90.4	–10.4	49.2	50.3	78.1	2.40
$Ce_{0.8}Zr_{0.18}Ta_{0.02}O_{2+\delta}$	87.0	–10.9	52.0	53.1	78.2	2.38
$Ce_{0.8}Zr_{0.17}Ta_{0.03}O_{2+\delta}$	86.7	–9.2	54.7	55.5	80.5	2.34
$Ce_{0.8}Zr_{0.16}Ta_{0.04}O_{2+\delta}$	83.6	–9.0	52.3	53.0	80.2	2.35
$Ce_{0.8}Zr_{0.15}Ta_{0.05}O_{2+\delta}$	82.6	–9.8	50.6	51.6	79.0	2.36

4.4.4 Thermal and chemical stability studies of the pigments

It is clear from the TG/DTA analysis (Fig. 4.6) of the typical pigment $Ce_{0.8}Zr_{0.16}Ta_{0.04}O_{2+\delta}$ that there is no loss of weight and phase transformation in the temperature range 50–1000 °C.

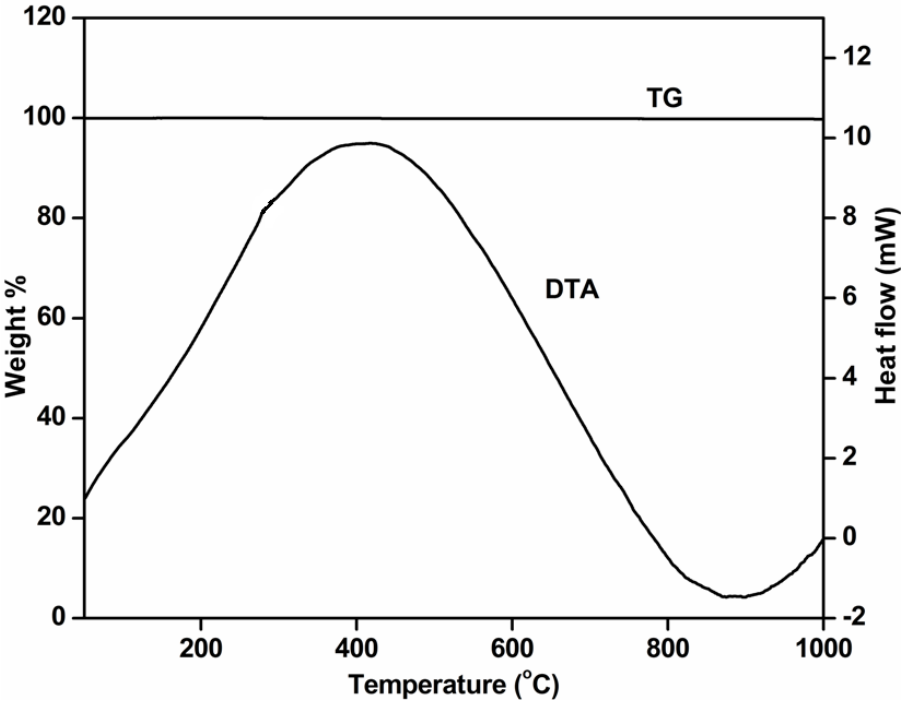

Fig. 4.6. TG/DTA of $Ce_{0.8}Zr_{0.16}Ta_{0.04}O_{2+\delta}$ pigment.

The typical pigment $Ce_{0.8}Zr_{0.18}Ta_{0.02}O_{2+\delta}$ was tested for its acid and alkali resistances. A pre–weighed quantity of the pigment was treated with 10% $HCl/H_2SO_4/HNO_3$ and NaOH, and soaked for half an hour with constant stirring using a magnetic stirrer. The pigments were then filtered, washed with water, dried and weighed. Negligible weight loss was noticed for the range of acids and alkali tested. The typical total color difference value (ΔE^*_{ab}) (Buxbaum and Pfaff 2005) after acid and alkali resistance tests were found to be negligible (ΔE^*_{ab} = 1.3 for HNO_3; ΔE^*_{ab} = 1.2 for H_2SO_4; ΔE^*_{ab} = 0.9 for HCl and ΔE^*_{ab} = 0.7 for NaOH). Thus the designed yellow pigments are found to be chemically and thermally stable.

4.4.5 Evaluation of mass tone/hiding power and tinting strength

The hiding power and tinting strength was evaluated by coating on an opacity chart at a thickness of 150 μm (Fig. 4.7). The CIELAB 1976 method of determination of *L**, *a** and *b** was employed to determine the hiding power and tinting strength of the colorants

by comparison of values when coated on a board with a checkered, white and black background and the results are summarized in Table 4.2. The color difference has been quantified on the CIELAB based color difference (ΔE_{ab}*), which is calculated using the equation (CIE 1986; CIE 2004; Ohno 2000).

$$\Delta E^*_{ab} = [(\Delta L^*)^2+(\Delta a^*)^2+(\Delta b^*)^2]^{½}$$

Table 4.2. The color coordinates (±0.1) of the $Ce_{0.8}Zr_{0.17}Ta_{0.03}O_{2+\delta}$ yellow powder pigment after hiding power and tinting strength analysis on a white and black surface

Surface	Hiding power				Tinting strength			
	L^*	a^*	b^*	ΔE^*_{ab}	L^*	a^*	b^*	ΔE^*_{ab}
Powder	86.7	–9.2	54.7	–	86.7	–9.2	54.7	–
Black	75.6	–5.9	48.3	13.2	87.4	1.8	22.6	32.9
White	84.4	–7.1	53.2	3.5	86.8	–5.7	27.8	27.1

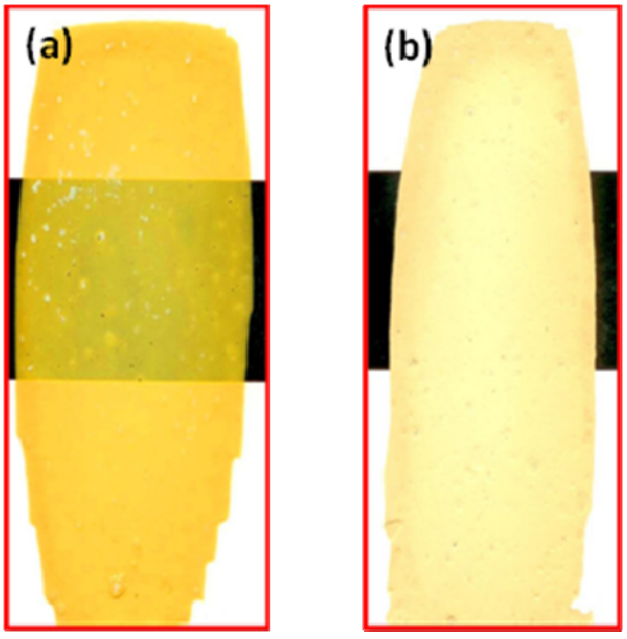

Fig. 4.7. Photographs of (a) hiding power and (b) tinting strength of $Ce_{0.8}Zr_{0.17}Ta_{0.03}O_{2+\delta}$ yellow pigment.

For mass tone, the color difference (ΔE^*_{ab}) between the white and black surfaces is 10.14 as against 8.95 for an industrial sample reported elsewhere (Aby *et al*. 2007). For the tinting strength, the color difference between the black and white regions was found

to be 6.52, as against 4.5 for the industrial sample (Aby *et al*. 2007). A reasonably lower value of ΔE^*_{ab} for the mass tone on the black vs the white region is indicative of the ability of the colorant to cover black and white regions uniformly well. Still lower values were obtained when tinted with TiO_2. Nevertheless, the color difference between the tinted and untinted colorants is high (Table 4.2), indicating the poor ability of the colorant to transfer its color completely to TiO_2.

4.4.6 Weather resistance studies

The typical paint formulation consisting of $Ce_{0.8}Zr_{0.17}Ta_{0.03}O_{2+\delta}$, was coated on a board with a checkered, white and black background and evaluated for its weather resistance by exposing to natural sunlight (12 h exposure, 45° angle facing the sun, 30 days). The CIELAB 1976 method of determination of *L**, *a** and *b** was employed to determine the weather resistance of the colorants by comparison of values when coated on a board with a checkered, white and black background against unexposed sample and the results are depicted in Table 4.3. The color coordinates were measured in the interval of five days. The negligible values of ΔE^*_{ab} reveal that the pigments posses good weather stability.

Table 4.3. The color coordinates (±0.1) of the white/black surface coated with $Ce_{0.8}Zr_{0.17}Ta_{0.03}O_{2+\delta}$ yellow pigment after exposed to sunlight

Time duration	White surface				Black surface			
	*L**	*a**	*b**	ΔE^*_{ab}	*L**	*a**	*b**	ΔE^*_{ab}
Unexposed sample	84.4	–7.1	53.2	–	75.6	–5.9	48.3	–
Day 5	84.3	–7.2	53.5	0.33	75.9	–6.2	48.4	0.44
Day 10	84.1	–7.0	52.9	0.43	75.7	–6.2	48.6	0.44
Day 15	83.9	–6.9	53.0	0.57	75.8	–6.1	48.9	0.66
Day 20	84.0	–7.3	53.2	0.44	75.9	–6.3	48.8	0.70
Day 25	83.8	–7.2	53.1	0.61	75.8	–6.1	48.7	0.49
Day 30	83.9	–7.1	53.3	0.50	75.7	–6.2	48.9	0.67

4.5 Conclusions

- Novel non–toxic inorganic pigments displaying colors ranging from white to yellow based on the general formula $Ce_{1-(x+y)}Zr_xTa_yO_{2+\delta}$ (x ranges from 0.15 to 0.2 and y ranges from 0 to 0.05) have been successfully designed and evaluated for surface coating applications.
- The coloring mechanism is based on the shift of the charge transfer band of CeO_2 to higher wavelengths, by introducing an additional energy level between O_{2p} valence band and the Ce_{4f} conduction band by forming a hybrid orbital of Ta_{5d} and $O_{2p.}$
- The synthesized powder pigment samples are found to possess thermal, chemical and weather stability.
- The hiding power of the yellow pigment was found to be good on a white surface. However the hiding power was not satisfactory on a black surface.

Chapter 5

Novel environmentally benign yellow inorganic pigments based on solid solutions of samarium–transition metal mixed oxides

5.1 Summary

A new class of environmentally benign yellow inorganic pigments having the general formula $Sm_{6-x}W_{1-y}Zr_xMo_yO_{12+\delta}$ (*x* ranges from 0 to 0.6 and *y* ranges from 0 to 1) have been synthesized by simple solid state route and characterized by various spectroscopic techniques. The systematic substitution of Mo^{6+} for W^{6+} in Sm_6WO_{12} gently shifted the absorption edge from 374 nm to 460 nm and consequently the designed compounds exhibit colors ranging from white to yellow. The band gap of the resultant pigments varied from 3.29 to 2.69 eV. The coloring mechanism is based on the O_{2p}–Mo_{4d} charge transfer transitions. Furthermore, the doping of Zr^{4+} for Sm^{3+} in Sm_6MoO_{12} lattice produced intrinsic strain, which further red shifted the absorption edge to 479 nm. This intensified the yellow hue of the resultant compounds with band gap decreasing to 2.58 eV. The designed pigments possess good chromatic properties, especially the hue angle which is found to be similar to those observed for industrial pigments such as $PbCrO_4$, $BiVO_4$, CdS, $NiTiO_3$ and praseodymium yellow and also show thermal and chemical stabilities. The coloring performance of the developed yellow pigments was evaluated by incorporating it into a polymer substrate material.

Vishnu, **V. S.**; Jose, S and Reddy, M. L. P. *J. Am. Ceram. Soc. 94*, **2011**, 997–1001

5.2 Introduction

Natural and synthetic inorganic pigments produced and marketed as fine powders are an integral part of many decorative and protective coatings and are used for mass coloration of many materials (Kar *et al*. 2005). Inorganic pigments are traditionally based on toxic metal ions (Smith 2002). Nevertheless, due to the high toxicity of these elements, research on ceramic pigments has lately been dedicated to improve traditional coloured systems from an environmental point of view and maintaining their colouring properties and technological requirements (Martos *et al*. 2007). Substitution of toxic elements by lanthanide ions represents an alternative and successful way to prepare more environmentally benign colored materials ([a]Martos *et al*. 2008). Doping a structure using metal species is one of the most frequently adopted practices to induce modifications, not only in its structural characteristics, but also in its composition and reactivity. Recent investigations reveal the utility of rare earth–transition metal mixed oxides as a host material for non–toxic inorganic pigments (George *et al*. 2011; Furukawa *et al*. 2006; Sreeram *et al*. 2007; Masui *et al*. 2006). The band gap of these oxides can be engineered to realize different color hues by suitable substitution of a chromophore metal ion.

Amorphous cerium tungstate, $Ce_{1-x}M_xW_2O_8$ (M = Zr or Ti, $0 \leq x \leq 0.6$) has been reported as a possible ecological inorganic yellow pigment. This pigment exhibits yellow color due the effective absorptions in the visible and ultraviolet regions (under 500 nm efficiently), which is originated from the O_{2p}–Ce_{4f} and the O_{2p}–W_{5d} double charge transitions (Furukawa *et al*. 2006). However, the concentration of tungsten metal ion used in the design of these pigments is significantly very high (66%). Moreover these pigments carry a slight red hue. An yellow pigment based on samarium sesquisulphide, suitable for the coloration of polymer substrates has been reported elsewhere (Busnot and Macaudiere 2002); but the preparation process consists in reacting starting compounds

with a gaseous mixture of hydrogen sulphide and of carbon disulphide. Praseodymium yellow is a renowned inorganic pigment which has been widely used in the industry for coloring of ceramics (Hill *et al*. 2000; Blonski 1994). Yet the hue angle values of these colorants deviate considerably from that of an ideal yellow hue. Keeping in mind the foregoing considerations, in the current work a series of novel yellow colored pigments of the formula $Sm_{6-x}W_{1-y}Zr_xMo_yO_{12+\delta}$ (x ranges from 0 to 0.6 and y ranges from 0 to 1) were developed and utilized to evaluate their use as colorants for plastics.

5.3 Experimental Section

5.3.1 Materials and Methodology

Ten compositions based on the general formula $Sm_{6-x}W_{1-y}Zr_xMo_yO_{12+\delta}$ (x ranges from 0 to 0.6 and y ranges from 0 to 1) were prepared by traditional solid state route using Sm_2O_3 (99.9 %), WO_3 (99.9 %), ZrO_2 (99.9 %) and $(NH_4)_6Mo_7O_{24}\cdot 4H_2O$ (99.9%) supplied by M/s. Sigma Aldrich as precursors at an optimized temperature of 1600 ^oC for 3 h in air atmosphere (heating rate 5 °C/min).The calcination process was repeated five times with intermittent grinding to ensure the completion of the reaction and to improve the color properties. The as–synthesized powders were refined and homogenized in an agate mill after the heat treatment. Satisfactory phase purity and better chromatic properties were obtained at the aforesaid calcination conditions.

5.3.2 Coloration of plastics

The coloring performance of the pigment was evaluated after incorporating it into a polymer substrate like poly(methyl methacrylate) (PMMA; Sigma Aldrich) using the typical pigment having the best chromatic properties, $Sm_{5.4}Zr_{0.6}MoO_{12+\delta}$. A viscous solution of PMMA with the pigment (4–12 wt%) was prepared with Acralyn cold curing liquid (Asian Acrylates, India) and the thick paste was allowed to set in cylindrical

molds. Each side of the polymer compact was lapped using a fine–grade emery sheet for obtaining a polished surface. The intensity of the color of polymer disc depended on the concentration of the pigment being incorporated.

5.3.3 Characterization Techniques

The instrumental techniques employed for the characterization of various pigments designed in the present study are the same as that described in the previous chapter 2.

5.4 Results and Discussion

5.4.1 Powder X–ray diffraction analysis

Fig. 5.1 summarizes the XRD patterns of the $Sm_{6-x}W_{1-y}Zr_xMo_yO_{12+\delta}$ (x = 0 and y ranges from 0 to 1) pigments. All the XRD patterns correspond to the characteristic reflection of the ordered defect fluorite structure of Sm_6WO_{12} with a lattice constant of 0.5419 nm (JCPDF 16–414). Systematic substitution of Mo^{6+} ions for W^{6+} into the lattice of Sm_6WO_{12} moderately enhances the lattice constant to 0.5438 nm. However, a significant change in lattice parameter was not observed because the ionic radii of W^{6+} and Mo^{6+} (0.060 and 0.059 nm, respectively) are almost close to each other (Shannon 1976).

The XRD patterns of $Sm_{6-x}W_{1-y}Zr_xMo_yO_{12+\delta}$ (y = 1 and x ranges from 0 to 0.6) are shown in Fig. 5.2. Analysis revealed that all patterns are symmetric in nature and match well with the sole presence of the fluorite type cubic phase of Sm_6MoO_{12} [JCPDF 24–1121]. From the XRD patterns it could be noted that doping of Sm_6MoO_{12} with Zr^{4+} leads to shifting of diffraction peaks to higher angle side. Furthermore, no peaks were observed corresponding to the precursor oxides. This distinct feature compared with the pure Sm_6MoO_{12} can be explained due to solid solution formation. The addition of Zr^{4+} ions for Sm^{3+} in Sm_6MoO_{12} decreases the lattice parameter from 0.5438 nm to 0.5396 nm. The contraction of the crystal lattice is expected as Zr^{4+} (0.084 nm) is smaller than

Sm^{3+} (0.096 nm). The sharp and intense peaks in both the XRD patterns reveal the crystalline nature of the phase.

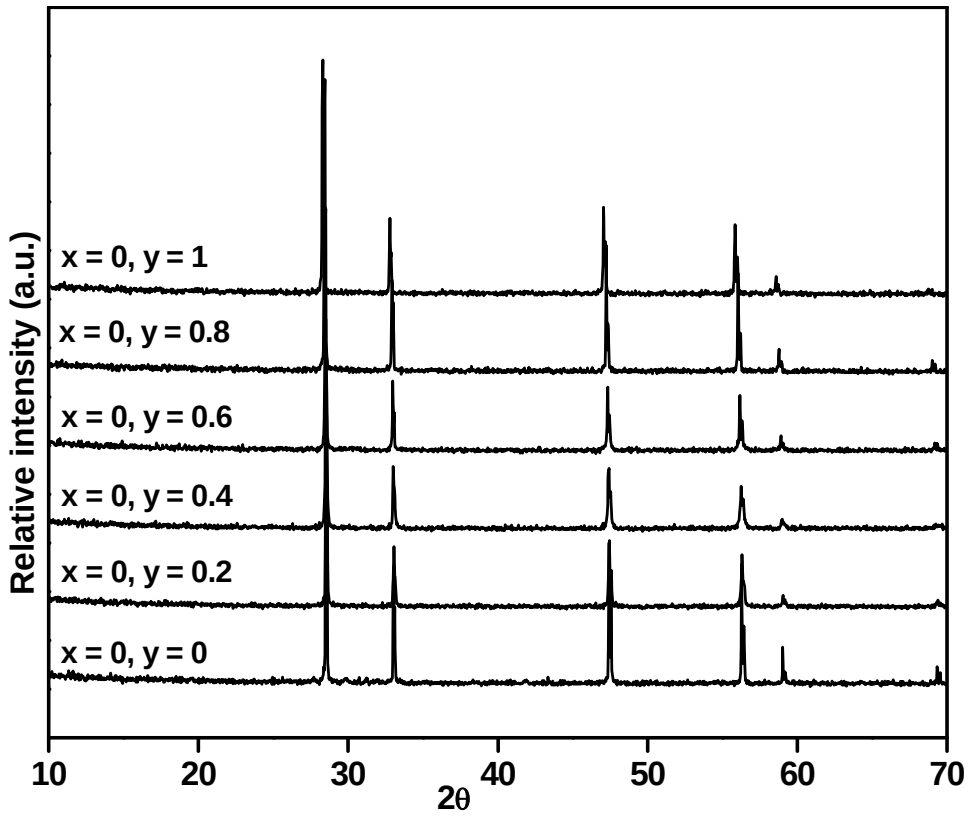

Fig. 5.1. XRD patterns of $Sm_{6-x}W_{1-y}Zr_xMo_yO_{12+\delta}$ (x = 0 and y ranges from 0 to 1).

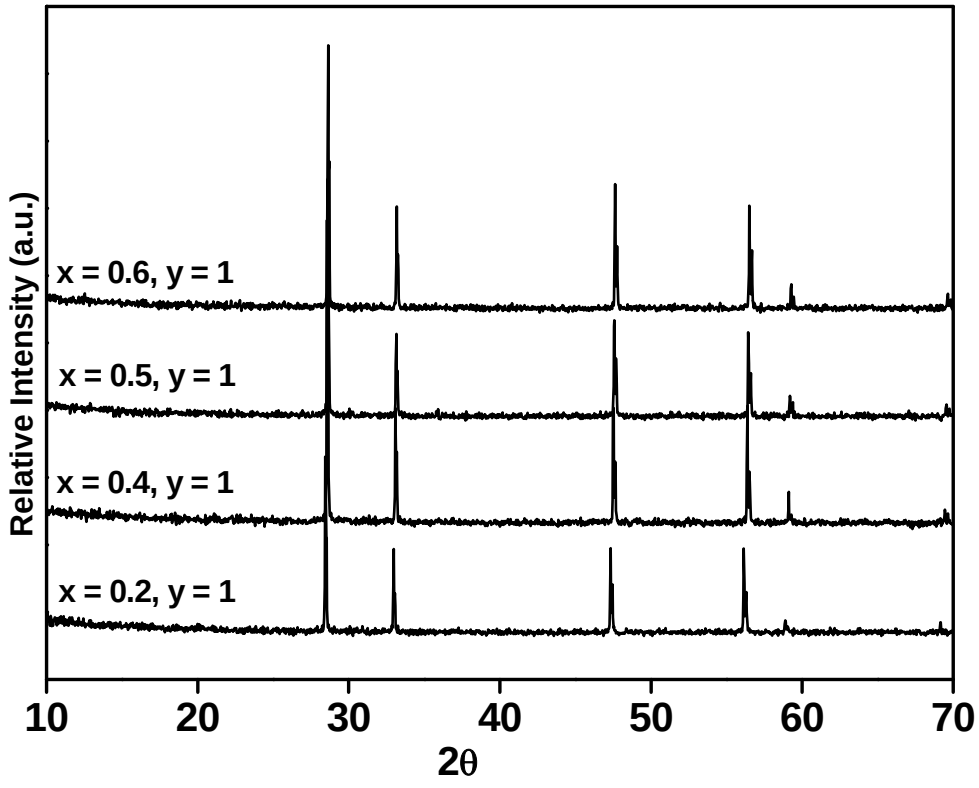

Fig. 5.2. XRD patterns of $Sm_{6-x}W_{1-y}Zr_xMo_yO_{12+\delta}$ (y = 1 and x ranges from 0.2 to 0.6).

5.4.2 Particle size and morphological analysis

Particle size analysis of the pigments using the representative samples Sm_6WO_{12}, Sm_6MoO_{12} and $Sm_{5.4}Zr_{0.6}MoO_{12+\delta}$ revealed a mean diameter of 8 μm, 9.73 μm and 10.78 μm, respectively. The distribution of particle sizes of these pigments is compiled in Table 5.1. The average particle size of the pigments as observed from the SEM images shown in Fig. 5.3 is less than 10 μm, which matches well with the results obtained from particle size analysis.

Table 5.1. Distribution of particle sizes of representative pigment samples

Sample	d_{90} (μm)	d_{50} (μm)	d_{10} (μm)	Mean diameter (μm)
Sm_6WO_{12}	1.63	6.14	18.09	8.00
Sm_6MoO_{12}	1.71	6.93	19.25	9.73
$Sm_{5.4}Zr_{0.6}MoO_{12+\delta}$	1.64	8.40	23.07	10.78

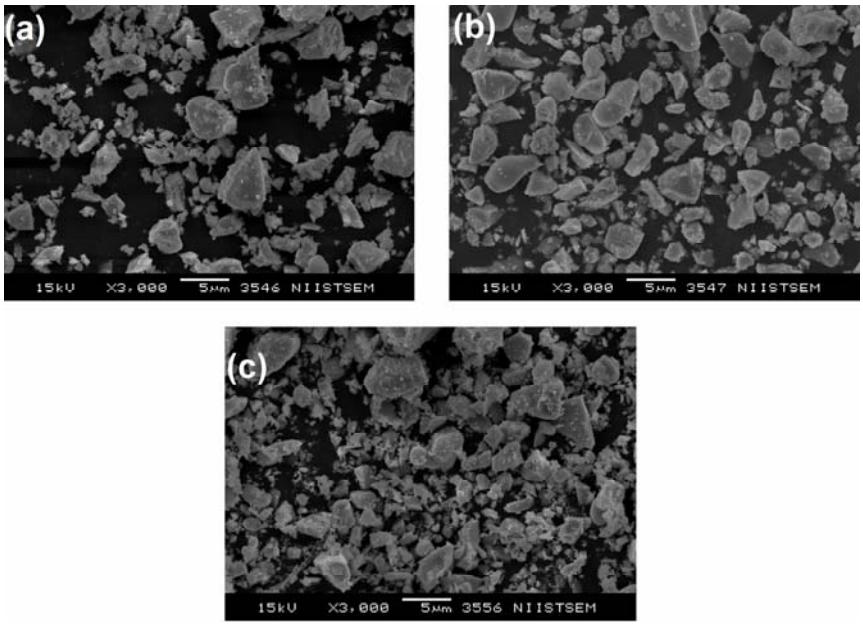

Fig. 5.3. SEM micrographs of (a) Sm_6WO_{12}, (b) Sm_6MoO_{12} and (c) $Sm_{5.4}Zr_{0.6}MoO_{12+\delta}$.

5.4.3 UV–vis spectroscopy

The diffuse reflectance spectra of the $Sm_{6-x}W_{1-y}Zr_xMo_yO_{12+\delta}$ (x = 0 and y ranges from 0 to 1) pigments in the UV–vis region displayed in Fig. 5.4 reveal a strong absorption at <

375 nm and is attributed to the $O^{2-} \rightarrow Sm^{3+}$ charge transfer transition in Sm_6WO_{12} (Han *et al.* 2007). Besides this, weak absorptions corresponding to *f–f* transitions of Sm^{3+} are also noticed in the visible region at ~ 404, 422, 469, 486, 528 and 568 nm. These can be assigned to the $^6H_{5/2} \rightarrow {}^6P_{3/2}$, $^4P_{5/2}$, $^4I_{13/2}$, $^4I_{11/2}$, $^4I_{9/2}$, $^4F_{3/2}$ and $^4G_{5/2}$ transitions of Sm^{3+}, respectively (Carnal *et al.* 1968). The main feature of the spectra is the shift in the absorption band from the UV region to 441 nm leading to a change in color of the pigment from white to greenish–yellow with the doping of 2.9 mol% of Mo^{6+}. More and more substitution of Mo^{6+} (14.3 mol%) for W^{6+} further red shifts the absorption edge, and reaches 460 nm upon complete replacement of W^{6+} with Mo^{6+} resulting in its yellow color. This observation can be explained on the basis of $O^{2-} \rightarrow Mo^{6+}$ charge transfer transitions. The change in color is also evident from the decrease in band gap of Sm_6WO_{12} from 3.29 eV to 2.69 eV with the formation of Sm_6MoO_{12} compound. The band gaps of the powder pigments were obtained from the absorption spectra (Fig. 5.5) by a straight forward extrapolation method ([b]George *et al.* 2008) and are given in Table 5.2.

The UV–vis diffuse reflectance and the corresponding absorption spectra of $Sm_{6-x}W_{1-y}Zr_xMo_yO_{12+\delta}$ (y = 1 and x ranges from 0 to 0.6) powder pigments is shown in Figs. 5.6. and Fig. 5.7, respectively. Doping of Zr^{4+} for Sm^{3+} shifts the $O^{2-} \rightarrow Mo^{6+}$ charge transfer absorption edge of Sm_6MoO_{12} to 479 nm and intensifies the yellow hue of the pigment. Introduction of Zr^{4+} into the lattice produces intrinsic strain, which will affect the O_{2p} valence band (Furukawa *et al.* 2008). This leads to an improvement of yellow hue of the pigment (Fig. 5.8). The increase in yellow hue of the pigment is also manifested by the change in band gap of the pigment from 2.69 eV (0 mol% of Zr^{4+}) to 2.58 eV (8.6 mol% of Zr^{4+}) as depicted in Table 5.2.

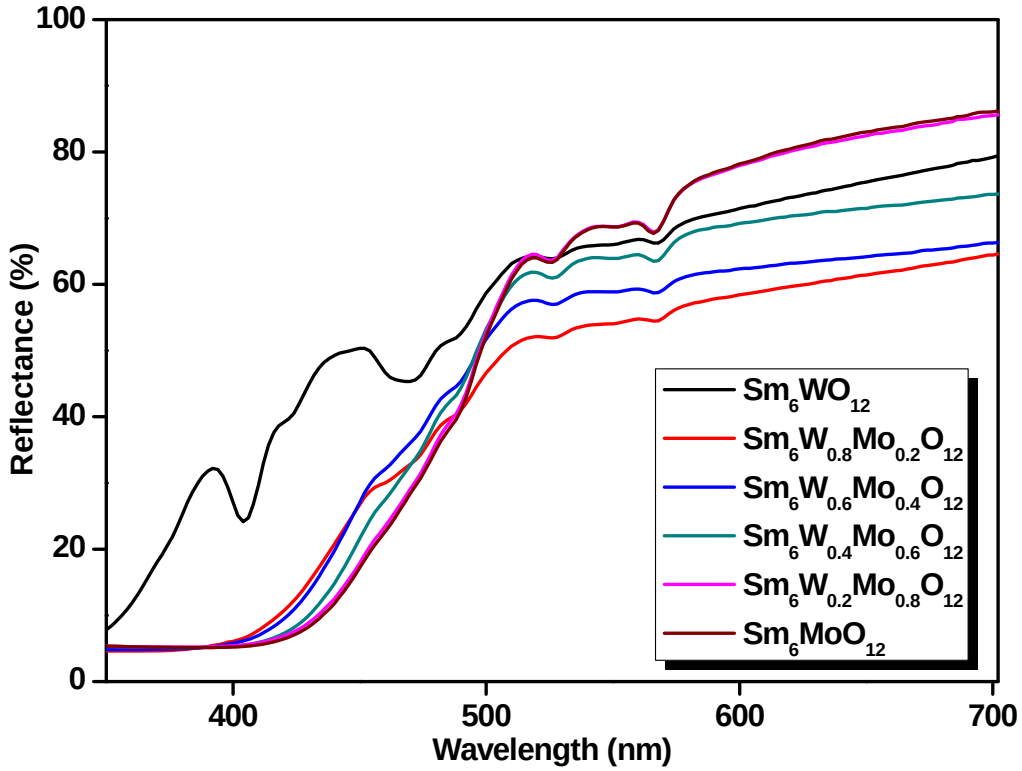

Fig. 5.4. Diffuse reflectance spectra of $Sm_{6-x}W_{1-y}Zr_xMo_yO_{12+\delta}$ (x = 0 and y = 0 to 1).

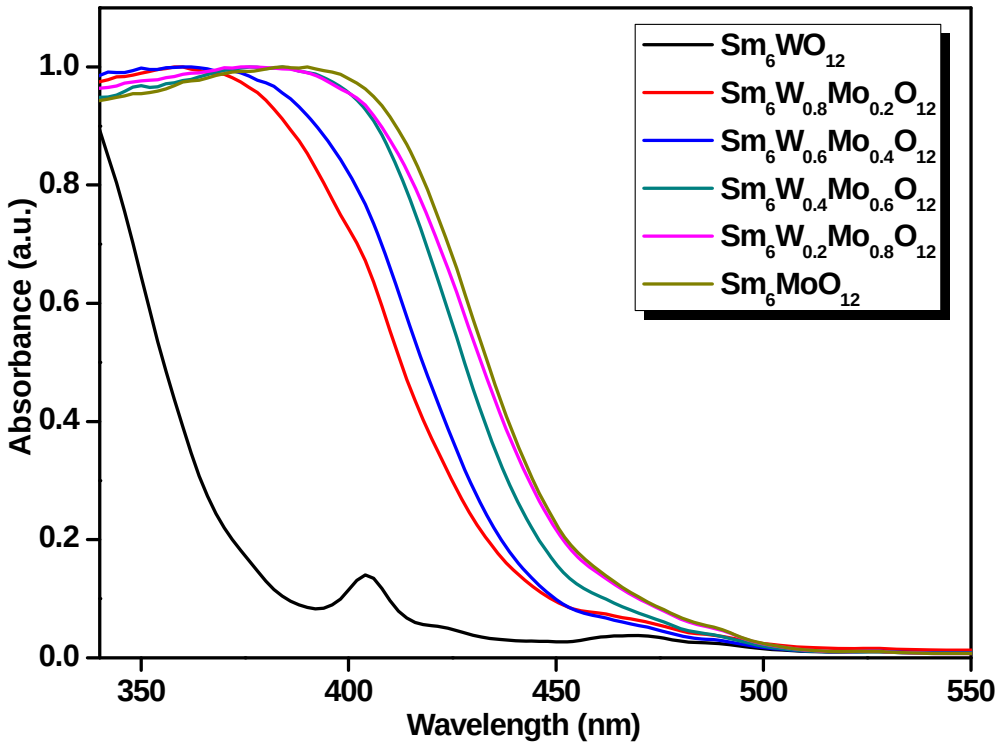

Fig. 5.5. Absorption spectra of $Sm_{6-x}W_{1-y}Zr_xMo_yO_{12+\delta}$ (x = 0 and y = 0 to 1).

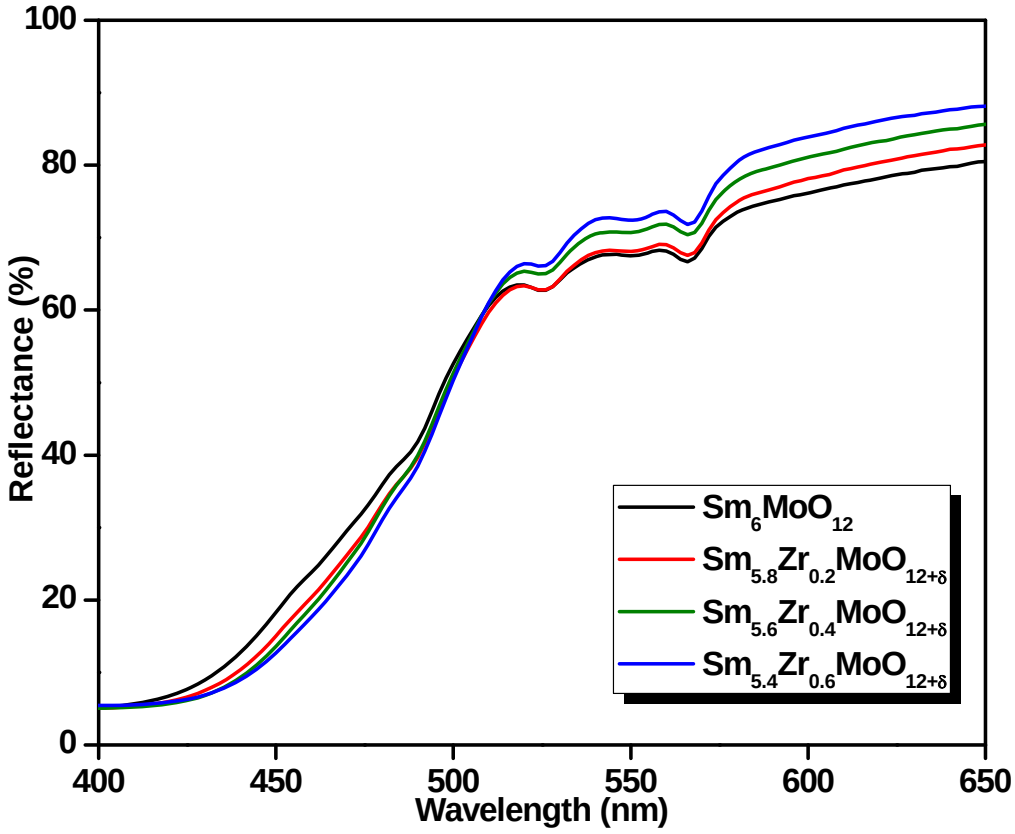

Fig. 5.6. Diffuse reflectance spectra of $Sm_{6-x}W_{1-y}Zr_xMo_yO_{12+\delta}$ (y = 1 and x ranges from 0 to 0.6).

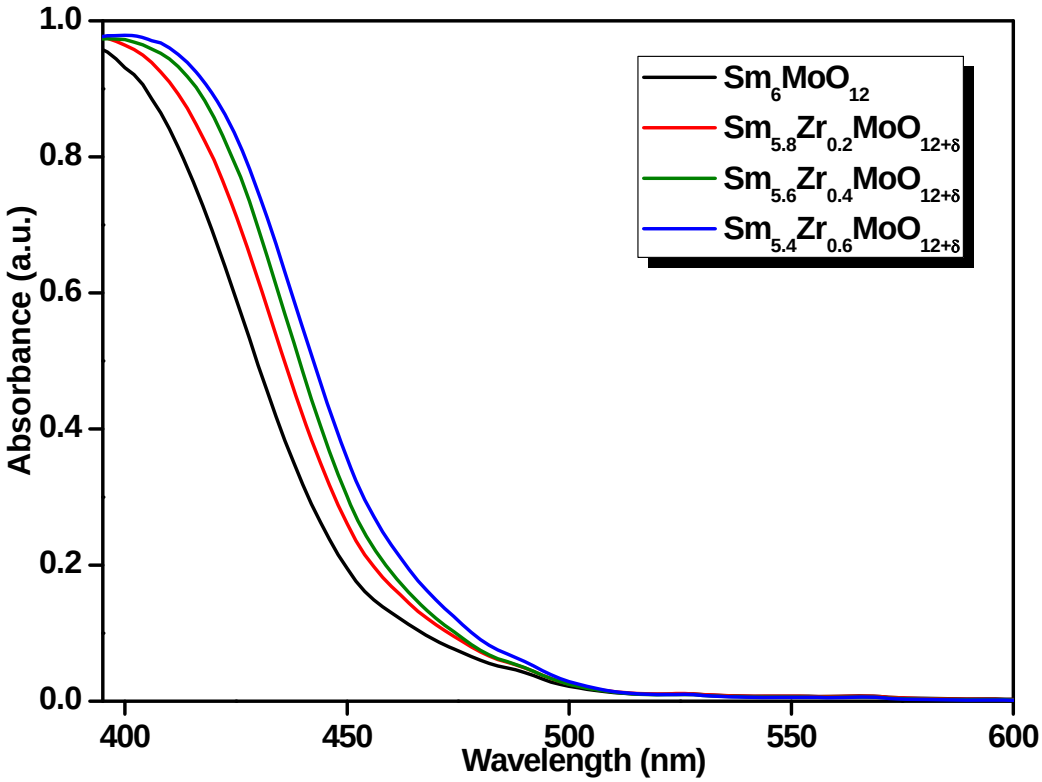

Fig. 5.7. Absorption spectra of $Sm_{6-x}W_{1-y}Zr_xMo_yO_{12+\delta}$ (y = 1 and x ranges from 0 to 0.6).

Fig. 5.8. Photographs of (a) Sm_6WO_{12}, (b) Sm_6MoO_{12} and (c) $Sm_{5.4}Zr_{0.6}MoO_{12+\delta}$.

5.4.4 Color characterization

The influence of time duration of heat treatment on the color coordinates (L^*, a^* and b^*) was analyzed using three representative pigment samples, Sm_6WO_{12}, Sm_6MoO_{12} and $Sm_{5.4}Zr_{0.6}MoO_{12+\delta}$ being calcined at 1600 °C for 3–15 h and the results are depicted in Figs. 5.9, 5.10 and 5.11, respectively. It was found that the time duration had negligible influence on the color coordinates of Sm_6WO_{12}. Conversely, for Sm_6MoO_{12} and $Sm_{5.4}Zr_{0.6}MoO_{12+\delta}$ pigments, the duration of calcination time played a noticeable role in the a^* and b^* values. A steady decrease in the green component ($-a^*$) and a systematic increase in the yellow component (b^*) was noticed in both the cases with increasing calcination time. However, the time duration has not influenced the brightness (L^*) of the pigments significantly. Hence it can be concluded that the calcination time duration has a profound influence in deciding the yellow hue and the best chromatic properties were obtained after calcining the sample at 1600 °C for 15 h.

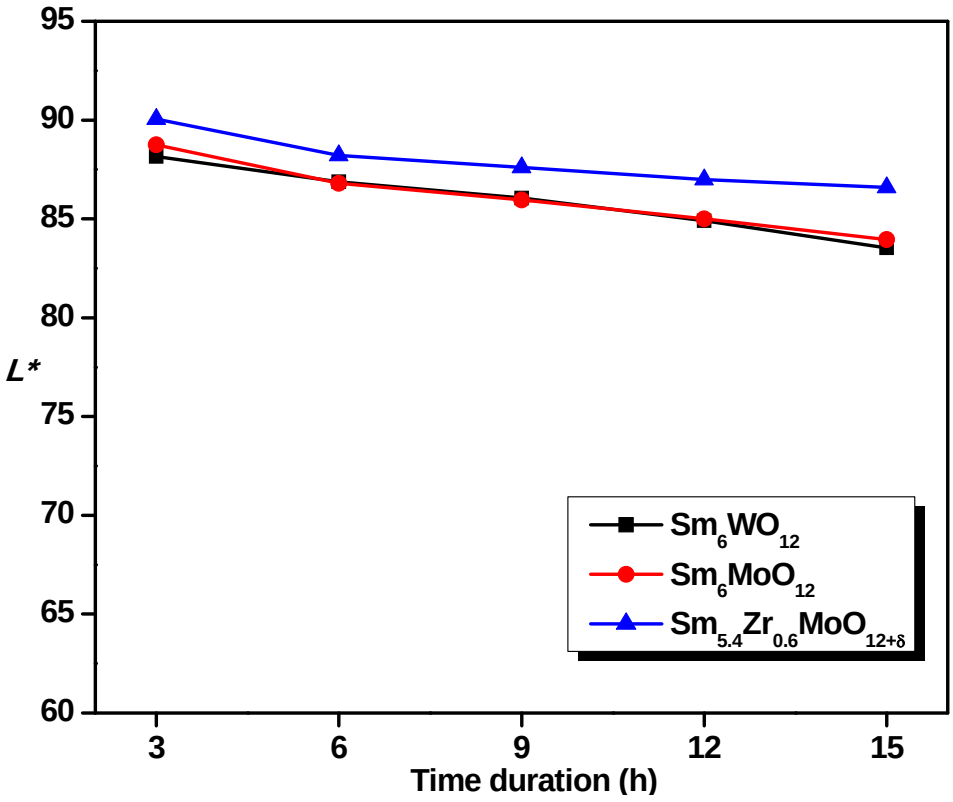

Fig. 5.9. Effect of time duration on the lightness parameter of Sm_6WO_{12}, Sm_6MoO_{12} and $Sm_{5.4}Zr_{0.6}MoO_{12+\delta}$ pigments.

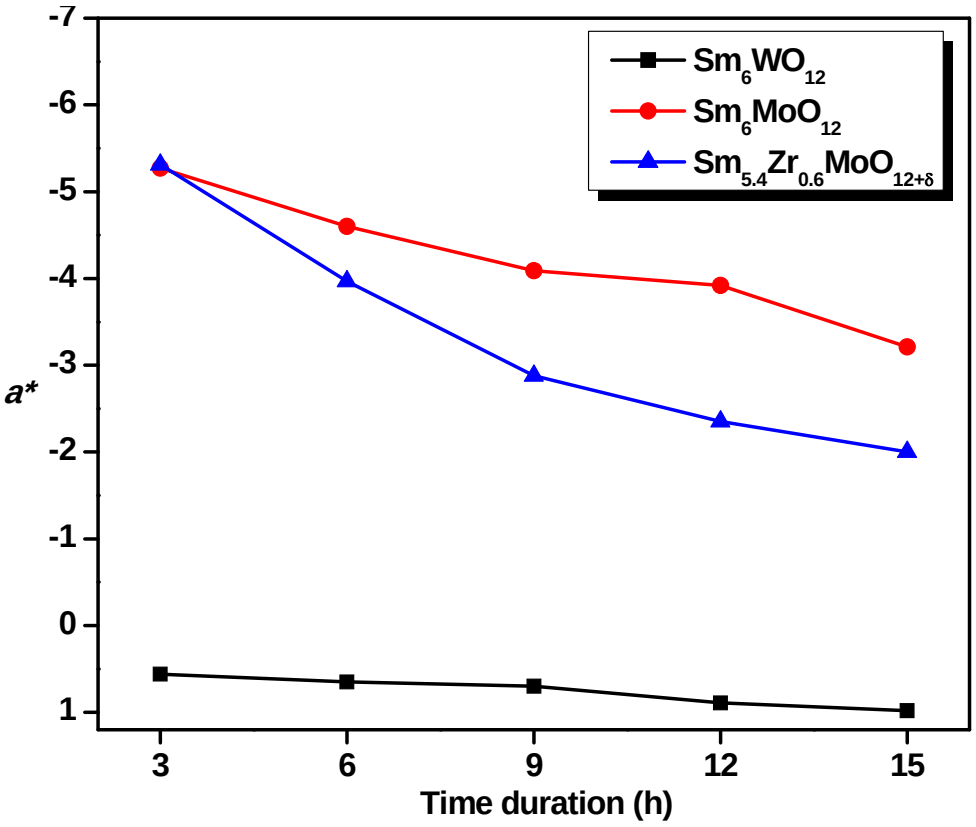

Fig. 5.10. Effect of time duration on the green hue of Sm_6WO_{12}, Sm_6MoO_{12} and $Sm_{5.4}Zr_{0.6}MoO_{12+\delta}$ pigments.

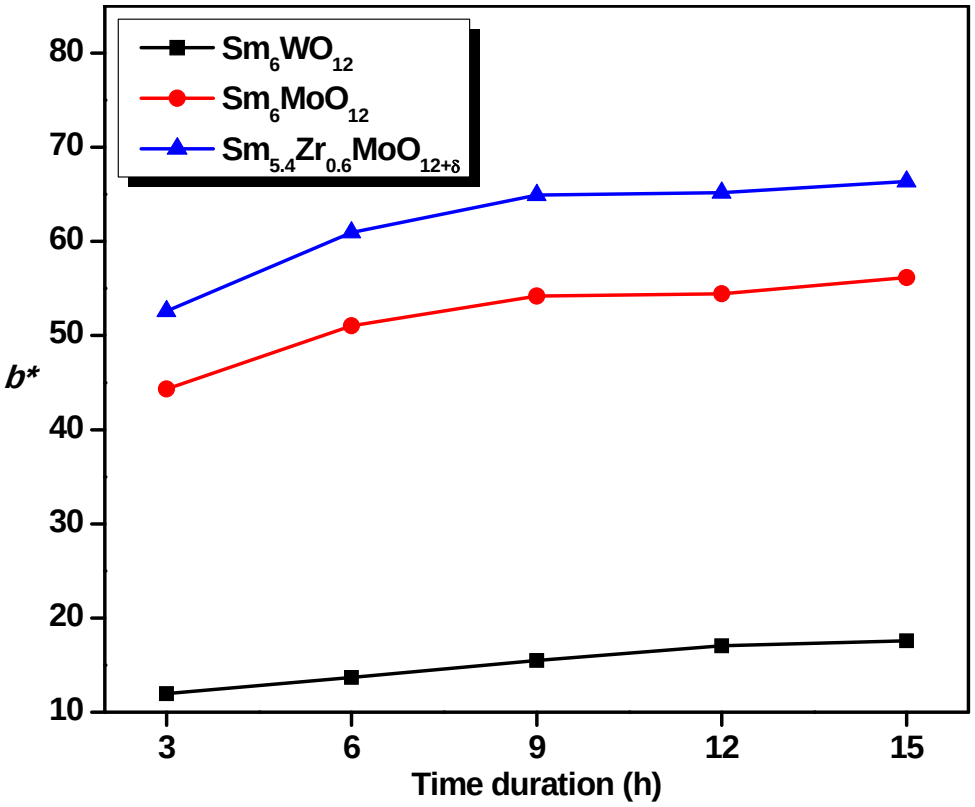

Fig. 5.11. Effect of time duration on the yellow hue of Sm_6WO_{12}, Sm_6MoO_{12} and $Sm_{5.4}Zr_{0.6}MoO_{12+\delta}$ pigments.

The colorimetric parameters of the $Sm_{6-x}W_{1-y}Zr_xMo_yO_{12+\delta}$ (x = 0 and y ranges from 0 to 1) powder pigments calcined at 1600 °C/15 h are given in Table 5.2. The partial substitution (2.9 mol %) of Mo^{6+} for W^{6+} in the Sm_6WO_{12} lattice enhances the yellow hue of the pigment which is expressed by the higher value of the color coordinate, b^*. It can be observed from the table that, increasing addition (up to 14.3 mol %) of Mo^{6+}, leading to complete replacement of W^{6+} greatly enhances the yellow component to 56.2. The green hue of the pigment as denoted by the color coordinate, a^* shows a slight increase upto 5.7 mol % of Mo^{6+} and decreases thereafter. The yellow hue gets purer as evident from the increase in Chroma (C^*) values from 17.6 to 56.3. The hue angle values of the pigments lie in the yellow region of the cylindrical color space ($h°$ = 70–105 for yellow) (Sulcova *et al.* 2007).

Table 5.2. The color coordinates (±0.1) and band gap values of the $Sm_{6-x}W_{1-y}Zr_xMo_yO_{12+\delta}$ (x ranges from 0 to 0.6 and y ranges from 0 to 1) powder pigments

Pigment composition	Color coordinates					|d = h°–90|	Band gap (eV)
	L*	a*	b*	C*	h°		
Sm_6WO_{12}	83.5	1.0	17.6	17.6	86.8	3.4	3.29
$Sm_6W_{0.8}Mo_{0.2}O_{12}$	77.1	–4.2	32.0	32.2	97.5	7.5	2.80
$Sm_6W_{0.6}Mo_{0.4}O_{12}$	78.0	–6.5	37.4	37.9	99.8	9.8	2.78
$Sm_6W_{0.4}Mo_{0.6}O_{12}$	80.6	–5.9	47.2	47.6	97.2	7.2	2.73
$Sm_6W_{0.2}Mo_{0.8}O_{12}$	83.8	–3.4	54.8	55.0	93.6	3.6	2.71
Sm_6MoO_{12}	84.0	–3.2	56.2	56.3	93.3	3.3	2.69
$Sm_{5.8}Zr_{0.2}MoO_{12+\delta}$	84.6	–2.6	60.6	60.6	92.5	2.5	2.64
$Sm_{5.6}Zr_{0.4}MoO_{12+\delta}$	86.0	–2.5	63.8	63.8	92.3	2.3	2.62
$Sm_{5.5}Zr_{0.5}MoO_{12+\delta}$	86.1	–2.4	65.1	65.2	92.1	2.1	2.59
$Sm_{5.4}Zr_{0.6}MoO_{12+\delta}$	86.6	–2.0	66.4	66.4	91.7	1.7	2.58

The color coordinates of $Sm_{6-x}W_{1-y}Zr_xMo_yO_{12+\delta}$ (y = 1 and x ranges from 0 to 0.6) powder pigments shows a significant enhancement in the yellow color of the pigment upon doping of zirconium (Table 5.2). Partial substitution of Zr^{4+} for Sm^{3+} in the lattice of Sm_6MoO_{12} steadily increases the yellow hue of the pigment as evident from the increase in the yellow parameter (b*) from 56.2 to 66.4. At the same time, a steady decrease in the green hue represented by the color parameter, –a* from –3.2 to –2.0 has been observed. There is an improved richness in the yellow color with systematic replacement of Zr^{4+} for Sm^{3+} (up to 8.6 mol %) in Sm_6MoO_{12} as can be observed from the increase in C* values. It can also be noted that the hue angle (h°) values for $Sm_{6-x}W_{1-y}Zr_xMo_yO_{12+\delta}$ (y = 1 and x ranges from 0 to 0.6) pigments approach close to 90° with increase in Zr^{4+} content expected for an ideal yellow color. The deviation from the ideal yellow color decreases with increasing amounts of Zr^{4+}. The low –a* value and high b* value of the typical pigment $Sm_{5.4}Zr_{0.6}MoO_{12+\delta}$ makes it a potential candidate for non–toxic yellow inorganic pigments. The chromatic properties, especially the hue angle (91.7) of this pigment is comparable with a number of industrial pigments such as

$PbCrO_4$ (87.8), $BiVO_4$ (95.8), $NiTiO_3$ (100.0), CdS (93.6) and praseodymium yellow (92.7) (Gauthier *et al.* 2003; Furukawa *et al.* 2008).

5.4.5 Chemical and thermal stability of the pigments

To facilitate the use of this colorant in various applications, it is necessary to establish its chemical and thermal stability. Chemical resistance of the pigment was assessed using 10% HCl/H_2SO_4/HNO_3/NaOH. A known weight of the pigment was taken in beaker containing acid/alkali, soaked for 30 min with constant stirring using a magnetic stirrer. It was then filtered, washed with water, dried and weighed. Negligible weight loss was noted in all the cases. The color coordinates of the ensuing powders were then measured and the results are given in Table 5.3. The total color difference (ΔE^*_{ab}) is negligible indicating an imperceptible color change to the human eye.

Thermal resistance of the typical pigment $Sm_{5.4}Zr_{0.6}MoO_{12+\delta}$ was performed in the temperature range 50–1000 °C. It is clear from the thermogram shown in Fig. 5.12 that the pigment has no weight loss or phase transition in the temperature range studied, thus illustrating its stability.

Table 5.3. The color coordinates (±0.1) of the $Sm_{5.4}Zr_{0.6}MoO_{12+\delta}$ powder pigments after chemical resistance tests

10% Acid/Alkali	Color coordinates			[a] ΔE^*_{ab}
	L^*	a^*	b^*	
HCl	86.2	–1.4	66.1	0.78
HNO_3	86.7	–1.0	65.3	1.48
H_2SO_4	87.0	–1.4	66.2	0.74
NaOH	87.6	–2.1	66.9	1.12

[a] $\Delta E^*_{ab} = [(\Delta L^*)^2 + (\Delta a^*)^2 + (\Delta b^*)^2]^{½}$

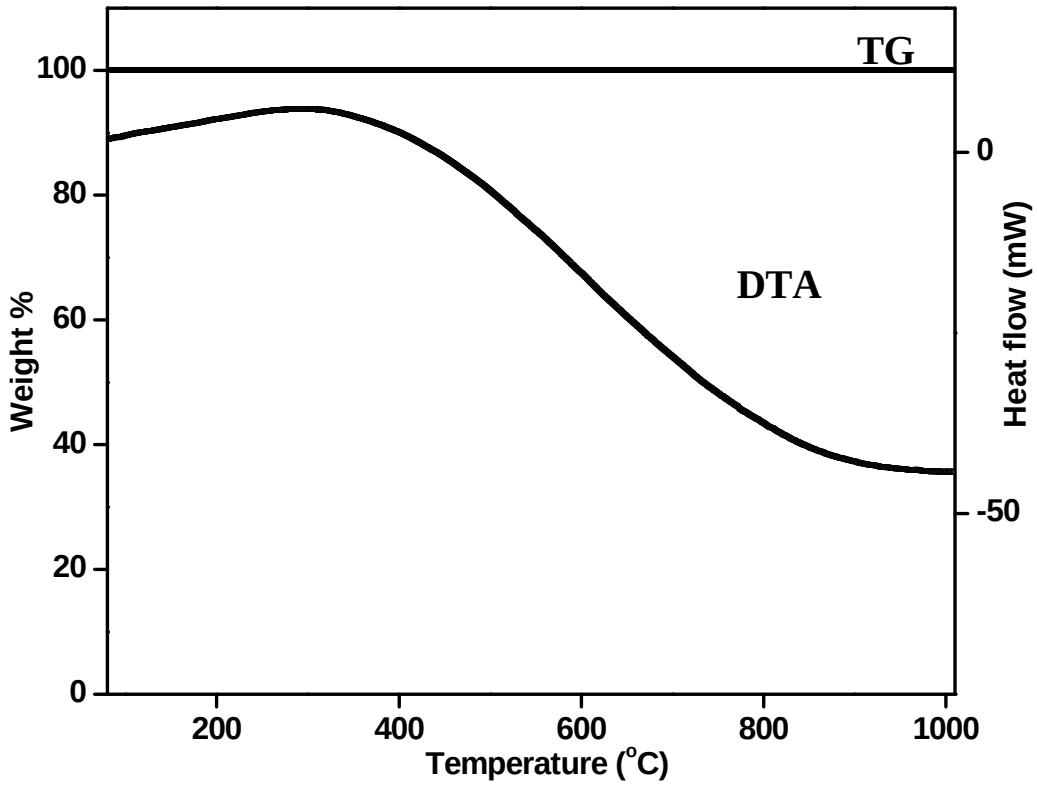

Fig. 5.12. TG/DTA of $Sm_{5.4}Zr_{0.6}MoO_{12+\delta}$.

5.4.6 Evaluation of coloring performance of the pigments

The pigment having the best chromatic properties, $Sm_{5.4}Zr_{0.6}MoO_{12+\delta}$ was evaluated for its coloring performance by incorporating it into a polymer substrate like PMMA. Typically 4–12 wt.% of the pigment sample was used for the purpose. The color coordinates of the polymer discs (Fig. 5.13) were analyzed at different locations on the surface and an average value is given in Table 5.4. The color coordinate values obtained were more or less the same, revealing the uniform distribution of the pigment particles in the polymer substrate. It is clear from the table that the intensity of the color of the polymer substrate depends on the concentration of the pigment being incorporated. It can be seen from the table that 12 wt.% incorporation of the pigment in the PMMA matrix can render its color totally to the matrix. Surprisingly, the deviation of the hue from the ideal yellow color is zero at this concentration.

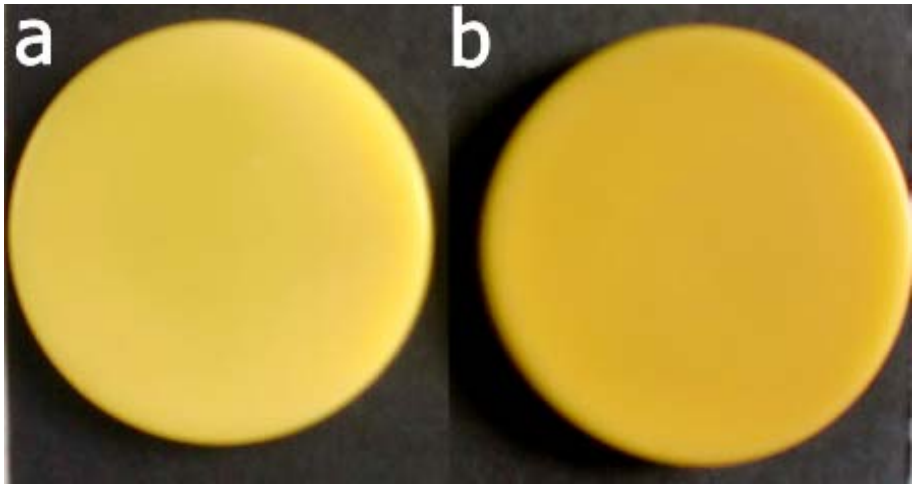

Fig. 5.13. Photographs of (a) $Sm_{5.4}Zr_{0.6}MoO_{12+\delta}$ (4%) + PMMA (b) $Sm_{5.4}Zr_{0.6}MoO_{12+\delta}$ (12%) + PMMA.

Table 5.4. The color coordinates (±0.1) of the PMMA substrate incorporated with various concentrations of $Sm_{5.4}Zr_{0.6}MoO_{12+\delta}$

Wt. % of pigment	Color coordinates					|d = *h*°–90|
	*L**	*a**	*b**	*C**	*h*°	
4	69.3	–6.9	50.9	51.4	97.7	7.7
8	74.5	–5.3	59.6	59.8	95.1	5.1
10	74.6	–4.3	62.3	62.5	93.9	3.9
12	72.0	0	65.3	65.3	90.0	0

5.5 Conclusions

- Eco–friendly yellow inorganic pigments having the general formula $Sm_{6-x}W_{1-y}Zr_xMo_yO_{12+\delta}$ (*x* ranges from 0 to 0.6 and *y* ranges from 0 to 1) with a cubic fluorite structure have been developed by traditional solid state route.
- The replacement of Mo^{6+} for W^{6+} in Sm_6WO_{12} shifts the absorption band from the UV region to 460 nm thereby producing a yellow color. The coloring mechanism is explained based on $O^{2-} \rightarrow Mo^{6+}$ charge transfer transitions.
- Doping of Zr^{4+} for Sm^{3+} shifts the $O^{2-} \rightarrow Mo^{6+}$ charge transfer absorption edge of Sm_6MoO_{12} to 479 nm and intensifies the yellow hue of the pigment. Introduction of Zr^{4+} into the lattice produces intrinsic strain, which will affect the O_{2p} valence band.
- The pigments exhibits intense yellow hue with hue angles (91.7) superior to that of commercial inorganic pigments such as $PbCrO_4$ (87.8), $BiVO_4$ (95.8), $NiTiO_3$ (100.0), CdS (93.6) and praseodymium yellow (92.7).
- The synthesized pigments possess good chemical and thermal stability.
- The current results clearly demonstrate the potential of the designed yellow pigments for the coloration of substrate materials like plastics.

List of Publications

LIST OF PUBLICATIONS

Publications from the thesis

1. **Vishnu**, **V. S.**; George, G.; Divya, V.; Reddy, M. L. P. "Synthesis and characterization of new environmentally benign tantalum–doped $Ce_{0.8}Zr_{0.2}O_2$ yellow pigments: Applications in coloring of plastics," *Dyes Pigm.*, *82*, **2009**, 53–57.
2. **Vishnu**, **V. S.**; George, G.; Reddy, M. L. P. "Effect of molybdenum and praseodymium dopants on the optical properties of $Sm_2Ce_2O_7$: Tuning of band gaps to realize various color hues," *Dyes Pigm.*, *85*, **2010**, 117–123.
3. **Vishnu**, **V. S.**; Reddy, M. L. P. "Near–infrared reflecting yellow inorganic pigments based on molybdenum–doped yttrium cerate: Synthesis, characterization, and optical properties," *Chem. Lett.*, *39*, **2010,** 820–821.
4. **Vishnu**, **V. S.**; Jose, S.; Reddy, M. L. P. "Novel environmentally benign yellow inorganic pigments based on solid solutions of samarium–transition metal mixed oxides," *J. Am. Ceram. Soc.*, *94*, **2011**, 997–1001.
5. **Vishnu**, **V. S.**; Reddy, M. L. P. "Near–infrared reflecting inorganic pigments based on molybdenum and praseodymium doped yttrium cerate: Synthesis, characterization and optical properties," *Sol. Energy Mater. Solar Cells,* d.o.i. 10.1016/j.solmat.**2011**.05.042

Publications not related to this thesis

1. George, G.; **Vishnu, V. S.**; Reddy, M. L. P. "The synthesis characterization and optical properties of silicon and praseodymium doped Y_6MoO_{12} compounds: environmentally benign inorganic pigments with high NIR reflectance," *Dyes Pigm.*, *88*, **2011**, 109–115.
2. George, G.; Kumari, L. S.; **Vishnu, V. S.**; Ananthakumar, S.; Reddy, M. L. P. "Synthesis and characterization of environmentally benign calcium–doped $Pr_2Mo_2O_9$ pigments: Applications in coloring of plastics," *J. Solid State Chem.*, *181*, **2008**, 481–492.

References

Aby, C. P.; Sreeram, K. J.; Nair, B. U.; Ramasami, T. "Doped oxides of cerium as inorganic colorants," *Color. Technol*., *123*, **2007**, 374–378.

Ali, M. F.; El–Ali, B. M.; Speight, J. G. "Handbook of industrial chemistry–organic chemicals," Mc–Graw Hill, New York, **2005**.

Ardit, M.; Dondi, M.; Cruciani, G.; Matteucci, F. "Ti–Ca–Al-doped $YCrO_3$ pigments: XRD and UV–vis investigation," *Mater. Res. Bull.*, *44*, **2009**, 666–673.

Arranz, A.; Perez–Dieste, V.; Palacio, C. "Electronic structure of stoichiometric and reduced Ta_2O_5 surfaces determined by resonant photoemission," *Phys. Rev. B: Condens. Matter Mater. Phys.*, *66*, **2002**, 075420–075425.

Aruna, S. T.; Ghosh, S.; Patil, K. C. "Combustion synthesis and properties of $Ce_{1-x}Pr_xO_{2-\delta}$ red ceramic pigments," *Int. J. Inorg. Mater.*, *3*, **2001**, 387–392.

[a]Badenes, J. A.; Llusar, M.; Tena, M. A.; Calbo, J.; Monros, G. "Praseodymium–doped cubic Ca–ZrO_2 ceramic stain," *J. Eur. Ceram. Soc.*, *22*, **2002**, 1981–1990.

[b]Badenes, J. A.; Vicent, J. B.; Llusar, M.; Tena, M. A.; Monros, G. "The nature of Pr–$ZrSiO_4$ yellow ceramic pigment," *J. Mater. Sci*., *37*, **2002**, 1413–1420.

Barnett, J. R.; Miller, S.; Pearce, E. "Color and art: A brief history of pigments." *Opt. Laser. Technol.*, *38*, **2006**, 445–453.

Bendiganavale, A. K.; Malshe, V. C. "Infrared reflective inorganic pigments," *Recent Patents on Chemical Engineering*, *1*, **2008**, 67–79.

Biju, S.; Reddy, M. L. P.; Cowley, C. H.; Vasudevan, K. V. "3–Phenyl–4–acyl–5–isoxazolonate complex of Tb^{3+} doped into poly–β–hydroxybutyrate matrix as a promising light–conversion molecular device," *J. Mater. Chem.*, *19*, **2009**, 5179–5187.

Biswas, S. K.; Dhak, D.; Pathak, A.; Pramanik, P. "Chemical synthesis of environment–friendly nanosized yellow titanate pigments," *Mater. Res. Bull.*, *43*, **2008**, 665–675.

Bittler, K.; Ostertag, W. "Developments in the field of inorganic pigments," *Angew. Chem. Int. Ed. Engl.*, *19*, **1980**, 190–196.

Blonski, R. P. "Stable heavy metal free zircon pigments for use in plastics and paints and method for coloring thereof," *U.S. Patent No.* 5,316,570, **1994**.

Bondioli, F.; Corradi, A. B.; Manfredini, T.; Leonelli, C.; Bertoncello, R. "Nonconventional synthesis of praseodymium–doped ceria by flux method," *Chem. Mater.*, *12*, **2000**, 324–330.

Bondioli, F.; Ferrari, A. M.; Leonelli, C.; Siligardi, C.; Hart, N. A.; Evans, N. G. "The application of microwaves in the synthesis of $Ce_{0.9}Pr_{0.1}O_2$ nanostructured powders," *J. Mater. Chem.*, *11*, **2001**, 2620–2624.

Bondioli, F.; Ferrari, A. M.; Lusvarghi, L.; Manfredini, T.; Nannarone, S.; Pasquali, L.; Selvaggi, G. "Synthesis and characterization of praseodymium–doped ceria powders by a microwave–assisted hydrothermal (MH) route," *J. Mater. Chem.*, *15*, **2005**, 1061–1066.

Bunzili, J. –C. G.; Piguet, C. "Taking advantage of lanthanide luminescent ions," *Chem. Soc. Rev. 34*, **2005**, 1048–1077.

Busnot, S.; Macaudiere, P. "Composition based on samarium sesquisulphide, preparation method and use as coloring pigment," *U.S. Patent No*. 6,419,735, **2002**.

Buxbaum, G.; Pfaff, G. "Industrial inorganic pigments," Wiley–VCH, Weinheim, **2002**.

Carnall, W. T.; Fields, P. R.; Rajnak, K. "Electronic energy levels in the trivalent lanthanide aquo ions. I. Pr^{3+}, Nd^{3+}, Pm^{3+}, Sm^{3+}, Dy^{3+}, Ho^{3+}, Er^{3+} and Tm^{3+}," *J. Chem. Phys.*, *49*, **1968**, 4424–4442.

Christie, R. M. "Color chemistry," Royal Society of Chemistry, UK, **2001**.

Chopin, T.; Dupuis, D. "Rare earth metal sulfide pigment compositions," *U.S. Patent No.* 5,401,309, **1995.**

Chopin, T.; Macaudiere, P. "Inorganic rare earth pigments/colorants and synthesis/applications thereof," *U.S. Patent No.* 6,284,033; **2001**.

CIE (Commission Internationale de l'Eclairage). Colorimetry – Technical Report. CIE Pub. No. 15, Second Edition (Vienna: CIE Central Bureau CIE, **1986**).

CIE (Commission Internationale de l'Eclairage). Colorimetry – Technical Report. CIE, Third Edition (Vienna: CIE Central Bureau CIE, **2004**).

Clemente, D. A.; Lucchini, E.; Meriani, S.; Furlan, N. "Crystal structures of CeO_2–ZrO_2–Ta_2O_5 ternary system studied by rietveld method," *J. Eur. Ceram. Soc.*, *25*, **2005**, 1863–1876.

Cornell, R. M.; Schwertmann, U. "The iron oxides; structure, properties, reactions, occurrence and uses," Wiley–VCH, Weinheim, **1996.**

Diot, N.; Larcher, O.; Marchand, R.; Kempf, J. Y.; Macaudiere, P. "Rare–earth and tungsten oxynitrides with a defect fluorite–type structure as new pigments," *J. Alloys Compd.*, *323–324*, **2001**, 45–48.

Dohnalova, Z.; Sulcova, P.; Trojan, M. "Synthesis and characterization of $LnFeO_3$ pigments," *J. Therm. Anal. Calorim.*, *91*, **2008**, 559–563.

Dohnalova, Z.; Sulcova, P.; Trojan, M. "Effect of Er^{3+} substitution on the quality of Mg–Fe spinel pigments," *Dyes Pigm.*, *80*, **2009**, 22–25.

Fernandez–Gonzalez, R.; Julian–Lopez, B.; Cordoncillo, E.; Escribano , P. "New insights on the structural and optical properties of Ce–Ti mixed oxide nanoparticles doped with praseodymium," *J. Mater. Chem.*, *21*, **2011**, 497–504.

Furukawa, S.; Masui, T.; Imanaka, N. "Synthesis of new environment–friendly yellow pigments," *J. Alloys Compd.*, *418*, **2006**, 255–258.

Furukawa, S.; Masui, T.; Imanaka, N. "New environment–friendly yellow pigments based on CeO_2–ZrO_2 solid solutions," *J. Alloys Compd.*, *451*, **2008**, 640–643.

Garcia, A.; Llusar, M.; Calbo, J.; Tena, M. A.; Monros, G. "Low–toxicity red ceramic pigments for porcelainised stoneware from lanthanide–cerianite solid solutions," Green *Chem.*, *3*, **2001**, 238–242.

Gauthier, G.; Jobic, S.; Evain, M.; Koo, H.–J.; Whangbo, M.–H.; Fouassier, C.; Brec, R. "Syntheses, structures and optical properties of yellow Ce_2SiS_5, $Ce_6Si_4S_{17}$ and $Ce_4Si_3S_{12}$ materials," *Chem. Mater.*, *15*, **2003**, 828–837.

[a]George, G.; Kumari, L. S.; Vishnu, V. S.; Ananthakumar, S.; Reddy, M. L. P. "Synthesis and characterization of environmentally benign calcium–doped $Pr_2Mo_2O_9$ pigments: Applications in coloring of plastics," *J. Solid State Chem.*, *181*, **2008**, 481–492.

George, G.; George, G.; Rao, P. P.; Reddy, M. L. P. "Synthesis and characterization of environmentally benign nontoxic pigments: $RE_2Mo_2O_9$ (RE = La or Pr)," *Chem. Lett.*, *34*, **2005**, 1702–1703.

George, G.; Rao, P. P.; Reddy, M. L. P. "Synthesis and characterization of CeO_2–TiO_2–Pr_6O_{11} solid solutions for environmentally benign nontoxic red pigments," *Chem. Lett.*, *35*, **2006**, 1412–1413.

George, G.; Vishnu, V. S.; Reddy, M. L. P. "The synthesis characterization and optical properties of silicon and praseodymium doped Y_6MoO_{12} compounds: environmentally benign inorganic pigments with high NIR reflectance," *Dyes Pigm.*, *88*, **2011**, 109–115.

[b]George, H. C.; Ming, –L. L.; Li, –D. C.; Fu, –Q. H.; Daniel, E. B.; Daniel, M. W.; John, R. I.; Mark, C. H.; Richard, P.; Van, D.; James, A. I. "Syntheses, crystal structures, and physical properties of $La_5Cu_6O_4S_7$ and $La_5Cu_{6.33}O_4S_7$," *Inorg. Chem.*, *47*, **2008**, 4368–4374.

Han, B.; Liang, H. B.; Lin, H. H.; Zhong, J. P.; Su, Q. "Vacuum ultraviolet–ultraviolet and x–ray excited luminescence properties of $Ba_3Gd(BO_3)_3:Ce^{3+}$," *J. Appl. Phys.*, *101*, **2007**, 1135301–1135308.

Hill, K.; Lehman, R.; Swiler, D. "Effects of selected processing variables on color formation in praseodymium–doped zircon pigments," *J. Am. Ceram. Soc.*, *83*, **2000,** 2177–2182.

Huguenin, D.; Pettini, F.; Seguelong, T. "Yellow/orange pigments comprising zirconium oxide and cerium, praseodymium and/or terbium values," *U.S. Patent* 5,560,772, **1996**.

Imanaka, N.; Masui, T.; Furukawa, S. "Novel nontoxic and environment–friendly inorganic yellow pigments," *Chem. Lett.*, *37*, **2008**, 104–105.

Imanaka, N.; Masui, T.; Itaya, M. "Synthesis of an environmentally friendly and nontoxic new pigment based on rare earth phosphate," *Chem. Lett.*, *32*, **2003**, 400–401.

Ishida, S.; Ren, F.; Takeuchi, N. "New yellow ceramic pigment based on codoping pyrochlore–type $Y_2Ti_2O_7$ with V^{5+} and Ca^{2+}," *J. Am. Ceram. Soc.*, *76*, **1993**, 2644–2648.

Jansen, M.; Letschert, H. P. "Oxonitrides of the formula $LnTaON_2$ with enhanced brightness and a process for their use," *U.S. Patent No*. 5,693,102, **1997**.

Jansen, M.; Letschert, H. P. "Inorganic yellow–red pigments without toxic metals," *Nature*, *404*, **2000**, 980–982.

Jayasankar, K.; Samal, S.; Bhattacharjee, S. "Synthesis of fluorite ceria based solid solutions from mixed rare earth carbonates," *Ceram. Int.*, *35*, **2009**, 3103–3109.

Jeevanandam, P.; Mulukutla, R. S.; Phillips, M.; Chaudhuri, S.; Erickson, L. E.; Klabunde, K. J. "Near infrared reflectance properties of metal oxide nanoparticles," *J. Phys. Chem. C.*, *111*, **2007**, 1912–1918.

Joergensen, C. K.; Rittershaus, E. "Powder–diagram and spectroscopic studies of mixed oxides of lanthanides and quadrivalents metals," *K. Dan. Vidensk. Selsk.,Mat. –Fys. Medd.*, 35**, 1967**, 1–37.

Kar, J. K.; Stevens, R.; Bowen, C. R. "Novel terbium–zircon yellow pigment," *J. Mater. Sci.*, *39*, **2004**, 5755–5763.

Kar, J. K.; Stevens, R.; Bowen, C. R. "Processing and characterization of Pr–zircon pigment powder," *Adv. Appl. Ceram.*, *104*, **2005**, 233–238.

Kar, J. K.; Stevens, R.; Bowen, C. R. "Effect of cerium oxide on colour hue of praseodymium–zircon yellow pigment," *Adv. Appl. Ceram.*, *106*, **2007**, 175–179.

Kar, J. K.; Stevens, R.; Bowen, C. R. "Rare–earth cuprates for ceramic colouring application–An investigation," *J. Alloys Compd.*, *455*, **2008**, 121–129.

Kido, J.; Okamoto, Y. "Organo lanthanide metal complexes for electroluminescent materials," *Chem. Rev.*, *102*, **2002**, 2357–2368.

Koelling, D. D.; Boring, A. M.; Wood, J. H. "The electronic structure of CeO_2 and PrO_2," *Solid State Commun.*, *47*, **1983**, 227–232.

Kroger, F. A.; Vink, H. J.; In:Sietz, F.; Turnbull, D. "Solid state physics," vol. 3. Associated Press, New York, **1956**.

Kumari, L. S.; George, G.; Rao, P. P.; Reddy, M. L. P. "The synthesis and characterization of environmentally benign praseodymium–doped $TiCeO_4$ pigments," *Dyes Pigm.*, *77*, **2008**, 427–431.

Kumari, L. S.; Rao, P. P.; Koshy, P. "Red pigments based on CeO_2–MO_2–Pr_6O_{11} (M = Zr and Sn): Solid solutions for the coloration of plastics," *J. Am. Ceram. Soc*., *93*, **2010**,1402–1408.

[a]Levinson, R.; Akbari, H.; Berdahl, P. "Measuring solar reflectance–Part I: Defining a metric that accurately predicts solar heat gain," *Solar Energy*, *84*, **2010**, 1717–1744.

[b]Levinson, R.; Akbari, H.; Berdahl, P. "Measuring solar reflectance–Part II: Review of practical methods," *Solar Energy*, *84*, **2010**, 1745–1759.

[a]Levinson, R.; Berdahl, P.; Akbari, H. "Solar spectral optical properties of pigments–Part I: model for deriving scattering and absorption coefficients from transmittance and reflectance measurements," *Sol. Energy Mater. Solar Cells*, *89*, **2005**, 319–349.

[b]Levinson, R.; Berdahl, P.; Akbari, H. "Solar spectral optical properties of pigments–Part II: Survey of common colorants," *Sol. Energy Mater. Solar Cells*, *89*, **2005**, 351–389.

Levinson, R.; Berdahl, P.; Akbari, H.; Miller, W.; Joedicke, I.; Reilly, J.; Suzuki, Y.; Vondran, M. "Methods of creating solar–reflective nonwhite surfaces and their application to residential roofing materials," *Sol. Energy Mater. Solar Cells*, *91*, **2007**, 304–314.

Lewis, P. A. "Pigment Handbook," J. Wiley & Sons, New York, **1988**.

Linke, E. A. E.; Zwart, C. H.; Smout, A. D. "Doped zirconium mixed silicate pigment, method for the preparation thereof and products containing such pigment or a thus prepared pigment," *U.S. Patent No.* 5,275,649, **1994**.

Llusar, M.; Calbo, J.; Badenes, J. A.; Tena, M. A.; Monros, G. "Synthesis of iron zircon coral by coprecipitation routes," *J. Mater. Sci., 36*, **2001**, 153–163.

Llusar, M.; Vitaskova, L.; Sulcova, P.; Tena, M. A.; Badenes, J. A.; Monros, G. "Red ceramic pigments of terbium–doped ceria prepared through classical and non–conventional coprecipitation routes," *J. Eur. Ceram. Soc.*, *30*, **2010**, 37–52.

Mandal, B. P.; Roy, M.; Grover, V.; Tyagi, A. K. "X–ray diffraction, μ–raman spectroscopic studies on CeO_2–RE_2O_3 (RE = Ho, Er) systems: observation of parasitic phases," *J. Appl. Phys.*, *103*, **2008**, 0335061–0335067.

[a]Martos, M.; J Julian, –L. B.; Cordoncillo, E.; Escribano, P. "Structural and spectroscopic study of a novel erbium titanate pink pigment prepared by sol−gel methodology," *J. Phys. Chem., B. 112*, **2008**, 2319–2325.

Martos, M.; Julian, –L. B.; Cordoncillo, E.; Escribano, P. "Structural and spectroscopic study of a new pink chromium–free $Er_2(Ti,Zr)_2O_7$ ceramic pigment," *J. Am. Ceram. Soc. 92*, **2009**, 2987–2992.

[b]Martos, M.; Julian, –L. B.; Folgado, J. V.; Cordoncillo, E.; Escribano, P. "Sol–Gel synthesis of tunable cerium titanate materials," *Eur. J. Inorg. Chem.*, **2008**, 3163–3171.

Martos, M.; Martinez, M; Cordoncillo, E.; Escribano, P. "Towards more ecological ceramic pigments: Study of the influence of glass composition on the colour stability of a pink chromium–doped ceramic pigment," *J. Eur. Ceram. Soc.*, *27*, **2007**, 4561–4567.

Maslennikova, G. N.; Pishch, I. V.; Gvozdeva, N. A. "Particularities of the synthesis of pigments with corundum–spinel structures," *Glass Ceram. 66*, **2009**, 5–7.

Maso, N.; Beltran, H.; Munoz, R.; Julian, B.; Carda, J. B.; Escribano, P.; Cordoncillo, E. "Optimization of praseodymium–doped cerium pigment synthesis temperature," *J. Am. Ceram. Soc., 86*, **2003**, 425–430.

Masui, T.; Furukawa, S.; Imanaka, N. "Preparation and characterization of amorphous $Ce_{1-x}M_xW_2O_8$ fine particles for environmental–friendly yellow pigments," *Chem. Lett., 34*, **2005**, 1322–1323.

Masui, T.; Furukawa, S.; Imanaka, N. "Synthesis and characterization of CeO_2–ZrO_2–Bi_2O_3 solid solutions for environment–friendly yellow pigments," *Chem. Lett., 35*, **2006**, 1032–1033.

[a]Masui, T.; Tategaki, H.; Imanaka, N. "Preparation and characterization of SiO_2–CeO_2 particles applicable for environment–friendly yellow pigments," *J. Mater. Sci., 39*, **2004,** 4909–4911.

[b]Masui, T.; Tategaki, H.; Furukawa, S.; Imanaka, N. "Synthesis and characterization of new environmentally–friendly pigments based on cerium phosphate", *J. Ceram. Soc.Jpn.*, *112*, **2004**, 646–649.

Melo, D. M. A.; Melo, M. A .F.; Martinelli, A. E.; Silva, Z. R.; Cunha, J. D.; Lima, A. C. "Synthesis and characterization of lanthanum– and yttrium–doped Fe_2O_3 pigments," *Ceramica*, *53*, **2007**, 79–82.

Modly, Z. M. "Pigment consisting of a mixture of chromium oxide and iron oxide useful in high infra red reflectance gray vinyl composition," *U.S. Patent No.* 4,624,710, **1986**.

Nero, G. D.; Cappelletti, G.; Ardizzonne, S.; Fermo, P.; Gilardoni, S. "Yellow Pr–zircon pigments: The role of praseodymium and of the mineralizer," *J. Eur. Ceram. Soc.*, *24*, **2004**, 3603–3611.

Nunes, M. G. B.; Cavalcante, L. S.; Santos, V.; Sczancoski, J. C.; Santos, M. R. M. C.; Santos–Junior, L. S.; Longo, E. "Sol–gel synthesis and characterization of $Fe_2O_3 \cdot CeO_2$ doped with Pr ceramic pigments," *J. Sol–Gel Sci. Technol.*, *47*, **2008**, 38–43.

Ocana, M.; Caballero, A.; Gonzalez–Elipe, A. R.; Tartaj, P; Serna, C. J. "Valence and localization of praseodymium in Pr–doped zircon,". *J. Solid State Chem.*, *139*, **1998**, 412–415.

Ohno, Y. "CIE Fundamentals for Color Measurements," Paper for IS&T NIP16 Conference, Vancouver, Canada, **2000**, Oct. 16.

Olazcuaga, R.; El Kira, A.; Le Flem, G.; Hagenmuller, P. "Pr–CeO_2 red pigment," *Revue de Chimie Minerale*, *23*, **1986**, 55–57.

Olazcuaga, R.; Le Polles, G.; El Kira, A.; Le Flem, G.; Maestro, P. "Optical properties of $Ce_{1-x}Pr_xO_2$ powders and their applications to the coloring of ceramics," *J. Solid State Chem.*, *71*, **1987**, 570–573.

Pailhe, N.; Gaudon, M.; Demourgues, A. "(Ca^{2+}, V^{5+}) co–doped $Y_2Ti_2O_7$ yellow pigment," *Mater. Res. Bull.*, *44*, **2009**, 1771–1777.

Perrin, M. –A.; Wimmer, E. "Color of pure and alkali–doped cerium sulfide: A local density–functional study," *Phys. Rev. B: Condens. Matter Mater. Phys.*, *54*, **1996,** 2428–2435.

Rao, P. P.; Reddy, M. L. P. "$(TiO_2)(CeO_2)_{1-x}(RE_2O_3)_x$–novel environmental secure pigments," *Dyes Pigm.*, *73*, **2007**, 292–297.

Raj, D. B. A.; Francis, B.; Reddy, M. L. P.; Butorac, R. R.; Lynch, V. M.; Cowley, A. H. "Highly luminescent poly(methyl methacrylate)–incorporated european complex supported by a carbazole–based fluorinated β–diketonate ligand and a 4,5–bis(diphenylphosphino)–9,9–dimethylxanthene oxide co–ligand," *Inorg. Chem.*, *49*, **2010**, 9055–9063.

Ray, E. H.; Carnahan, T. D.; Sullivan, R. M. "Tin–vanadium yellows and praseodymium yellows," *Am. Ceram.* Soc. *Bull.*, *40*, **1961**, 13–16.

Reddy, B. M.; Khan, A. "Raman and x–ray photoelectron spectroscopy study of CeO_2–ZrO_2 and V_2O_5/CeO_2–ZrO_2 catalysts," *Langmuir*, *19*, **2003**, 3025–3030.

Seabright, C. A.; Draker, H. C. "Ceramic stains from zirconium and vanadium oxides," *Am. Ceram.* Soc. *Bull.*, *40*, **1961**, 1–4.

Seabright, C. A. "Yellow ceramic pigments," *U.S. Patent No.* 2,992,123, **1961**.

Shannon, R. D. "Revised effective ionic radii and systematic studies of interatomic distances in halides and chalcogenides," *Acta Crystallogr. Sect. A: Found. Crystallogr.*, *32*, **1976**, 751–767.

Shirpour, M.; Sani M. A. F.; Mirhabibi, A. "Synthesis and study of a new class of red pigments based on perovskite $YAlO_3$ structure," *Ceram. Int.*, *33*, **2007**, 1427–1433.

Shoyama, M.; Nasu, H.; Kamiya, K. "Preparation of rare earth–zircon pigments by the sol–gel method," *J. Ceram. Soc. Jpn. Int. Ed.*, *106*, **1998**, 279–284.

Sivakumar, V.; Varadaraju, U. V. "Environmentally benign novel green pigments: $Pr_{1-x}Ca_xPO_4$ (x = 0–0.4)," *Bull. Mater. Sci.*, *28*, **2005**, 299–301.

Smith, H. M. "High performance pigments," Wiley–VCH, Weinheim, **2002**.

Smith, A. E.; Mizoguchi, H.; Delaney, K.; Spaldin, N. A.; Sleight, A. W.; Subramanian, M. A. "Mn^{3+} in trigonal bipyramidal coordination: A new blue chromophore," *J. Am. Chem. Soc*., *131*, **2009**, 17084–17086.

Sliwinsky, T. R.; Pipoly, R. A.; Blonski, R. P. "Infrared reflective color pigment," *U.S. Patent No.* 6,454,848, **2002**.

Sorly, S.; Tena, M. A.; Badenes, J. A.; Calbo, J.; Llusar, M.; Monros, G. "Structure and color of $Ni_xA_{1-3x}B_{2x}O_2$ (A = Ti, Sn; B = Sb, Nb) solid solutions," *J. Eur. Ceram. Soc.*, *24*, **2004**, 2425–2432.

[a]Sreeram, K. J.; Aby, C. P.; Nair, B. U.; Ramaswamy, T. "Colored cool colorants based on rare earth metal ions," *Sol. Energy Mater. Solar Cells*, *92*, **2008**, 1462–1467.

[b]Sreeram, K. J.; Aby, C. P.; Nair, B. U. "Synthesis and characterization of doped rare earth oxides for environmentally benign nontoxic reddish–yellow pigments," *Chem. Lett.*, *37*, **2008**, 902–903.

[c]Sreeram, K. J.; Kumeresan, S., Radhika, R., Sundar, V. J., Muralidharan, C., Nair, B. U., Ramasami, T. "Use of mixed rare earth oxides as environmentally benign pigments," *Dyes Pigm.*, *76*, **2008**, 243–248.

Sreeram, K. J.; Radhika, S.; Devi, J. M.; Nair, B. U.; Ramasami, T. "Cerium molybdenum oxides for environmentally benign pigments," *Dyes Pigm.*, *75*, **2007**, 687–692.

Sulcova, P.; Trojan, M. "Thermal synthesis of the CeO_2–PrO_2–La_2O_3 pigments," *J. Therm. Anal. Calorim.*, *77*, **2004**, 99–104.

Sulcova, P.; Trojan, M. "Thermal synthesis of the $(Bi_2O_3)_{1-x}(Er_2O_3)_x$ pigments," *J. Therm. Anal. Cal.*, *88*, **2007**, 111–113.

Sulcova, P.; Trojan, M. "Thermal analysis of the $(Bi_2O_3)_{1-x}(Y_2O_3)_x$ pigments," *J. Therm. Anal. Calorim.*, *91*, **2008**, 151–154.

[a]Sulcova, P.; Trojan, M. "The synthesis of the $Ce_{0.95-y}Pr_{0.05}La_yO_{2-y/2}$ pigments," *Dyes Pigm.*, *44*, **2000**, 165–168.

[b]Sulcova, P.; Trojan, M. "The synthesis of the $Ce_{0.95-y}Pr_{0.05}Nd_yO_{2-y/2}$ pigments," *Dyes Pigm.*, *47*, **2000**, 285–289.

Sulcova, P. "The synthesis of the $Ce_{0.95-y}Pr_{0.05}Gd_yO_{2-y/2}$ pigments," *Dyes Pigm.*, *52*, **2002**, 89–93.

[a]Sulcova, P.; Trojan, M. "The synthesis of the $Ce_{0.95-y}Pr_{0.05}Sm_yO_{2-y/2}$ pigments," *Dyes Pigm.*, *58*, **2003**, 59–63.

[b]Sulcova, P.; Trojan, M. "Study of $Ce_{1-x}Pr_xO_2$ pigments," *Thermochim. Acta.*, *395*, **2003**, 251–255.

Sulcova, P.; Trojan, M.; Solc, Z. "Cerium dioxide fluorite type pigments," *Dyes Pigm.*, *37*, **1998**, 65–70.

Sulcova, P.; Vitaskova, L.; Trojan, M. "Thermal analysis of the $Ce_{1-x}Tb_xO_2$ pigments," *J. Therm. Anal. Calorim.*, *99*, **2010**, 409–413.

Sumaletha, N.; Rajesh, K.; Mukundan, P.; Warrier, K. G. K. "Environmentally benign sol–gel derived nanocrystalline rod shaped calcium doped cerium phosphate yellow–green pigment," *J Sol–Gel. Sci. Technol.*, *52*, **2009**, 242–250.

Swiler, R. D. "Manganese vanadium oxide pigments," *U.S. Patent No.* 6,485,557, **2002**.

Swiler, R. D.; Axtell, E. A. "Rare earth manganese oxide pigments," *U.S. Patent No.* 6,541,112, **2003**.

Swiler, R. D.; Detrie, T. J.; Axtell, E. A. "Rare earth–transition metal oxide pigments," *U.S. Patent No.* 6,582,814, **2003**.

Taniguchi, H.; Kido, J.; Nishiya, M.; Sasaki S. "Europium chelate solid state laser based on morphology–dependent resonances," *Appl. Phys. Lett.*, *67*, **1995,** 1060–1062.

Thongkanluang, T.; Kittiauchawal, T.; Limsuwan, P. "Preparation and characterization of Cr_2O_3–TiO_2–Al_2O_3–V_2O_5 green pigment," *Ceram. Int.*, *37*, **2011**, 543–548.

Thongkanluang, T.; Limsuwan, P.; Rakkwamsuk, P. "Preparation and using of high near–infrared reflective green pigments on ceramic glaze," *J. Ceram. Soc. Jpn.*, *118*, **2010**, 349–352.

Urones–Garrote, E.; Martinez, F.; Landa–Canovas, A. R.; Otero–Diaz, L. C. "New inorganic pigments in the Ca–Nd–S system: Stabilization of γ phase," *J. Alloys Compd.*, *418*, **2006**, 86–89.

van Roosmalen, J. A. M.; Cordfunke, E. H. P. "A new defect model to describe the oxygen deficiency in perovskite–type oxides," *J. Solid State Chem.*, *93*, **1991**, 212–219.

Volz, H. G. Industrial color testing: Fundamentals and techniques, 2nd Ed., Wiley–VCH, Weinheim, **2002**

Wang, Y.; Mori, T.; Ji–Guang, Li.; Ikegami, T. "Low–temperature synthesis of praseodymium–doped ceria nano powders," *J. Am. Ceram. Soc.*, 85, **2002**, 3105–3107.

Yamamura, H.; Nishino, H.; Kakinuma, K.; Nomura, K. "Crystal phase and electrical conductivity in the pyrochlore type composition systems, $Ln_2Ce_2O_7$ (Ln = Ln, Nd, Sm, Eu, Gd, Y, Tb)," *J. Ceram. Soc. Jpn.*, *111*, **2003**, 902–906.

Yamamura, H.; Nishino, H.; Kakinuma, K.; Nomura, K. "Relationship between oxide–ion conductivity and ordering of oxide ion in the $(Y_{1-x}La_x)_2(Ce_{1-x}Zr_x)_2O_7$ system with pyrochlore type composition," *Solid State Ionics*, *178*, **2007**, 233–238.

Zhukov, V.; Mauricot, R.; Gressier, P.; Evain, M. "Band electronic structure study of some doped and undoped γ–Ln_2S_3 (Ln = La, Ce, Pr, and Nd) rare earth sulphides through LMTO–TB calculations," *J. Solid State Chem.*, *128*, **1997**, 197–204.